KTH ROYAL INSTITUTE
OF TECHNOLOGY

Doctoral Thesis in Civil and Architectural Engineering

The influence of multiscale hyporheic flow on solute transport

Implications for stream restoration enhancing nitrogen removal

IDA MORÉN

Stockholm, Sweden 2022

The influence of multiscale hyporheic flow on solute transport

Implications for stream restoration enhancing nitrogen removal

IDA MORÉN

Academic Dissertation which, with due permission of the KTH Royal Institute of Technology, is submitted for public defence for the Degree of Doctor of Philosophy on Monday the 5th September 2022, at 10:00 a.m. in F3, Lindstedtsvägen 28, Stockholm.

Doctoral Thesis in Civil and Architectural Engineering
KTH Royal Institute of Technology
Stockholm, Sweden 2022

ISBN 978-91-8040-305-4
TRITA-ABE-DLT-2232

Printed by: Universitetsservice US-AB, Sweden 2022

Swedish summary

Vattendrag utgör en volumetrisk liten men viktig del av den hydrologiska cykeln. Vattendrag fungerar som snabba transportleder för vatten, lösta ämnen och energi och ytvattnet interagerar även kontinuerligt med utströmmande grundvatten i den så kallade hyporheiska zonen, vilket är sedimenten närmast vattendragen. Flödet av ytvatten in och ut ur den hyporheiska zonen kallas hyporheiskt utbyte och kan påverka vattenkvalitén i det lokala vattendraget och i nedströms recipienter genom att skapa förutsättningar för retention och nedbrytning. På grund av antropogena aktiviteter har många vattendrag blivit fysikaliskt, kemiskt och biologiskt nedbrytna, och naturliga funktioner såsom hyporheiskt utbyte har gått förlorade. För att skydda vattendrag från fortsatt destruktion, och för att restaurera vattendrag och förbättra vattenkvalitén i lokala vattendrag och nedströms recipienter krävs en ökad fysikalisk förståelse och tillförlitliga modeller för prognosering av hyporheiskt utbyte. Trots att den hyporheiska zonen studerats ingående under de senaste decennierna misslyckas ofta befintliga modeller med att inkludera alla väsentliga temporala och spatiala skalor, och de är därför svårt att generalisera resultaten för större avrinningsområden. Det generella syftet med denna avhandling var att öka den fysikaliska förståelsen för hur flödet genom den hyporheiska zonen i små vattendrag drivs och att undersöka hur det hyporheiska utbytet påverkar ämnestransporten i små enskilda vattendrag och nätverk av vattendrag. Dessutom syftade avhandlingen till att undersöka betydelsen av restaurering av vattendrag för det hyporheiska utbytet och transporten av kväve i små jordbruksdiken. Metoderna som användes i den här avhandlingen inkluderar både omfattande undersökningar i fält och semi-analytisk matematisk modellering. Ett ramverk av modeller etablerades, vilket inkluderade både en deduktiv, hydromekanisk modell som utvärderar korrelationen mellan den flerdimensionella bottentopografin och hydrologin i ett vattendrag och det hyporheiska utbytet, samt en endimensionell longitudinell transportmodell som inducerar de parametrar som beskriver det hyporheiska utbytet från spårämnesförsök i vattendrag. Dessa två modeller kors-validerades i tio lokala vattendrag och ramverket av modeller användes sedan på nätverks-skalan i två studier, då understött med omfattande observationer.

Resultaten visar att hyporheiskt utbyte kan ha stor inverkan på ämnestransporten i nätverk av vattendrag samt på det utströmmande grundvattnets flödesmönster. Resultaten underbygger dessutom tidigare studier som visar att fördelningen av hydraulisk tryckhöjd längsmed vattendragens botten till stor del kontrollerar det hyporheiska utbytet i små alluviala vattendrag med lågt flöde, litet djup, och måttlig lutning. Bottens och ytvattnets longitudinella profilers fraktala egenskaper är särskilt betydande för den hyporheiska utbyteshastigheten. Inmätningar av bottentopografin och ytvattenprofilen i tio små alluviala vattendrag visade att det var de longitudinella variationerna i hydraulisk tryckhöjd över korta våglängder (0.1-5m) som drev majoriteten av det hyporheiska utbytet, samt att variationer i den hydrostatiska tryckhöjden var viktigare än variationer i den hydrodynamiska tryckhöjden. Det

etablerade modellramverket visade också att nedbrytningen av kväve i den hyporheiska zonen i huvudsak beror på balansen mellan flödet av vatten till sedimenten och transporttiden däri. Specifikt visar studien att det existerar ett optimalt Damkhölers tal, definierat som produkten mellan medeluppehållstiden i den hyporheiska zonen, och denitrifikationshastigheten längsmed hyporheiska flödeslinjer, som motsvarar den optimala nedbrytningshastigheten av kväve, givet en konstant ratio mellan djupet på den hyporheiska zonen och vattendjupet i vattendraget. Det betyder att nedbrytningshastigheten av kväve i vattendragen antingen är transport eller reaktionsbegränsad, och när det nuvarande Damlkhölers tal bestämdes för alla små vattendrag i jordbruksområden i Sverige, varierade denna begränsning både mellan vattendrag och mellan olika flödessituationer. Den stora spatiotemporala variationen i potentialen pekar på behovet av en hög lokal förståelse för de processer som faktiskt driver det hyporheiska utbytet samt noggrann och platsspecifik design av specifika åtgärder. Modellering visade att om detta görs finns potential att minska mängden kväve som transporteras till Östersjön genom att förstärka det hyporheiska utbytet i små, alluviala vattendrag.

List of publications

Two published journal papers and two journal papers submitted for review, along with an extensive initial summary, form the basis for this compilation thesis. Throughout the thesis, the papers are referred to by their Roman numerals:

I. **Morén, I.**, Wörman, A., and Riml, J. (2017). Design of remediation actions for nutrient mitigation in the hyporheic zone. *Water Resources Research, 53*, 8872–8899. https://doi.org/10.1002/2016WR020127

II. **Morén, I**., Wörman, A., and Riml, J. (2021). Cross-validating hydromechanical models and tracer test assessments of hyporheic exchange flow in streams with different hydromorphological characteristics. *Water Resources Research, 57*, e2021WR030248. https://doi.org/10.1029/2021WR030248

III. Riml, J., **Morén, I.**, and Wörman, A., (2022). Potential of stream restorations to enhance hyporheic removal of agricultural nitrogen in Sweden. Submitted to *Ecological Engineering*.

IV. **Morén, I.**, Mojarrad, B., Riml, J. and Wörman, A. (2022). Geographic and hydromorphologic controls on surface water–groundwater interactions averaged at different spatial scales. Submitted to *Hydrogeology Journal*.

The contributions of the author for each paper are as follows:

I. The author, Ida Morén (IM), was the main responsible for the scientific planning; modelling; evaluation of modelling results and field data. Supervised by Anders Wörman (AW), IM derived the analytical solutions presented in the paper. IM planned the fieldwork and collected the field data together with Joakim Riml (JR) and colleagues. IM wrote the initial manuscript and the revised version of the paper, while JR and AW contributed with editing.

II. IM was the main responsible for the scientific planning; theoretical development; modelling; evaluation of modelling results and field data; and writing, while both co-authors did contribute with editing and scientific advice. IM planned the fieldwork together with JR and collected the included field data together with other colleagues and students.

III. IM was jointly responsible for the scientific planning and theoretical development of the manuscript. The manuscript is based on a report prepared by IM (Morén et al., 2018), which was then extensively revised by JR together with IM and AW. In the final version of the manuscript, IM was responsible for the modelling in HEC-RAS and the evaluation of restoration strategies at the local scale, while JR performed and evaluated the network scale modelling. IM wrote the parts of the paper (methods, results and discussion) considering the local scale evaluation and contributed with editing the full paper.

IV. IM was together with Brian Mojarrad (BM) responsible for the scientific planning and theoretical development. IM performed the processing of the digital elevation model, analytical modelling of the hyporheic flow and the regression analysis, while BM performed the groundwater flow modelling and the PCA. IM wrote the main parts of the manuscript, except for the method section on modelling of groundwater flow, which was written by BM. All co-authors did contribute with editing the final version of the manuscript.

Listed below are reports written by IM, which are related to, but not included in, the thesis:

- Riml, J., **Morén, I.**, Wörman, A., Zięba, D., and Wachniew P. Tracer Tests and the effect of solute retention and attenuation on the stream reach scale. BONUS Soils2Sea Deliverable 4.2. Royal Institute of Technology (KTH), Stockholm, December 2016, www.Soils2Sea.eu

- **Morén, I.**, Riml, J. and Wörman, A., Design of water-course remediation measures to increase nutrient mitigation. BONUS SOILS2SEA Deliverable 4.3. Royal Institute of Technology, Stockholm, November 2017, www.SOILS2SEA.eu

- **Morén, I.**, Riml, J. and Wörman, A., In-stream water management strategies for reducing nutrient loads to the Baltic Sea. BONUS Soils2Sea Deliverable 4.4. KTH Royal Institute of Technology, Stockholm, March 2018, www.Soils2Sea.eu

Acknowledgements

At last, I have finalized this thesis, and I would like to acknowledge the many people who helped me along the way. First, I gratefully acknowledge the financial support that made this work possible. The study was part of the BONUS Soils2Sea project (Art 185), which was jointly funded by the EU's Seventh Program for research, technological development and demonstration and by The Swedish Environmental Protection Agency. Furthermore, the Swedish Radiation Safety Authority, SSM (Dnr SSM2019-1195) contributed to the funding of this work, as did the Swedish Research Council Formas.

Second, I want to thank my main supervisor professor Anders Wörman for giving me the opportunity to study at KTH, and for letting me stay for so long. Thank you for introducing me to the world of research, for sharing your time and your knowledge and for believing in this project even when I did not. I would also like to thank my second supervisor Joakim Riml, for always being available with valuable advice. I enjoyed our discussions in the office as well as in the field. Without Anders and Joakim, I would never have finalized this thesis. I am also thankful to past and present colleagues at the Department of Civil and Architectural Engineering and at the Department of Sustainable Development, Environmental Science and Engineering (SEED) for making the time at KTH pleasant and for inspiring me to do research that actually matters. A special mention goes to Anna, Nicholas, Peng Hua, Babak, Shuang, Bijan and Luigia. Thank you for the good times we had together and for your personal and academic support. I am also happy to have met many great researchers outside of KTH during my PhD studies, both within the BONUS Soils2Sea project and in the HypoTrain group. Furthermore, I am thankful to all of you who helped me in the field. In addition to those of you already mentioned above, I would like to acknowledge Damian, Oscar, Jakob, Sunna, Jenny and Olivia. Furthermore, I want to thank Johnny and Katrine at Tullstorpsåns Ekonomiska Förening for interest in our project and Bertil for storing all our equipment.

On a personal note, I want to thank my parents for giving me the confidence and eagerness to keep learning new things and for supporting me in all ways possible. Many thanks goes also to my siblings, parents in law and extended family for taking care of my children so that I could write. Finally, I want to acknowledge my own and endlessly loved little family. Thank you Enar for constantly reminding me of what is actually important in life and Hedda for keeping me company while writing this thesis, on the inside as well as on the outside. Anders, my husband rock, thank you for staying calm when I worry and for giving me time and space to finish this thesis. Now I look forward to the next chapter of our life together.

Ida Morén, Falun, Sweden, July 2022

Contents

Swedish summary i
List of publications iii
Acknowledgements v
List of Figures ix
List of Tables xii
Notations and Abbriviations xiii
Abstract 1
1 INTRODUCTION 2
1.1 The hyporheic zone and the groundwater-surface water continuum 2
1.2 Biochemical reactions in the hyporheic zone 4
1.3 Degradation and restoration of streams and hyporheic zones 7
1.4 Objectives and scope of the thesis 9
1.5 Thesis limitations 10
2 THEORY ON HYPORHEIC FLOW MODELLING 11
2.1 In-stream solute transport modelling 12
2.1.1 The transport equation 12
2.1.2 Transient storage and HEF in solute transport models 14
2.2 Hydromechanical subsurface flow modelling 15
2.2.1 The governing equation for groundwater flow 15
2.2.2 Longitudinal pressure distributions at streambed interfaces 16
2.2.3 Multiscale hyporheic exchange flow and fractality 18
2.3 Modelling nutrient cycling in streams 20
3 METHODS 22
3.1 Field and modelling sites 22
3.2 Field measurements and data processing 27
3.2.1 In-stream tracer tests 27
3.2.2 Hydraulic conductivity 28
3.2.3 Elevation surveying 28
3.2.4 Discharge and nitrogen load data 29
3.2.5 Processing topography data 29
3.3 The reactive advection storage path model 30
3.3.1 Solutions to the transport equation using the Laplace method 32
3.3.2 Estimating the mass removal in stream reaches and networks 32
3.3.3 Calibrating the advective storage path model 33
3.3.4 Sensitivity analysis 34

3.4 A hydromechanical model for hyporheic exchange flow 35
3.4.1 The flow-weighted average exchange velocity 36
3.4.2 Estimating hydraulic head power spectral densities 37
3.4.3 The geological damping factor 38
3.4.4 The hyporheic residence time 39
3.5 Estimating hydraulic variables in nongauged streams 41
3.6 Generalization of the average hyporheic exchange velocity 42
3.6.1 Tested dependent and independent variables 42
3.6.2 Regression analysis 43
3.7 Testing the potential of stream restoration 44
3.7.1 The local effects of specific stream restoration designs 44
3.7.2 The theoretical potential of stream restoration at the national scale 45
4 RESULTS AND DISCUSSION 46
4.1 Physical controls on hyporheic exchange flow 47
4.1.1 Cross-validating two approaches for estimating hyporheic exchange 47
4.1.2 Static and dynamic hyporheic exchange at different spatial scales 50
4.1.3 Reach and catchment characteristics controlling hyporheic exchange 53
4.2 Impact of hyporheic exchange on stream nitrogen removal 57
4.2.1 Analytical solutions for nitrogen removal at the reach scale 57
4.2.2 Current hyporheic nitrogen removal at the national scale 59
4.2.3 Potential hyporheic nitrogen removal at the national scale 61
4.2.4 Impacts of stream restoration design on nitrogen mass removal 62
4.3 Surface water and deep groundwater interactions 67
5 FUTURE PROSPECTS 68
6 CONCLUSIONS 70
References 73
Appendix: Papers 89

List of Figures

Figure 1. Overview of field sites including both locations of local stream reaches studied in Papers I, II and III, and the regional catchments studied in Paper IV.... 25

Figure 2. Example of tracer test data from Malsta Brook (reach R3 in Paper II), including a) a standard calibration curve linking the fluorimeter reading in mV to Rhodamine WT (RWT) concentration in μg/L; and b) the resulting upstream (us) and downstream (ds) observed break through curve (BTC) in μg/L, as well as the best (optimized) advective storage path (ASP) model of the us and ds BTC, and all the behavioral models of the ds BTC. 27

Figure 3. Dotty plots from Monte Carlo sensitivity analysis of the advective storage path (ASP) model calibrated using tracer test data from Malsta Brook (reach R3 of Paper II). Each dot represents a model run with randomly selected variables and the red dots represents behavioural models, with an error smaller than 15% of the minimal error. The vertical black line illustrates the parameter value from the formal optimization. 35

Figure 4. Power spectral density (PSD) of static and dynamic hydraulic head fluctuations as well as stream bottom elevation fluctuations along the thalweg of the stream based on a) elevation measurements along reach R6a of Paper II and b) data extracted from the DEM at the same position as reach R6a..... 38

Figure 5. The interlinkages between different models and papers in this thesis, indicating both subsurface and surface water modelling (lower and upper boxes) and modelling at different spatial scales (increasing scale towards the right in the figure). The big white arrows illustrates the models that are part of the framework including the multiscale, hydro mechanical (HM) model used for 2D subsurface flow modeling; the advective storage path (ASP) model used to quantify the 1D solute transport with surface water; temporal moment derivation to estimate the reach scale mass removal; and aggregation of the reach scale response to estimate the network scale mass removal. The cross-validation between the surface and subsurface models is also shown to the left. The brown fields and small arrows denotes the data needed to limit the models, and the blue markers illustrates which models that were part of which papers. 46

Figure 6. Cross-validation of inductive assessments of tracer tests using the advective storage path (ASP) model and deductive modelling using the mulstiscale hydro mechanical (HM) model, in terms of: a) the average exchange velocity, $\langle W \rangle$; b) the average of the hyporheic residence time, $\langle T \rangle$; and c) the coefficient of variation of the residence time distribution, $CV[T]$. Horizontal error bars represents the variable range leading to behavioral models, while the vertical error bars represents the sensitivity in the variables due to different assumptions of the hyporheic zone depth, ε, and streambed porosity, η. (From Paper II) 48

Figure 7. The power spectral densities (PSDs) of the static, dynamic and total head driven hyporheic exchange flow (HEF) velocity distributed over observed and extrapolated wavelength. Note that the blue lines (solid and dashed) are disappearing behind the black line for larger wavelength, since the dynamic head is too small to influence the total HEF velocity at these scales. This is an example from Malsta Brook (Reach R3), while results from the rest of the reaches are found in Paper II. 51

Figure 8. The average hyporheic exchange flow (HEF) velocity calculated with increasingly high cutoff wavelength (λ_{max}) and normalized with the HEF velocity calculated with the maximal upper wavelength equal to the stream reach length (X), for the ten different study reaches of Paper II. (Modified from Paper II).....52

Figure 9. The hyporheic exchange flow velocity, $\langle W \rangle$, normalized with the hydraulic conductivity, K, as a function of; a) the standard deviation in the water surface profile along the reach normalized with the stream reach length σ_{hs}/X; b) the standard deviation in streambed topography normalized with stream depth, σ_{yb}/d; c) the Reynold number calculated from streamdepth, $Re = Ud/v$; and d) the squared Froude number $Fr^2 = U^2/dg$. Triangles and circles represents values estimated with the multiscale hydromechanical (HM) model and the advective storage path (ASP) model, respectively. Colors refer to the reaches investigated in Paper II, according to the legend. Lines between markers indicate that the data is coming from the same reach; thus longer lines indicates a higher disagreement between the models. (Modified from Paper II).....55

Figure 10. The best performing regression models, estimating the average hyporheic exchange flow (HEF) velocity at a) the reach scale (r), b) the intermediate catchment (IC) scale and, c) the regional catchment (RC) scale. Adjusted R^2 and predictive R^2 are shown in each graph. The different markers indicates that data are derived from the different regional catchments Bodals Brook (BB), Säva Brook (SB), Tullstorps Brook (TB), Forsmark Brook (FB) and Krycklan Catchment (KC) and the grey line represents the I:I reference. (From Paper IV).....57

Figure 11. Probability density functions of the system reaction rate, R_{HZ}, in all small local agricultural stream reaches in Sweden at yearly mean discharge (MQ), yearly mean low discharge (MLQ) and yearly mean high discharge (MHQ) conditions. (Modified from Paper III).....60

Figure 12. The hyporheic removal rate, R_{HZ}, as a function of the denitrification Damkhöler number Da_{den} at conditions of yearly mean discharge (MQ), yearly mean low discharge (MLQ) and yearly mean high discharge (MHQ). The black vertical line denotes the optimal Damkhöler number $Da_{den,opt}$. Presented results are based on the assumption that ε=0.1, r_{den}=0.1 h^{-1} and τ_{oxy}=1 h while stream hydraulics varies between stream reaches (Modified from Paper III). 61

Figure 13. Variability in a) the current and potential hyporheic removal rate, R_{HZ} and b) the current and potential relative mass removal, D, in all local agricultural

stream reaches during mean flow conditions (MQ). Presented results are based on the assumption that ε=0.1, r_{den}=0.1 h^{-1} and τ_{oxy}=1 h in all reaches, while stream hydraulics varies between stream reaches. (Modified from Paper III) 62

Figure 14. The nitrogen removal rate, R_{HZ}, as a function of hyporheic zone depth, ε, derived assuming hydraulic head variations along the streambed estimated from measurements in the Tullstorps Brook, and hydraulic head distributions shaped as a generic horizontal step. Two different step sizes were tested, which differed in length (*L*) and height (*H*), but had the same ratio height/length equal to the stream slope. (Modified from Paper I) 64

Figure 15. Effect of stream different stream restoration design scenarios (S1-S4) in Malsta Brook compared to base-case (BC) conditions on a) the denitrification Damkhöler number and its impact on the nitrogen removal rate of the hyporheic zone, R_{HZ}, and b) the in stream residence time, and its impact on the relative mass removal, D. The scenarios were tested in mean low discharge conditions (MLQ), mean discharge conditions (MQ) and mean high discharge conditions (MHQ). The grey lines in the upper panel represents different values of the ratio $\frac{P}{A}\frac{WT}{2} = \varepsilon\frac{P}{A}$, and the gray lines in the lower panel represents different values of R_{HZ} in 1/day. In both the base-case conditions and the different scenarios the hyporheic zone depth was assumed to be ε=0.05, and the denitrification rate r_{den}=0.1 h^{-1} and the oxygen consumption time τ_{oxy}=1 h. (Modified from Paper III) 65

Figure 16. The empirical cumulative distribution function of the ratio between the average deep GWF discharge velocity and the average flow weighted HEF velocity at the streambed-water interface, $\delta_{W,r}$, in all stream segments in the five catchments modelled in Paper IV. (From Paper IV) 67

List of Tables

Table 1. Characteristics of investigated stream reaches in Paper I including surrounding environment, geomorphology, in-stream vegetation, streambed material, stream length X, stream slope S, stream depth d and streambed hydraulic conductivity K, as well as the discharge at the time of the tracer test, Q0. (Modified from Paper I) 24

Table 2. Characteristics of investigated stream reaches from the five catchments in Paper II, including surrounding environment, geomorphology, in-stream vegetation, streambed material, stream length *X*, stream slope *S,* stream depth *d* and streambed hydraulic conductivity *K*, as well as the discharge at the time of the tracer test, Q_0. (Modified from Paper II) 26

Table 3. The base case condition and restoration designs tested in Malsta Brook (Paper III), including in-stream structures in the form of weirs of varying height (H) and in-between distance (L) and modification of the average hydraulic conductivity (K) of the streambed. (From Paper III) 45

Notations and Abbriviations

A	Stream cross section area	m^2
ADE	Advection Dispersion Equation	-
ASP	Advective Storage Path	-
A_{CM}	Catchment area	m^2
A_U	Regression constants in model estimating stream width	-
a_{f}	level of power spectrum of signal f	[unit of f]
$A_{\mathrm{f,i}}$	Amplitudes of harmonic i, in signal f	[unit of f]
b_{f}	Slope of power spectrum of signal f	-
B	Relative mass recovery	-
B_U	Regression constants in model estimating stream width	-
c	Solute concentration	kg/m^3
C	Time and volume average solute concentration	kg/m^3
C_{d}	Fehlmans constant	-
C_1	Constant associated with equation for residence time	-
c_{K}	Hydraulic conductivity decay constant	$1/m$
C_U	Regression constants in model estimating stream width	-
CV	Coefficient of Variation	-
d	Average stream depth	m
D	Relative mass removal	-
D_L	Dispersion coefficient	m^2/s
D_{QD}	Average catchment quaternary deposit depth	m
Da_{den}	Denitirification Damkhöler number	-
Da_{oxy}	Oxygen consumption Damkhöler number	-
E	Elevation above sea	m
EaS	Elevation above stream	m
e	Error between observed and simulated concentration	-
Fr	Froude number	-
f	Darcy-Weisbash friction factor	-
$f(T)$	Flow weighted residence time distribution	$1/s$
G	Solute concentration in streambed pour water	kg/m^3
GtS	Gradient to stream	-
g	Gravitational acceleration	m/s^2
H	Bedform height or weir height	m
HEF	Hyporheic Exchange Flow	-
HM	Hydro-mechanical	-
HZ	Hyporheic Zone	-
h	Hydraulic head of streambed	m
h_{d}	Dynamic hydraulic head at streambed-water interface	m
h_{s}	Static hydraulic head at streambed-water interface	m
J	Fluid flux	kg/m^2s
J_{CS}	Transversal flux over the permeable streambed surface	kg/m^2s

K	Hydraulic conductivity at top of streambed sediments	m/s
K_{CM}	Average hydraulic conductivity of catchment top soil	m/s
L	Distance between weirs or steps in water surface profile	m
M	Solute mass	kg
M_{inj}	Injected mass of tracer	kg
M_{in}^{i}	Mass load to stream segment i	kg
MR	Absolute Mass Removal	kg
MLQ	Annual mean low discharge	m^3/s
MHQ	Annual mean high discharge	m^3/s
MQ	Annual mean discharge	m^3/s
MSC	Median Subcatchment Area	m^2
n	Manning's Coefficient	$s/m^{1/3}$
n_{c}	Corrected Manning's Coefficient	$s/m^{1/3}$
n_j	jth Temporal Moment	-
P	Wet Perimeter	m
PDF	Probability Density Function	-
PSD	Power Spectral Density	-
p	Laplace Variable	-
Q	Reach Average Stream Discharge	m^3/s
Q_0	Discharge at the injection point during tracer tests	m^3/s
q	Darcy Velocity in Streambed	m/s
R_h	Hydraulic radius	m
R_{sys}	Nitrogen removal rate in the full stream system	1/s
R_{HZ}	Nitrogen removal rate in the hyporheic zone	1/s
R_{MC}	Nitrogen removal rate in main channel	1/s
R^2	Coefficient of determination	-
R^2_{Adj}	Adjusted coefficient of detemination	-
R^2_{Pred}	Predictive coefficient of determination	-
r_{den}	Hyporheic zone denitrification rate	1/s
Re	Reynolds number	-
s	Stream sinousity	-
S	Average stream slope	-
S_{CM}	Average catchment slope	°
S_{f}	Power spectral density of signal f	[unit of f]^3
T	Residence time along hyporheic streamline	s
$\langle T \rangle_{opt}$	The optimal, average hyporheic residence time	s
t	Time	s
u	Cross section average in-stream velocity	m/s
U	Reach Average in-stream velocity	m/s
V_x	Horizontal pour velocity component in streambed	m/s
V_y	Vertical pour velocity component in streambed	m/s
W	Hyporheic exchange velocity	m/s

W_{dGWF}	Discharging deep groundwater velocity	m/s
WSP	Water Surface Profile	-
X	Stream reach length	m
X_U	Regression constants in model estimating in-stream velocity	-
x	Coordinate longitudinal along stream	m
y	Coordinate perpendicular to flat streambed	m
Y	True dependent variables of regression model	-
$\hat{Y}$	Predicted dependent variables of regression model	-
Y_U	Regression constant in equation for sream velocity	-
y_b	Elevation along streambed	m
Z_U	Regression constant in equation for sream velocity	-
z	Coorinate along streamtube	m
α	Geological damping factor associated with HM model	-
γ_s	Static head damping factor associated with HM model	-
γ_s	Dynamic head damping factor associated with HM model	-
∇	nabla operator	1/m
δ	Dirac delta function	1/s
δ_W	Ratio between HEF velocity and dGWF velocity	-
ε	Hyporheic zone depth	m
ζ	Area reduction factor	-
ζ_n	Manning coefficient correction factor	-
TS	Transient Storage	-
τ	Characteristic time within hyporheic zone	s
τ_{oxy}	Oxygen consumption time in HZ	s
η	Streambed porosity	-
λ	Wavelength of power spectrum	m
λ_{min}	Minimal wavelength of power spectrum	m
λ_{max}	Maximal wavelength of power spectrum	m
σ_f	Standard deviation of signal f along streambed	[unit of f]
σ_E	Standard deviation in elevation above sea	m
σ_{logT}	Standard deviation of the logarithm of T	log(s)
μ_{logT}	Mean of the logarithm of T	log(s)
$\forall$	System control volume	m^3
Ω	Stream power per unit stream length	kgm/s^2

Abstract

Stream water that flows into and out of streambeds is called hyporheic exchange flow (HEF). It continuously interacts with groundwater and thereby affect the water quality of local stream reaches as well as downstream recipients by providing an environment where solutes and energy can be retained and degraded. Because of anthropogenic activities, many streams and rivers have been physically, chemically and biologically degraded during the last centuries and natural functions, such as HEF, have to some extent been lost. The general aim of this thesis was to advance the understanding of the physical controls of HEF in small streams and to investigate how HEF influences solute reactive transport in streambeds and surface water networks before and after stream restoration. To reach the aim, the consistency and deviation between HEF parameters evaluated with two common approaches were investigated in ten different alluvial streams with low discharge, shallow depth and moderate slope. The two approaches were: 1) developing and using a deductive hydro-mechanical model to assessed the relationship between the multiscale streambed geomorphology and the reach scale average HEF parameters, and 2) evaluating HEF parameters from in-stream tracer tests using a 1D longitudinal transport model. The relatively high consistency between the approaches connects theories that previously have been relatively fragmented and provides a tool for upscaling (parameterizing) of HEF in solute transport models over stream networks based on independent observations of stream topography, streambed sediment properties and in-stream hydraulics. Applying the modelling framework at the network scale and supporting it with comprehensive datasets provided information regarding physical mechanisms and spatial variability of HEF as well as its influence on longitudinal solute transport. Specifically, the fractal properties of the water surface profile were shown to represent the average HEF velocity well. Furthermore, hydraulic head variations over shorter wavelengths (0.1-5 m) were found to drive the main part of the HEF and the static hydraulic head variations dominated over dynamic hydraulic head variations as drivers of HEF in all investigated streams. Moreover, this thesis highlights the importance of the hyporheic zone as a bio-chemical and mechanical filter for stream water. It shows that common engineered stream restorations can influence HEF and improve the water quality in local stream reaches as well as downstream recipients. Specifically, the thesis presents exact solutions to the nitrogen transport, which shows that the mass removal of nitrogen in the hyporheic zone is either transport or reaction limited and that the maximal removal rate corresponds to an optimal hyporheic residence time and a typical denitrification Damköhler number. The results also show that potential exists to reduce the agricultural nitrogen load to the Baltic Sea by stream restorations that optimize the hyporheic residence times. However, the large spatiotemporal variability in the potential between reaches stresses the importance for further studies on which processes that are driving HEF under specific hydromorphologic conditions and careful design of stream restoration measures at each local stream reach.

Keywords: Hyporheic exchange flow, Hydrological modeling, Solute transport, Stream restoration, Nitrogen, Power spectral analysis

1 INTRODUCTION

Streams and rivers are extremely important for the natural environment as well as society, and they contribute to many different ecological, economic and societal functions. The stream network serves as roadways in the landscape, by distributing drinking, bathing and irrigation water, while also providing important ecological habitats and corridors for many aquatic species. Furthermore, while streams and rivers can transport contaminants, natural solutes and particulate matters over large areas, they also have self-cleaning capacities depending on different hydrologic conditions. This thesis studies the self-cleaning capacity of streams achieved by flow through the so-called hyporheic zone (HZ) and investigates how this process can be observed, quantified and enhanced through stream restoration actions. This section provides a summary of the hydrological aspects of this scientific discipline and sets out the motivation of the thesis. It also introduces the HZ and its importance for local streambed hydrology, the groundwater-surface water continuum and biogeochemical reactions in the stream, with a focus on nitrogen cycling. Furthermore, this section summarizes the ongoing degradation of many stream functions and the potential of stream restoration as a method to improve water quality. Finally, the main objectives and scope, as well as the limitations of the thesis, are presented in this section.

1.1 The hyporheic zone and the groundwater-surface water continuum

It has been known since the mid 20th century that the water in streams is a mix of surface runoff and old groundwater (Rodhe et al., 1996, McDonnell et al., 2010). More recently, it was discovered that streamwater flows into the subsurface and, after some time, returns to the stream, and the stream network has therefore been increasingly acknowledged as an integrated part of the catchment (e.g., Bencala, 1993, Winter et al., 1998, Cardenas, 2015). The area closest to the streambed, where groundwater and surface water meets is part of both the surface water and the groundwater continuum and is commonly referred to as the hyporheic zone. The term hyporheic originates from the Greek words hypo, which means under and rheos, which means river, and was initially introduced by Orghidan (2010). The flow of water through the HZ is called hyporheic exchange flow (HEF) and is defined here as surface water that flows into the streambed and soon returns to the stream (Harvey and Bencala, 1993). By this definition, hyporheic flow paths are bidirectional and enter and leave the streambed several times within the study reach, which is contradictory to groundwater flow paths that are unidirectional and only cross the streambed interface once, recharging from or discharging to the stream (Harvey and Wagner, 2000). However, since both groundwater flow and HEF occur over a wide range of spatial scales, creating a complex hierarchical pattern of flow cells (Tóth, 1963, Winter et al., 1998, Wörman et al., 2007), the separation of the two types of flows is not always straightforward and will depend on the research focus (Bencala et al., 2011, Boano et al., 2014). HEF along a specific

stream reach is impacted by the larger-scale groundwater circulation and, thus, is controlled by large-scale catchment processes, while at the same time, it reflects an aggregation of processes operating on smaller scales (Tonina and Buffington, 2009, Ward and Packman, 2019). Thus, this mutual influence between groundwater and HEF demonstrates that the two types of flows are part of an integrated hydrological system.

The impact of regional groundwater flow on the patterns of the HEF has been estimated at the catchment scale in modelling studies by superimposing the two flow fields. Such studies have shown that groundwater flow causes a fragmentation of HEF, resulting in patchier HEF characteristics than occurs when the groundwater flow is not accounted for (Wörman et al., 2007, Stonedahl et al., 2013, Caruso et al., 2016, Mojarrad et al., 2019). The superimposing approach also reveals that the interaction between groundwater and surface water is mutual, so that the groundwater flow patterns and magnitudes likewise are impacted by the HEF (Winter et al., 1989, Mojarrad, 2021). A highly intensive HEF will force groundwater to discharge over smaller areas, and this funneling of groundwater flow paths results in higher discharge velocities close to the streambed-water interface. The importance of having a multiscale perspective in HEF research has been acknowledged for a long time, but is still often neglected (Stream Solute WorkshopWorkshop, 1990, Boano et al., 2014, Pinay et al., 2015, Ward and Packman, 2019). This thesis adds to the increasing body of research on the multiscale nature of HEF by utilizing a spectral model that acknowledges the importance of a wide distribution of spatial scales wen studying HEF.

The wide range of spatial and temporal scales related to HEF reflects its broad range of drivers, even within a shorter stream reach. HEF is mainly driven by hydraulic head variations at the streambed-water interface, and is controlled by the geological properties of the streambed (Boano et al., 2014). The hydraulic head variations at the streambed-water interface can be divided into static and dynamic parts, both related to the streambed geomorphology. At a specific point at the streambed-water interface, the static head is the sum of the streambed elevation and the stream water depth. The variation in static head along the streambed interface was first studied as a driver of HEF by Vaux (1968). Static head gradients that drive the HEF are created across relatively large geomorphological features in the stream such as riffle and pool sequences, dunes or cascades and steps (e.g., Harvey and Bencala, 1993, Woessner, 2000, Tonina and Buffington, 2007, Tonina and Buffington, 2011, Hassan et al., 2015). Static head gradients can also arise across obstacles, such as boulder clusters and dead wood (e.g., Kasahara and Hill, 2006, Lautz et al., 2006, Sawyer and Cardenas, 2012, Sawyer et al., 2012), and across meander bends (e.g., Wroblicky et al., 1998, Boano et al., 2006). Dynamic head variations are the drag and lift forces that arise when flowing water interacts with streambed roughness features such as bedforms and stones as described early by Thibodeaux and Boyle (1987), Savant et al. (1987) and Elliott and Brooks (1997a).

Dynamic head driven HEF is particularly important in lowland rivers, which have sandy bottoms and entail submerged bedforms and where overlying water surfaces are relatively flat; however, it can also exist in combination with static head driven HEF (Wondzell et al., 2019). The relative importance of static and hydraulic head drivers has been raised only occasionally in previous research. This thesis more thoroughly addresses the separate impacts of dynamic and static heads on HEF. An improved understanding of these phenomena is needed in order to upscale reach and sub-reach mechanisms to the scale of stream networks and catchments. A better understanding can also improve the design of stream restoration measures with specific remediation targets. Other processes and phenomena that can cause flow of surface water across the streambed interface are not discussed extensively in this thesis but are acknowledged here since they can be substantial in certain types of streams. First, stream meandering can result in pressure variations at the streambed that cause lateral HEF through the meander bars (e.g., Boano et al., 2006, Cardenas, 2009). Another important phenomenon that can cause HEF is the penetration of turbulent surface water across the streambed interface (e.g., Nagaoka and Ohgaki, 1990, Packman et al., 2004, Boano et al., 2011, Voermans et al., 2017, Grant et al., 2018, Voermans et al., 2018). Furthermore, changes in stream and groundwater stages cause occasional and mainly lateral HEF, often referred to as bank storage (e.g., Pinder and Sauer, 1971, Wu et al., 2018, Singh et al., 2019). Finally, different types of biological processes create a flow of water across the streambed-water interface, such as, e.g., burrowing and feeding by benthic organisms (Boudreau, 2000, Song et al., 2010, Shrivastava et al., 2021).

1.2 Biochemical reactions in the hyporheic zone

The HZ has been identified as a hotspot for biochemical reactions (McClain et al., 2003, Zhao et al., 2021). Flow of water through the HZ increases the contact time between the surface water and mineral surfaces and biofilms in the streambed sediments, where reactions can occur. Furthermore, groundwater and surface water have very different chemical and physical compositions. While groundwater is generally anoxic and slow moving, with relatively stable temperatures and reduced chemical conditions, surface water is highly illuminated, oxygenated, well-mixed and fast moving, with highly variable temperatures (Brunke and Gonser, 1997, Krause et al., 2011, Boano et al., 2014). Mixing of these waters makes the HZ a transition environment with steep physiochemical gradients (Triska et al., 1993, Rutherford et al., 1995, Hedin et al., 1998, Lautz and Fanelli, 2008, Zarnetske et al., 2011, Zarnetske et al., 2012). Groundwater flow and HEF bring essential nutrients, organic carbon and oxygen into the HZ, which together with physically stable streambed sediments provides an attractive habitat for microbes (Hedin et al., 1998, Findlay and Sobczak, 2000). Aerobic catalyzing microbes colonize in areas where surface water is recharged into the HZ and normally has high dissolved oxygen concentrations. High aerobic microbial activity in those areas subsequently leads to oxygen depletion along streamlines, resulting in colonization of anaerobic

metabolizing microbes furthere down in the streambed sediments or in discharge areas along the streambed. The highly reactive sediments can influence the fate of water contaminants traveling through a watershed. First, groundwater contaminated with heavy metals, nutrients and organic solutes that are discharged in streams can be substantially modified after passing through the HZ (Hedin et al., 1998, Nagorski and Moore, 1999, Conant et al., 2004, Krause et al., 2013). Second, after reaching the surface water, multiple circulations of the contaminant through streambeds with HEFs can influence the stream water quality and the final concentration exported to the recipient (Harvey et al., 2013, Mallard et al., 2014, Ensign and Doyle, 2006, Wörman et al., 2002)

Nitrogen is one of the most important components in stream ecosystems, and its biogeochemical cycling in the HZ has been studied extensively. Nitrogen, together with phosphorous, carbon, oxygen and hydrogen is essential for all living organisms. However, imbalances in the nitrogen cycle can lead to eutrophication, resulting in collapsed aquatic ecosystems. Nitrogen makes up just below 80% of the atmosphere in the form of nitrogen gas (N_2), which is not available for biological metabolism by most living organisms (Galloway et al., 2004). Nitrogen reaches the geosphere through biological nitrogen fixation (BNF), where the reduction of N_2 into ammonia (NH_4) is catalyzed by specific groups of bacteria. Furthermore, lightning can produce enough energy to turn atmospheric N_2 into NO_2. Nitrogen is subsequently loaded to the surface water system from point sources or diffuse sources such as surface runoff and groundwater discharge, in organic as well as inorganic forms. If the upstream catchment is small, fixation of nitrogen gas directly into the water can also be substantial but occurs primarily in slow-moving waters such as wetlands and lakes (Howarth, 2014). In undisturbed terrestrial areas, nitrogen is mainly apparent in the surface water system in organic forms such as detritus or dissolved organic matter (Bernot and Dodds, 2005). The relatively low levels of inorganic nitrogen that enter such pristine streams are rapidly denitrified or taken up by biota (Peterson et al., 2001, Galloway et al., 2003). In contrast, in many areas that are impacted by human activities, the nitrogen cycle has been altered by the cultivation of legumes, utilization of industrialized fertilizers, and fossil fuel combustion (Galloway et al., 2004). Therefore, many soils are saturated with nitrogen, which then leaches to surface water (Galloway et al., 2003, Bernot and Dodds, 2005, Royer et al., 2006). Nitrogen saturation can occur when organism growth is no longer limited by the nitrate concentration, when organisms mineralize a greater part of their food because it is nitrogen-rich, and when abiotic adsorption places are saturated (Bernot and Dodds, 2005). So-called legacy nitrogen has been shown to accumulate within the root zone of agricultural soils for several decades before being transported to streams with relatively deep and old groundwater (Tesoriero et al., 2013, Van Meter et al., 2016). Climate change is also expected to alter the transport of nitrogen from land to surface waters, and intensify the eutrophication of lakes and oceans (Teutschbein et al., 2008). The leaching of nitrogen into groundwater, and subsequently into streams, is mainly in

inorganic forms, i.e. nitrite and nitrate, since those species are highly movable in water. The transport of inorganic nitrate in stream networks is thus high and accounts for a large part of the nitrate transported to oceans (Boyer et al., 2006). In the Baltic Sea, where eutrophication is an extensive problem, it is estimated that around 70% of the total nitrogen load to the sea is riverine transport (HELCOM 2018)

Nitrogen cycling refers here to the transformation process between different inorganic nitrogen species, through nitrification, denitrification and bacterial N fixation (Duff and Triska, 2000). Nitrification is when ammonium is oxidized into nitrate, which is an energy-yielding process that is catalyzed by chemolithotrophic nitrifying bacteria. Denitrification occurs in anoxic conditions and reduces nitrate into nitrite, nitrous oxide, and nitrogen gas, and the process is catalysed by specific denitrifying bacteria that derive most of their energy from degradation and use nitrate or nitrite as an electron acceptor. As described in previous paragraphs, the HZ is an important environment for nitrogen cycling due to its steep oxygen gradients and diverse microbial community. Depending on whether denitrification or nitrification dominates, the HZ can function as both a sink and a source of surface water nitrogen (Jones and Holmes, 1996, Zarnetske et al., 2011, Zarnetske et al., 2012). Hence, nitrification can be the dominating process in some streams (e.g., Jones et al., 1995, Holmes et al., 1996), but often the nitrification rate is relatively fast in comparison to the residence times in the HZ, and nitrate is an intermediate product subsequently reduced through denitrification (Jones and Holmes, 1996, Storey et al., 2004, Zarnetske et al., 2011). Therefore, when the sediments have relatively low permeability, when dissolved organic carbon is not the limiting factor and when the stream is the dominant source of nitrogen, the HZ is generally a nitrogen sink (Duff and Triska, 2000, Birgand et al., 2007). This was also concluded by a number of field studies at the catchment scale (Alexander et al., 2000, Peterson et al., 2001, Mulholland et al., 2008, Mulholland et al., 2009), and it is the benchmark of this thesis. The abovementioned field studies also observed differences in nitrogen removal related to watercourse size and concluded that small streams remove nitrogen more efficiently than larger rivers (removal in proportion to the nitrogen load). This is due to higher cumulative length, and generally higher connectivity with groundwater, indicated by the higher ratios between HEF rates and in in-stream discharge, in small streams compared to in large rivers (Lowe and Likens, 2005, Wollheim et al., 2006, Wondzell, 2011). Furthermore, the upstream position of small streams means they are the source of nitrogen for the downstream network, and that the condition in these streams can set the chemical signature of a full catchment (Lowe and Likens, 2005). However, large rivers can be a more important nitrogen sink in terms of absolute mass because of the possibly higher mass load in these streams and their downstream position in the stream network (Wollheim et al., 2006, Mulholland et al., 2008, Ensign and Doyle, 2006).

1.3 Degradation and restoration of streams and hyporheic zones

In pristine streams, that is streams that are not impacted by human activities, groundwater-surface water interactions in the HZ can largely affect the surface water quality within a catchment. However, accelerating exploitation of streams and rivers during the last century has led to the physical, chemical and biological degradation of streams and rivers and the loss of many natural functions (Ward et al., 2001, Newcomer Johnson et al., 2016). Most streams and rivers in the developed world have been geomorphologically simplified to reduce the risk of flooding and improve transportation of people and goods (Ward et al., 2001, Wohl et al., 2015). In agricultural areas, drainage systems have been installed and streams have been channelized, with the purpose of lowering groundwater levels and increasing the area of arable land (Krug, 1993, Åkesson et al., 2016, Newcomer Johnson et al., 2016). These simplifications of stream geomorphology have resulted in a disconnection between streams and their adjacent streambeds and generally decreased in-stream residence times and nitrogen removal rates (Opdyke et al., 2006, Royer et al., 2006, Gooseff et al., 2007, Fehér et al., 2012). The eutrophication of both local streams and many large lakes and coastal areas around the world is probably caused predominately by nutrient enrichment originating from land-based activities such as agriculture and atmospheric deposition (Schindler, 1974, Howarth, 2014, EEA, 2019). However, the problem has likely been amplified by the degradation of the streams' self-cleaning capacity (Hancock, 2002).

Because of the abovementioned problems, several international directives and policies have been implemented to protect our waterbodies. For example, according to the European Union water framework directive (WFD) (2000/50/EC), all waterbodies in Europe should be in good ecological and chemical status before 2015, a deadline that have now been extended to 2027. The WFD has been successful in reducing point source chemical pollution, and monitoring has indicated that nitrogen concentration in European rivers generally decreased between 1982 and 2018 (EEA, 2022). However, as of 2018, only approximately half of EU water bodies were in good status (EEA, 2018). Generally, surface water bodies (rivers, lakes, transitional and coastal waters) are in worse shape than groundwater bodies, and hydromorphological pressures and diffuse sources (most often related to agricultural practices) have been identified as the most severe pressures, affecting 40% and 38% of all EU water bodies, respectively. Hydromorphological pressures include physical alteration of the channel geomorphology, streambed sediments properties or riparian zone conditions, and river restoration is proposed as a potential measure for reducing such pressures. The WFD is accompanied by the Nitrates Directive (ND), which requires EU member states to both identify waters affected and at risk of being affected by nitrate pollution and develop action programs designed to reduce and prevent nitrates pollution. However, stream restoration is not mentioned specifically as a way of reaching this goal. Furthermore, several more localized initiatives exist. For

example, the countries within the catchment of the Baltic Sea have agreed on the Baltic Sea Action Plan (BSAP). It has the goal of eliminating eutrophication of the Baltic Sea by 2030, which is defined as a total maximum nitrate input to the Baltic Sea of 792,209 tonnes per year. HELCOM has acknowledged that agricultural practices represents the main part of the diffuse sources of nitrate exported to the Baltic Sea (HELCOM, 2021). One of several actions suggested against eutrophication is the application of innovative water management measures where appropriate and different types of stream restoration measures and implementation of wetlands are mentioned as examples.

River and stream restoration includes a variety of actions that enhance river processes or forms and addresses the improvements of the ecological, physical or chemical conditions of a local watercourse and downstream recipients. Restoration goals vary largely between projects and includes improvements in, e.g., fish habitats and passage, in-stream habitat of other specific species, river connectivity (longitudinal, with flood plains and with the HZ), bank stability and river esthetics (Bernhardt et al., 2005, Wohl et al., 2015). Furthermore, one of the most common restoration goals today, which is of increasing importance, is the improvement of water quality (Wohl et al., 2015, Newcomer Johnson et al., 2016, Lammers and Bledsoe, 2017). The HZ is known to impact stream water quality, but its functions have rarely been mentioned as a specific objective of stream restoration (Hester and Gooseff, 2010). Even in cases where the HZ is mentioned as an important ecotone, specific guidelines for how to modify the HEF are often lacking, although this is slowly changing (Berg et al., 2014). Generally, the HEF can be amplified in three ways through engineering practices: 1) modifying the hydraulic head variations at the streambed interface, 2) changing the streambed surface area (i.e. stream width and length) and 3) changing the hydraulic conductivity of the streambed (Hester and Gooseff, 2011). Specifically the first of these practices motivated the research performed in this thesis, which focused on how hydraulic head variations at the stream interface control HEF, and on how stream restoration measures can affect the hydraulic head variations and thus the solute transport at the reach and stream network scale. Restoration measures that modify the stream geomorphology and water surface profile include artificial riffle and pool structures, cross-vanes, boulder weirs and log dams (Kasahara and Hill, 2006, Hester and Doyle, 2008, Lautz and Fanelli, 2008, Gordon et al., 2013, Rana et al., 2017).

Stream restoration that aims to improve water quality has fast increased in numbers; however, in reality, improvements are uncertain, and their effects are lagging in time (Melland et al., 2018, Chen et al., 2021, Fisher et al., 2021). Most restoration projects lack long-term monitoring data, which complicates the evaluation of projects and designs at the relevant scales (Newcomer Johnson et al., 2016, Lammers and Bledsoe, 2017). Specifically, stream restoration projects are often implemented at the stream reach scale, while the resulting water quality is

monitored at the stream catchment outlet (Wohl et al., 2015). Modelling and field studies have concluded that stream restoration that modifies the HEF needs to be implemented across long watercourses to be effective (Azinheira et al., 2014, Hester et al., 2016, Thompson et al., 2018). Thus, it is important to position stream restorations in locations with high potential for HEF or in areas within the catchment where most nitrogen is loaded to the surface water (Refsgaard et al., 2019, Magliozzi et al., 2019). Furthermore, stream restoration measures should be designed to be most effective at times when the nitrogen load to the stream is the largest. This becomes complicated because the correlation between discharge and nitrogen load as well as discharge and HEF are not yet fully understood. The nitrogen load has been shown to increase with high discharge due to increasing nitrogen mobilization but also to decrease with high discharge due to dilution effects (Royer et al., 2006, Minaudo et al., 2019). Similarly, hyporheic fluxes have both been shown to increase and decrease with stream discharge, since the discharge impact the different physical controls of HEF differently (Ward et al., 2019). The temporal and spatial variation in both HEF and nitrogen load emphasize the importance of understanding the functions of the stream prior to restoration (Ward et al., 2001, Dufour and Piégay, 2009). For example, stream restoration measures have increased the static head-induced HEF while simultaneously decreasing the dynamic head-driven HEF, consequently resulting in minor changes in the total HEF and stream water quality (Mason et al., 2012, Rana et al., 2017). Furthermore, an understanding of how and where HEF influences groundwater flow properties, such as the exact position of discharge and transport rates through the upper streambed sediments, is needed to position stream restoration measures correctly (Mojarrad, 2021). This motivates further research on how to generalize the HEF at the catchment scale from common stream and catchment characteristics. Such generalizations do exist, but the complexity of the HEF and its high variability in both time and space have complicated the use of scaling models for predictive purposes at the catchment scale and more research is needed.

1.4 Objectives and scope of the thesis

The first aim of this thesis was to advance the understanding of the primary physical controls of HEFs at different spatial scales and to investigate how HEFs influence solute transport in local stream reaches and surface water networks. Therefore, the consistencies and deviations between two common approaches for estimating HEF was investigated. The two approaches were: 1) to assess HEF inductively from tracer tests using a transport model and 2) to estimate HEF deductively by developing a 2D multiscale mechanical model. A possible consistency between models would provide means for upscaling of sub-reach processes to the reach scale and for parameterization of transport models. The second aim of this thesis was to investigate whether and how nitrogen removal can be enhanced by stream restoration that modifies stream hydromorphology and

alters the HEF. This was done by deriving exact solutions to the nitrogen transport and subsequently aggregating these at the stream network scale. Specifically, the thesis was based on four separate but interlinked studies, with the objectives as stated below:

- The objective of **Paper I** was to formulate remediation targets for stream restoration in the form of exact solutions for mass removal in the HZ. A second aim of the paper was to evaluate the effect of stream restoration in a specific stream, using the derived equations parameterized through in-stream tracer tests, and to compare different ways to utilize the available hydraulic head drop along a stream reach to control the HEF velocity across the streambed-water interface.

- In **Paper II**, the linkages between streambed geomorphology and the parameters quantifying HEF were examined through a cross-validation between two approaches commonly used for estimating HEF, as described in the paragraph above. The paper included the performance of in-stream tracer tests and topographical and geological surveying of ten small stream reaches with varying characteristics. Furthermore, the paper investigated the relative importance of different spatial scales of stream topography as well as static and dynamic hydraulic head drivers on the reach average HEF velocity.

- The objective of **Paper III** was to use the modelling framework defined in Paper I to evaluate the current nitrogen removal in the HZ, as well as the potential for stream restoration to increase nitrogen removal, at the national scale. The paper also included modelling of a few simple restoration measures in a local reach, with the intent of examining the practical potential of stream restoration, in comparison to the theoretical potential, which was evaluated at the national scale.

- In **Paper IV**, the linkage between stream hydromorphology and HEF was utilized to map the HEF velocity along the stream network of five different catchments with varying hydromorphologic characteristics. In addition to illustrating the possible variation in HEF velocity within and between catchments, this paper aimed to investigate how the HEF is controlled by catchment and stream reach hydromorpholigic characteristics at different spatial scales and to understand the type of conditions under which the HEF can impact upwelling groundwater flow patterns and transport rates.

1.5 Thesis limitations

The results of this thesis are limited in a number of ways, related both to the modeling framework, and to the data used to calibrate and parameterize the used

models. Firstly, there is an underlying assumption of steady state within the timeframe of the field measurements, which had to be made to evaluate the performed tracer tests in the proposed way. Therefore, bank storage driven by temporal discharge fluctuations were not considered in this thesis. Secondly, this thesis mainly considers small watercourses with relatively low discharge and shallow depth, and the results will not be transferable directly to HEF in large rivers. The focus on small streams is because these are thought to be more important nitrogen sinks than large rivers (see section 1.2) and because restoring small streams are more practical and easier than restoring large rivers. Furthermore, the high accumulative length and the upstream position of small streams means they can set the chemical signature of a full catchment. However, the characteristics of the streams where field measurements were performed also assets a limitation on the results. In addition to being small, with relatively low discharge and shallow depth, the investigated stream reaches were also relatively straight and therefore, lateral HEFs through meander bends are not investigated as part of this thesis. Instead, the thesis focused on multiscale vertical HEFs driven by longitudinal head fluctuations at the streambed interface, often referred to as pumping. Thirdly, a major limitation of the reactive modelling results are the underlying assumptions that the HZ is a nitrogen sink; that nitrogen reaches the stream water mainly as nitrate or nitrite; that denitrification is the predominant process controlling the mass removal; and that first order reactive modelling can capture the essentialness of the removal. It should also be noted that stream restoration in the context of this thesis only refers to enhancement of the water quality, and that it was referred to as stream remediation in Paper I. Finally, groundwater discharge is accounted for in a simplistic way in this thesis. In Paper II, the groundwater flow was quantified as a dilution factor, and in the studies investigating the impacts of stream restoration on nitrogen mass removal (Papers I and III), neutral conditions were assumed (neither groundwater discharge nor recharge). Although the interactions between groundwater flow and HEF is the focus of Paper IV, the models for these two flows were completely separated so that the constraining impact that groundwater discharge can have on HEF was not accounted for. Furthermore, the parts of the stream network where groundwater was recharging at the streambed was not included in the investigation.

2 THEORY ON HYPORHEIC FLOW MODELLING

This thesis studies the transport of fluids in open channels and porous media, and a modeling framework was established to mechanistically represent the local HEF and its impact on 1D longitudinal solute transport. A large part of the thesis is focused on the technical aspect of how HEF is quantified in this modelling framework. Generally, existing models for HEF can be divided into two groups that are based on two fundamentally different approaches (Packman and Bencala, 2000, Boano et al., 2014, Cardenas, 2015). The first approach uses breakthrough curves from in-stream tracer tests to calibrate longitudinal transport models,

resulting in induced parameter values of the flow across the streambed interface. The second approach uses mechanistic groundwater models with varying complexity to deduce parameters quantifying hyporheic flow. In this thesis, both approaches are applied and combined to obtain a more holistic picture of the effect of HEF on solute transport in streams. In sections 2.1 and 2.2, a theoretical background of both methods will be presented, including examples of previously developed models. In addition, section 2.3 provides a theoretical background on the modelling of reactive solute transport in streams, mainly focusing on the transport of nitrogen removal through denitrification. Throughout this section, as well as the rest of this thesis, SI-units will be used when introducing new model parameters.

2.1 In-stream solute transport modelling

The first approach for modelling the HEF is an inductive approach, which looks at the HEF from the perspective of the transport of solutes in the surface water. HEF variables are estimated by calibration of differential equations, commonly referred to as the transport equations, using break-through curves from in-stream tracer tests. Tracer tests provide a unique way to measure the combined effects of all transport pathways and mechanisms that occur between two sampling points; and relate the longitudinal transport and the solute spread to specific transport mechanisms. The methodology essentially consists of the injection of a traceable solute in the stream or river and the measurement of breakthrough curves (concentration over time) at one or several positions downstream of the injection point (e.g., Kilpatrick and Wilson, 1989). The measured input signal, i.e. the concentration at the injection point, and the downstream breakthrough curves can then be used to calibrate the transport model. This section introduces the transport equations as well as different ways of accounting for HEF in such models; the tracer tests performed as part of this thesis are described in the methods section 3.2.1.

2.1.1 The transport equation

To derive the transport equation, the eulerian view of motion is used, in which fluid is considered a continuum and observed within a fixed frame in space, a so-called control volume. The Reynolds transport theorem is used to apply physical laws to a fluid flowing through such a control volume (Chow et al., 1988). The theorem defines two types of fluid properties, where the first is the extensive property (B), which is dependent on the mass of the studied system (M), and the second is the intensive property (β), which is defined according to $\beta = dB/dM$. In words, the Reynolds theorem states that the total rate of change of an extensive property with time (dB/dt), is equal to (1) the total rate of change of the extensive property stored in the control volume (CV) and (2) the net outflow of the extensive property through the control surface (CS). When solute mass M (kg) is used as the

extensive property in the Reynolds transport theorem, the intensive property is one, and we obtain the continuity equation:

$$\frac{dM}{dt} = \frac{d}{dt}\left(\iiint_{CV} c d\forall\right) + \iint_{CS} \boldsymbol{J} \cdot d\boldsymbol{A} \quad (2.1)$$

in which $\frac{dM}{dt}$ (kg/s) is any source or sink of the solute, c (kg/m^3) is the solute concentration that varies in both time and space and $\mathrm{d}\forall$ (m^3) is a small part of the control volume. Further, $\boldsymbol{J}$ (kg/m^{2}s) is the flux of the fluid across a small area $\mathbf{dA}$ (m^2) of the control surface. By utilizing Gauss's divergence theorem to transform the surface integral into a volume integral, the continuity equation transforms into its differential form according to:

$$\frac{dM}{dt} = \frac{dc}{dt} + \nabla \cdot \boldsymbol{J} \quad (2.2)$$

where $\nabla = \left(\frac{\partial}{\partial x}, \frac{\partial}{\partial y}, \frac{\partial}{\partial z}\right)$ is the nabla operator. In this thesis, the solute transport is studied along the stream network (coordinate *x*) using the common 1D advection-dispersion equation (ADE), which is derived by double averaging Equation 2.2 over time as well as space (Fischer et al., 1979). The 1D ADE reads:

$$\frac{dC}{dt} + \boldsymbol{u}\frac{dC}{dx} + D_L\frac{d^2C}{dx^2} = \frac{P}{A}\boldsymbol{J_{CS}} + \frac{dM}{dt} \quad (2.3)$$

where C (kg/m^3) denotes the time and volume average solute concentration, $\mathbf{u}$ (m/s) is the cross-sectional average stream velocity in the x direction, D_L (m^2/s) is the dispersion coefficient, *P* (m) is the wet perimeter, *A* (m^2) is the stream cross-sectional area and $\boldsymbol{J_{CS}}$ (kg/m^{2}s) is the transversal flux over the permeable streambed surface. Equation 2.3 is valid when the studied solute is completely mixed over the cross section of the stream, and describes the downstream transport of the solute or contaminant pulse and the Gaussian, symmetrical spreading of this pulse (Fischer et al., 1979). The advective transport, which is the transference of a species or particle from one place to another with the bulk flow field, is represented by the second term of the left hand side of Equation 2.3. The solute spreading from high to low concentration, a process referred to as hydrodynamic dispersion, is represented by the third term. The spreading occurs due to three processes: molecular diffusion, turbulent diffusion and mechanical dispersion, which are lumped together since their effects are difficult to separate, and since they all have mathematical expressions analogous to Fick's law, i.e. they are proportional to the concentration gradient (e.g., Fischer et al., 1979). The transversal transport over the main channel boundary, i.e. the right hand side of Equation 2.3, results from deviations from the mean velocity and concentration caused by turbulent flow and variations in the longitudinal stream geomorphology. This flux can be diffusive, dispersive and advective and is of great importance in

natural streams, where it induces an exchange between the main channel and zones with stagnant or slow moving water. The parameterization of the term J_{CS} was studied thoroughly in this thesis and previous work related to this term is presented in the next section.

2.1.2 Transient storage and HEF in solute transport models

The importance of the transversal flux across the streambed in natural streams was first acknowledged because in-stream tracer tests resulted in skewed tracer breakthrough curves with a characteristic tail related to late time arriving solutes. Initially, tailings were attributed to exchange with stagnant surface water adjacent to the main stream, so called dead zones, and models that coupled two differential equations were developed to address this process (Hays, 1966, Thackston and Schnelle, 1970). However, Bencala and Walters (1983) emphasized that the observed tailings did not necessarily have to be flow through strictly dead zones within the open stream body, but any process that temporarily removed the tracer from the main stream and returned it again at a later time. They therefore introduced the concept of transient storage and recognized that the same equations as those used to describe the dead zone storage could describe this longitudinally distributed exchange process. They also presented the extensively used transient storage model (TSM), where the transversal flow is conceptually described as a first order mass transfer that is proportional to the difference in solute concentration in the main channel and the storage zone, which is described as a well mixed box.

Since the TSM was first introduced, it has been adapted in several ways to increase its physical realism and thereby its complexity (Knapp and Kelleher, 2020). Most often, the adaptations have considered how the transversal flux across the streambed, J_{CS}, is formulated. A number of models have separated the transient storage into multiple storage zones, for example letting one zone represent stagnant surface water and another the HZ (Choi et al., 2000, Briggs et al., 2009, Neilson et al., 2010a, Neilson et al., 2010b). Another approach has been to account for the multiscale aspects of transient storage by extending the solute residence times within the transient storage zone to a wider range. This has been done in the multi-rate mass transfer model (MRMT) by mathematically defining the flux across the streambed as a convolution between the in-stream concentration breakthrough and a memory function, whose derivative is proportional to the residence time distribution in the storage zone (Carrera et al., 1998, Haggerty et al., 2000). As described by Boano et al. (2014), a special case of the MRMT model is the advective storage path model (ASP) (Wörman et al., 2002), which specifies the transient storage as advective flow through the streambed sediments. Both the MRMT and the ASP are advantaged over the TSM since they provide flexible ways (higher degrees of freedom) of defining the residence time distribution compared to the TSM, which implicitly uses an exponential residence time distribution with only one distribution parameter. If an exponential residence time distribution is used in

the ASP model, it equals the TSM exactly (Wörman et al., 2002). However, skewed distributions such as the truncated power law distribution (Haggerty et al., 2000, Haggerty et al., 2002, Gooseff et al., 2003) or the log-normal distribution (Wörman et al., 2002) have been shown to accurately describe the late time behavior of in-stream tracer test breakthrough curves.

2.2 Hydromechanical subsurface flow modelling

The second approach for quantifying the HEF is deductive and includes the utilization of hydromechanical models. Such models are based on the physical principles of mass and momentum balances and solve the governing equations for groundwater flow at the stream-subsurface interface. Existing models are highly variable in terms of their conceptual setup and mathematical complexity but generally rely on the governing equations for groundwater flow. In this section, these equations are described for saturated, steady and isotropic conditions. Furthermore, ways to model the constraining streambed geology and the driving hydraulic head fluctuations at the streambed interface are described.

2.2.1 The governing equation for groundwater flow

Below streambeds, the groundwater flow of water is often assumed to be saturated and thus driven by gravity and commonly modelled using the empirical Darcy´s law. The law assumes that the flow is laminar and states that the specific discharge through a porous medium, often referred to as Darcy's velocity, is proportional to the gradient of the energy potential across the medium. The energy within the groundwater domain is quantified in terms of hydraulic head, and for inertia free flow, the velocity field in the streambed becomes:

$$\boldsymbol{q} = \boldsymbol{K}\nabla h(x,y) \tag{2.4}$$

where $\boldsymbol{q}$ (m/s) is the Darcy velocity vector, $\boldsymbol{K}$ (m/s) is the hydraulic conductivity vector and $h(x,y)$ (m) is the hydraulic head of the streambed. Furthermore, we know that for steady and incompressible flow the continuity equation (Equation 2.2) simplifies to:

$$\nabla \cdot \boldsymbol{q} = 0 \tag{2.5}$$

By substituting $\boldsymbol{q}$ in Equation 2.5 with Darcy's law, the groundwater equation for steady state flow through a saturated, anisotropic porous medium in two dimensions becomes:

$$\frac{\partial}{\partial x}\left(K_x \frac{\partial h}{\partial x}\right) + \frac{\partial}{\partial x}\left(K_y \frac{\partial h}{\partial y}\right) = 0 \tag{2.6}$$

where K_x (m/s) is the hydraulic conductivity in the x direction and K_y (m/s) is the hydraulic conductivity in the y direction. Isotropic conditions subsequently result in the two-dimensional Laplace equation for groundwater flow:

$$\frac{\partial^2 h}{\partial x^2} + \frac{\partial^2 h}{\partial y^2} = 0 \tag{2.7}$$

The groundwater flow equation as well as the Laplace equation can be analytically solved if certain types of boundary conditions are used. The following two sections (2.2.2-2.2.3) describes the upper hydraulic head boundary condition and how it commonly has been defined in HEF research.

2.2.2 Longitudinal pressure distributions at streambed interfaces

HEF modelling is distinguished from general groundwater flow modelling in the definition of the upper hydraulic head boundary condition, applied at the streambed-water interface. The energy content of open surface water consists of four parts: potential energy related to the elevation of the streambed; pressure energy related to the weight of the water; kinetic energy related to the movement of the water and internal energy coming from the viscous properties of the water and its interaction with the streambed and banks (Chow, 1959). The gradient of this energy in the direction of the flow is referred to as the energy grade line, which always has a negative slope in the direction of flow and drives the longitudinal flow of water in the stream. It is the projection of the total energy of the water column at the streambed that causes the pressure gradients assumed to drive the main part of the HEF. At the streambed, if assuming no slip conditions, the velocity head is zero, and the energy thus consists only of the streambed elevation and the pressure head, which can be divided into two parts. The first part is the static pressure head, which is the weight of water at the streambed and thus equal to the stream depth. The second part is the dynamic pressure head, which is the transformation of the kinetic energy of the flowing water into pressure and occurs when flowing water interacts with the streambed. The high computational power now available allows for highly detailed numerical models that describe the spatially- and time-varying surface water flow through Naiver-Stokes equations and the resulting (dynamic and static) pressure distribution at the streambed interface (e.g, Cardenas and Wilson, 2007, Janssen et al., 2012, Ren et al., 2019, Betterle et al., 2021). These models can also account for HEF driven by turbulence, which can be an important process, specifically in high velocity, plane-bed streams with course streambed material (Packman et al., 2004, Voermans et al., 2017, Grant et al., 2018, Voermans et al., 2018). The drawback of these complex models is that they depend on high quality and dense input data in terms of stream geomorphology. Furthermore, for generalizing the results from a specific study, analytical models or simplified numerical models might be preferred over complex numerical solutions. Therefore, throughout the history of hyporheic exchange research, most existing models have used simplified expressions to account for the upper hydraulic head

boundary condition and focused mainly on the pressure-driven, advective flow through the HZ, which is referred to as advective pumping. In this thesis, these simplified equations are used but extended by accounting for the multiscale distribution of the pressure head along the streambed and including the static as well as the dynamic head, which will be described in more detail below.

2.2.2.1. Static head driven hyporheic exchange flow

In gradually varying flow, changes in the flow depth in the direction of the bulk movement are minor, and the hydrostatic law of pressure distribution applies (Chow, 1959). The law states that the vertical pressure distribution over the cross-section is close to static, and the total energy fluctuations along the stream, relative to a specific datum, are exactly defined by variations in the water surface profile. This has been utilized in several models for HEF. Early studies by Vaux (1962) and Vaux (1968) approximated changes in the total energy line with the surface water profile in a small gravel bottomed stream with riffle pool geomorphology. Vaux concluded that the water is upwelling where the profile is concave and downwelling at sites where the stream water profile is convex. A few decades later, Harvey and Bencala (1993) identified flow paths through the HZ of a mountain stream in Colorado and related the flow to breaks in the water surface profile and the streambed. Later research also verified that the water surface elevation is a good approximation for the total hydraulic head at the streambed interface and that it can be used to model the main part of the HEF (Anderson et al., 2005, Gooseff et al., 2007). As an alternative to measuring the stream bottom elevation and depth, hydraulic routing of the water surface profile can be used to examine the static hydraulic head at the streambed (e.g., Saenger et al., 2005, Hester and Doyle, 2008, Marzadri et al., 2014). In this thesis, both measurements and hydraulic routing was performed to quantify the static head fluctuation at the streambed, as described in section 3.4.2.

2.2.2.2. Dynamic head-driven hyporheic exchange flow

When studying the hydraulic conditions in rivers, or the longitudinal transport of solutes therein, it is often suitable to treat the flow as gradually varying over the main part of the reach. However, it is also known that natural stream flow often varies rapidly over short distances. This causes deviations around the hydrostatic pressure that in some conditions can be substantial. Compared to static head variations, dynamic pressure fluctuations generally occur across smaller spatial scales that are important to consider when modelling HEFs (e.g., Stonedahl et al., 2013, Gomez-Velez and Harvey, 2014). Specifically, the head gradients occurring across small roughness features due to drag and lift forces created by flow deflections have been acknowledged as important drivers of HEF. In early studies, it was shown that head pressure distributions over dune-like bedforms had an approximate shape of a sinusoidal wave, with wavelengths equal to the length of the bedforms (Savant et al., 1987, Elliott and Brooks, 1997a, Elliott and Brooks,

1997b). Drag forces at the stream bottom, induced by triangular bedforms, were therefore modelled as a single sine curve, whose amplitude was related to the bedform height and streamflow properties. The model was parameterized by combining theoretical knowledge on the drag force coefficient and empirical results of head measurements over triangular bedforms (Fehlman, 1985). The parameterization resulted in an expression of dynamic head h_d at the streambed-water interface ($y = 0$) according to:

$$h_d(x, y = 0) = C_d H \sin\left(\frac{2\pi}{\lambda} x\right) \tag{2.8}$$

where H (m) is the bedform height, λ (m) is the wavelength of the hydraulic head fluctuations, equal to the wavelength of the bedform and the so called Fehlmans constant C_d (-) is estimated as:

$$C_d = 0.28 \frac{U^2}{2gH} \begin{cases} \left(\frac{H/d}{0.34}\right)^{\frac{3}{8}} & H/d \leq 0.34 \\ \left(\frac{H/d}{0.34}\right)^{\frac{3}{2}} & H/d \geq 0.34 \end{cases} \tag{2.9}$$

where d (m) is the average stream depth, U (m/s) the average longitudinal stream velocity and g (m/s^2) is the gravitational acceleration. This idealization of hydrodynamic head across the bedforms was then used as the boundary condition at the streambed interface, to solve the groundwater flow equation (Equation 2.6), resulting in the advection pumping model (APM). Since its development, the APM has been widely used and extended to account for effects of, e.g., a limited HZ depth, groundwater discharge, unsteady flow conditions, and the transport and fate of contaminants and small particles in the HZ (e.g., Packman et al., 2000, Cardenas and Wilson, 2004, Wörman et al., 2006, Boano et al., 2009, Bottacin-Busolin and Marion, 2010, Grant et al., 2014, Azizian et al., 2015, Caruso et al., 2016).

2.2.3 Multiscale hyporheic exchange flow and fractality

The multiscale nature of groundwater flow and HEF has long been recognized and linked to the multiscale topography of the landscape and streambeds (e.g., Tóth, 1963, Winter et al., 1998). Modelers have considered this multiscale behavioral, and extended the original APM for utilization in streams with more complex streambed geomorphologies than triangular bedforms (Wörman et al., 2006, Stonedahl et al., 2010, Marzadri et al., 2014, Mojarrad et al., 2019). These extended models are all based on superposition principles, which apply to both the hydraulic head distribution within the streambed and the final velocity fields, since they are both linear properties. Specifically, the HEF is calculated over a wide range of spatial and temporal scales by defining the upper hydraulic head boundary condition, $h(x, y = 0)$, as a Fourier sum acting on a flat surface. This can be done in two dimensions to represent the effect of the 2D landscape topography on the 3D

subsurface flow (Wörman et al., 2006), but here, the simpler 1D boundary condition is applied to calculate the 2D HEF along the stream network. The boundary condition applies:

$$h(x, y = 0) = \sum_{i=1}^{N} A_{h,i} \sin\left(\frac{2\pi}{\lambda_i} x\right) + S \quad (2.10)$$

where $A_{h,i}$ (m) is the amplitude and λ_i (m) is the wavelength of the hydraulic head harmonic i, and S (-) is the average slope of the hydraulic head, equal to the slope of the stream. The more harmonics that are added to the sum, the better the equation will mimic the real hydraulic head fluctuations at the streambed interface. If Equation 2.10 is substituted into the steady state groundwater equation (Equation 2.6), the pour velocity flow field in the HZ can be derived according to:

$$V_x(x, y) = \sum_{i=1}^{N} \frac{2\pi K}{\eta} \frac{A_{h,i}}{\lambda_i} \cos\left(\frac{2\pi}{\lambda_i} x\right) \alpha(\lambda_i) + KS \quad (2.11a)$$

$$V_y(x, y) = \sum_{i=1}^{N} \frac{2\pi K}{\eta} \frac{A_{h,i}}{\lambda_i} \sin\left(\frac{2\pi}{\lambda_i} x\right) \alpha(\lambda_i) \quad (2.11b)$$

where V_x (m/s) is the horizontal velocity component, V_y (m/s) is the vertical velocity component, η (-) is the streambed porosity and α (-) is a factor that accounts for the common decrease in velocity with depth in the HZ. The factor α originates from the lower boundary condition assumption, which will be discussed in more detail in the methods section 3.4.3, and K in Equation 2.11 represents either the hydraulic conductivity at $y = 0$, or the average hydraulic conductivity of the streambed depending on which expression for α that is used. The HEF velocity at the streambed interface can then be defined as the vertical velocity component at $y = 0$, according to $W(x) = V_y(x, y = 0)\eta\zeta$ (m/s), where ζ (-) is a constant referred to ass the area reduction factor and accounting for the fact that all streamlines do not enter the streambed perpendicular to the bed, (Wörman et al., 2002).

It is relatively simple to separate the hydraulic head fluctuations into static and dynamic components according to $A_{h,i} = A_{h,d,i} + A_{h,s,i}$, where $A_{h,d,i}$ (m) is the dynamic head amplitude and $A_{h,s,i}$ (m) is the static head amplitude. In some studies, the static head was only considered as an average slope, while the dynamic head was distributed across scales according to Equations 2.8 and 2.9 (e.g., Wörman et al., 2006), while in other studies, both the static and dynamic head distributions were defined over a spectrum of scales (Marzadri et al., 2014, Mojarrad et al., 2019). The dynamic head can be calculated for complex streambeds by defining the streambed topography as a Fourier sum according to $y_b = \sum_{i=1}^{N} A_{y_b,i} \sin\left(\frac{2\pi}{\lambda_i} x\right) + S$ and calculating the dynamic head amplitudes as $A_{h,d,i} = C_d(H = \sigma_{y_b}) A_{y_b,i}$, thus substituting the bedform height with the streambed

elevation standard deviation σ_{y_b} (m) (Elliott, 1990, Wörman et al., 2006). Similarly, in Stonedahl et al. (2010) the bedform height was estimated as $H = 2\sqrt{2}\sigma_{y_b}(x)$, to more exactly represent a sinusoidal topography.

Previous studies have also illustrated that power spectral analysis and fractal theory can be important tools for understanding the multiscale aspects of HEFs. It has been acknowledged that both landscapes and riverbed topographies often follow a fractal geometry (Hino, 1968, Rodríguez-Iturbe et al., 1992, Turcotte, 1992, Nikora et al., 1997). The concept of fractals means that although the topography can seem complex and chaotic, the signal is ordered when represented on a spectral form with a power-law distribution of amplitudes versus wavelength of the constituent signal harmonics. That is, if a property that varies longitudinally along the streambed is treated as a signal and is mathematically represented by a Fourier series, then there is a power-law relationship between the amplitude, and the wavelength according to:

$$A_{y_b} = a_f \lambda^{b_f} \tag{2.12}$$

where a_f and b_f are constants, and f defines the property of the signal. For streambed topography elevation, denoted y_b, scaling variable a_{y_b} reflects the size of the streambed geomorphologic features (length and height), while b_{y_b} reflects their roughness (Lee et al., 2020). Previous studies in flumes as well as natural streams have shown that b_{y_b} generally varies between 2 and 3 (Hino, 1968, Nikora et al., 1997, Wörman et al., 2007, Aubeneau et al., 2015). Wörman et al. (2007) also showed that fractal landscapes and streambed topographies result in fractal distributions of subsurface patterns of both large-scale groundwater flow and HEF. Subsequently, later research has shown that fractal streambeds produce fractal distributions of hyporheic residence times (Aubeneau et al., 2015), and that the constants a_{y_b} and b_{y_b} can function as scaling parameters of HEF, where generally the hyporheic flux increases with increasing a_{y_b} and decreases with increasing b_{y_b} (Marzadri et al., 2014, Lee et al., 2020).

2.3 Modelling nutrient cycling in streams

Solutes that are transported through streams and the HZ may also interact with the surrounding environment through chemical reactions. These reactions are species specific and can be reversible, solely causing retention of the solute, or irreversible, removing the species from the studied stream system. In addition to investigating the transport of conservative solutes, this thesis considers the fate and transport of nitrogen within streams. As described in the introduction, streams and rivers are generally thought of as nitrogen sinks, and the main removal process is thought to be denitrification.

The reactive solute transport in streams can be modelled by specifying the solute source or sink term of the ADE (Equation 2.3). The removal of nitrogen in streams is often assumed a first order reaction that is directly proportional to the nitrogen concentration in the steam water according to

$$\frac{dM}{dt} = \frac{dC\forall}{dt} = -R_{sys}C\forall \quad (2.13)$$

where R_{sys} (1/s) is the first order reaction rate of the stream system and $\forall$ (m^3) is the system volume. This system reaction rate can be related to other common measures of nutrient removal such as the uptake length, which is equal to U/R_{sys}, or the uptake per unit area, which is equal to $R_{sys}Cd$ (Newbold et al., 1982, Stream Solute Workshop, 1990) . However, none of these quantifiers of mass removal are specifying the exact processes through which the mass is removed and are often determined experimentally through reactive in-stream tracer tests (Mulholland et al., 2009, Lammers and Bledsoe, 2017). The drawback of Equation 2.13 and the system removal rate is that it does not distinguish between reactions in the main channel and reactions in the HZ, which for example is relevant when using models in stream restoration work. To specify such a distinction, previous studies have extended the TSM by accounting for first order removal also within the storage zone (Böhlke et al., 2004, Runkel, 2007, Böhlke et al., 2009, O'Connor et al., 2010, Harvey et al., 2013). By doing so, it can be shown that R_{sys} is the sum of the uptake rate in the main channel, R_{MC} (1/s), and an effective uptake rate of the storage zone, R_{HZ} (1/s), which depend both on the biogeochemical and hydraulic conditions of the storage zone (Runkel, 2007). Using first order kinetics to model denitrification in the HZ is legitimated if the conditions are nitrate limited, and controlling factors, such as the number of bacteria, temperature and the concentration of dissolved organic carbon are not varying with time (Pell and Wörman, 2008, Marzadri et al., 2011, Hester et al., 2016). Nevertheless, slightly more complex models have been developed by coupling HEF hydromechanical estimations with so-called Monod kinetics or the Michaelis–Menten equation, which are nonlinear, mathematical models for microbial growth and redox reactions (Boano et al., 2010, Marzadri et al., 2011, Azizian et al., 2015). These models acknowledged that nitrogen removal along hyporheic streamlines is strongly linked to the redox gradients observed within HZs (Triska et al., 1993, Zarnetske et al., 2011, Zarnetske et al., 2012). A simpler approach that also acknowledges this gradient was used by Gomez-Velez et al. (2015) when estimating nitrogen removal in the HZ of the full Mississippi River network. In their model, nitrification was not accounted for, but the nitrogen removal was specified to occur only at hyporheic travel times longer than a threshold time, τ_{oxy} (s). τ_{oxy} is the travel time along an hyporheic streamline, after which oxygen is reduced to a degree that denitrification becomes significant, and this time will hereafter be referred to as the oxygen consumption time.

3 METHODS

Both mathematical modelling and extensive field investigations were performed in this thesis to increase the mechanistic understanding of HEF, its primary physical controls, and its effect on solute transport at larger scales. Specifically, a modelling framework was established by combining a number of different analytical and semi-analytical models, which were partly developed in this thesis. This section describes the field sites were measurements and modelling were done; the performed field measurements and data processing; as well as some results that constitute important stream characterizing information. Furthermore, the development of the model framework is described here. First, the advective storage path model is described, including calibration towards tracer tests and sensitivity analysis of the model. Then, the derivation of a multiscale hydromechanical model for HEF is described, including how the estimation of the hydraulic head boundary condition at the water-streambed interface was done; how geological constraints was accounted for through the geological damping factor and how the hyporheic residence times were estimated differently in the different papers. Finally, this methodology section describes how stream hydraulic variables were estimated in non-gaughed streams; how regression analysis was performed to generalize results from the field measurements and extensive modelling; and how the potential for stream restoration to enhance nitrogen removal was estimated in this theses.

3.1 Field and modelling sites

This thesis mainly considers HEF processes in relatively small streams in Sweden. All field investigations (Papers I and II) were made at the reach scale, and reaches varied in length between approximately 200 m and 1500 m (Tables 1 and 2). In the models that were set up at the catchment scale (Papers III and IV), the stream network was also divided into stream reaches (sometimes referred to as segments) with assumed constant hydraulic and geomorphologic characteristics and without any tributaries. Compared to the large rivers of the world, the water courses of Sweden are generally shorter (interspersed with lakes) and have smaller catchment areas (Petersen et al., 1995). Here, the type of streams investigated were restricted further to streams of low discharge, shallow depth and relatively low slope, in part resulting from the need to conduct measurements through wading. However, focusing on small (low-order) streams is also desired since these streams have demonstrated their importance for the overall solute transport in catchments due to their relatively long accumulative lengths, high connectivity with the terrestrial environments and upstream catchment positions, as described more comprehensively in Section 1.3. Furthermore, the stream restoration designs that were considered in this thesis are not applicable for very large rivers.

In Paper I, measurements were performed in the catchment of Tullstorps Brook, which is a small stream draining an agricultural area located in Scania at the south

cost of Sweden that discharges into the Baltic Sea. The catchment has an area of 57 km^2, and the yearly mean discharge at the mouth of the catchment is approximately 0.74 m^3/s according to models by SMHI (Lindström et al., 2010). As in most catchments in Scania, and in other agricultural areas of Sweden, the stream network has been channelized and is partly buried in culverts to lower groundwater levels and increase agricultural capacity (Krug, 1993, Vought and Lacoursière, 2010). However, to improve water quality and limit flooding, a large part of the stream network has been restored in an extensive restoration project that started in 2009 and was still ongoing in 2022 (Tullstorpsån Ekonomisk Förening, 2022). Measurements were performed in four different reaches of Tullstorps Brook; two were defined as agricultural, one as natural and one as restored. These reaches are described in more detail in the appended Paper I. The discharge was low at the time of the measurements, never reaching above 0.05 m^3/s; the average water depth varied among reaches between 0.11 m and 0.28 m; and the slope was between 0.24% and 0.46%.

In Paper II, investigations were performed in a relatively large variety of stream types (compared to in Paper I) to draw more general conclusions. Tullstorps Brook was also included in Paper II, but only a shorter part of the reach was referred to as natural in Paper I. In addition, measurements were performed in reaches flowing through both agricultural land and mixed coniferous and deciduous forests, which varied in both stream discharge, slope and streambed material. The reaches were located in five different catchments (Figure 1). The discharge at the time of the measurements was relatively low and varied among reaches between 0.005 m^3/s and 0.11 m^3/s and stream depths between 0.12 and 0.56 m on average. A more thorough description of the reaches is found in the appended Paper II and summarized in Table 2.

Paper III aimed to estimate the current nitrogen removal and the potential of stream restoration to increase nitrogen removal in all agricultural streams of Sweden. The study included only agricultural ditches small enough for the implementation of restoration measures, with yearly average discharge less than 1 m3/s and agricultural N load of more than 0 kg/year according to the SVAR database (Lindström, 2010). Furthermore, a local scenario analysis of a number of restoration designs was performed in Malsta Brook, a reach which also was investigated in Paper II. The modelled reach was 240 m long, had an average gradient of 0.12%, and flowed through an agricultural landscape. Malsta Brook had an estimated yearly average discharge of 0.12 m3/s, but the model was calibrated for the low flow conditions observed and reported in Paper II.

Table 1. Characteristics of investigated stream reaches in Paper I including surrounding environment, geomorphology, in-stream vegetation, streambed material, stream length X, stream slope S, stream depth d and streambed hydraulic conductivity K, as well as the discharge at the time of the tracer test, Q0. (Modified from Paper I)

	Surrounding environment	Geomorphology and in stream vegetation	Stream-bed material	X (m)	S (%)	d (m)	K (m/s) †	Q0 (m3/s) §
Reach 1 – restored	Agriculture	Restored, meandering, riffle and pools, two step ditches, boulders and logs regularly at stream bottom, dense, submerged vegetation.	Sand and gravel. Clay in pools	520	0.31	0.28	1.1E-03	0.03
Reach 2 – agriculture	Agriculture	Straight, channelized, dense submerged vegetation.	Sand and gravel	1530	0.44	0.25	1.2E-03	0.03
Reach 3 – natural	Agriculture. Mixed forest closest to stream	Sinuous, riffle and pools.	Sand and gravel	480*	0.46	0.11	9.9E-04	0.05
Reach 4 – agriculture	Agriculture	Straight, channelized, dense submerged vegetation.	Sand and gravel	1430	0.24	0.24	7.7E-04	0.03

*The elevation survey was performed over 455 m of the reach. †Hydraulic conductivity just below the streambed interface (y=0). § Discharge estimated by SMHI using the HYPE model.

The main aim of Paper IV was to understand how the HEF velocity, the upwelling deep groundwater velocity, and the ratio between them vary within and between catchments and to determine which catchment and reach characteristics that control this variation. Therefore, five catchments were selected to represent a range of topographies, land uses and soil depths that are common in Sweden (Figure 1). The first three of the catchments of Paper II were also included in Paper IV (Tullstorps Brook, Bodals Brook and Säva Brook) because some prior knowledge about the stream network was considered valuable for the study. Furthermore, the Krycklan catchment, which is a well monitored study catchment (Laudon et al., 2013), was selected to represent the boreal landscapes and the relatively steep streams that are common in the northern parts of Sweden (Petersen et al., 1995). Finally, a subcatchment of the Forsmarks Brook watershed was selected to represent the low gradient, surface water systems that are heavily interspersed with lakes and wetlands, which are common in south-central Sweden (Petersen et al.,

1995). Forsmarks Brook was also interesting because of its location near the planned Swedish final disposal of high-level nuclear waste. A thorough description of the five catchments is found in the appended Paper IV.

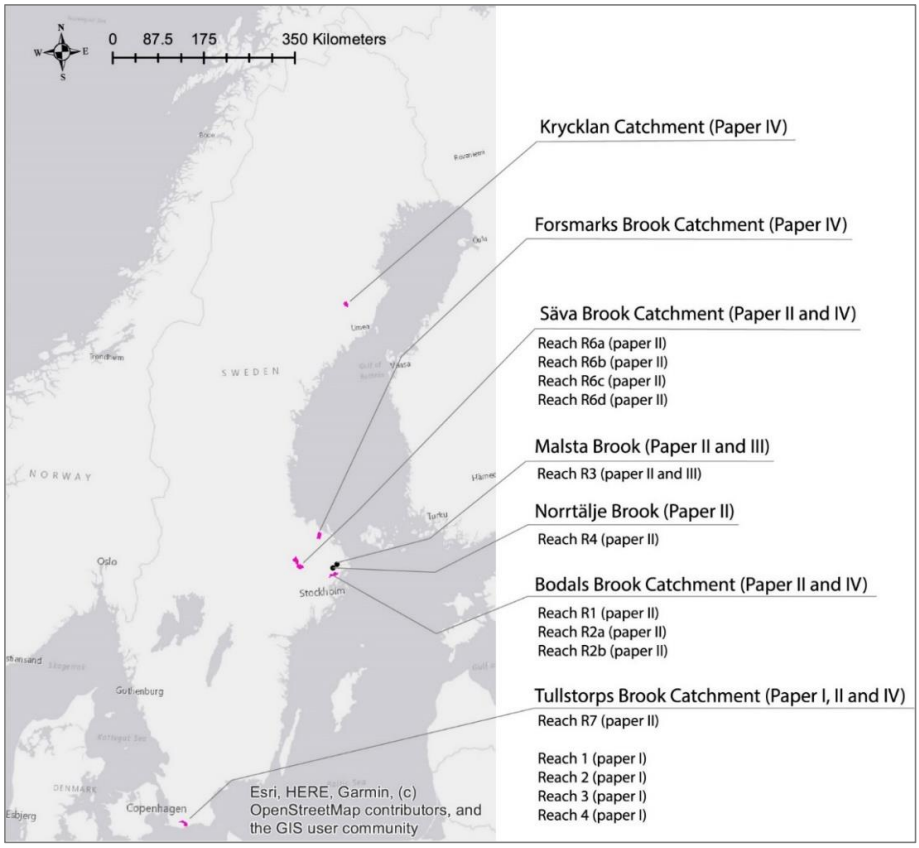

Figure 1. Overview of field sites including both locations of local stream reaches studied in Papers I, II and III, and the regional catchments studied in Paper IV.

Table 2. Characteristics of investigated stream reaches from the five catchments in Paper II, including surrounding environment, geomorphology, in-stream vegetation, streambed material, stream length *X*, stream slope *S,* stream depth *d* and streambed hydraulic conductivity *K*, as well as the discharge at the time of the tracer test, Q_0. (Modified from Paper II)

	Catchment	Surrounding environment	Geomorphology and in stream vegetation	Stream-bed material	X (m)	S (%)	d (m)	K (m/s)	Q_0 (m^3/s)
R1	Bodals Brook	Coniferous forest	Sinuous, riffle and pool with occasional cascades, pristine, perennial	Sand, gravel and stones	273	2.44	0.12	3.03E-04	0.006
R2a	Bodals Brook	Coniferous forest	Meandering, riffle and pool with occasional cascades, pristine, perennial	Sand, gravel and stones	338	1.66	0.14	3.36E-04	0.005
R2b	Bodals Brook	Mixed forest	Straight, riffle and pool, pristine	Sand	288	0.09	0.19	3.37E-04	0.005
R3 *	Malsta Brook	Agriculture	Straight, partly channelized with stone walls, occasional steps	Sand and gravel, clay in pools	197	0.12	0.2	3.55E-04	0.005
R4	Norrtälje Brook	Agriculture. Mixed forest closest to stream	Sinuous, flat bottom, partly channelized with stone walls	Sand and gravel	578	0.29	0.45	4.72E-04	0.109
R6a	Säva Brook	Coniferous forest	Straight, riffle and pool, pristine.	Sand and gravel	386	0.26	0.18	5.44E-04	0.003
R6b	Säva Brook	Agriculture	Sinuous. Partly dense submerged vegetation.	Sand and gravel, clay in pools	495	0.004	0.34	5.76E-04	0.012
R6c	Säva Brook	Agriculture. Mixed forest closest to stream	Straight. Pristine.	Sand, gravel and stones, clay in pools	226	0.43	0.34	5.13E-04	0.065
R6d	Säva Brook	Agriculture	Straight, channelized, partly dense vegetation	Clay and sand	208	0.08	0.56	6.86E-04	0.099
R7	Tulls-torps Brook	Agriculture. Mixed forest closest to stream	Straight, riffle and pool.	Sand and gravel	204	0.49	0.18	9.9E-04	0.041

*A longer reach of Malsta Brook, including R3, was surveyed and modelled in HEC-RAS as part of Paper III.

3.2 Field measurements and data processing

3.2.1 In-stream tracer tests

Tracer tests were conducted to obtain an integrated measure of HEF within the investigated reaches of Papers I and II and to parameterize the transport equations that will be described in detail in Section 3.3. The same experimental design was used in all conducted tracer tests. The fluorescent rhodamine WT (RWT) was injected directly into the stream water column through a slug injection, and a break through curve (BTC) was measured upstream as well as downstream of each investigated stream reach using in-situ submersible fluorimeters (Cyclops C7, Turner Designs, Inc., U.S.A.). The injection was made at a distance upstream from the first measured BTC that assured complete mixing within the cross section, which was essential in order to use the measurements to calibrate longitudinal, cross-section averaged, transport models (Kilpatrick and Wilson, 1989). The fluorimeters were also left in the stream long enough to capture the characteristic BTC tails, created when parts of the solute are retained in slow moving zones and thus arriving to the measuring point considerably later than the bulk of the solute (Haggerty et al., 2000, Haggerty et al., 2002, Wörman and Wachniew, 2007, Bottacin-Busolin et al., 2011, Drummond et al., 2012). The used fluorimeters measured the electric potential of the emitted fluorescence in mV and measurements were subsequently transformed into the concentration of RWT by creating a standard calibration curve using water from the stream. An example of a calibration curve and RWT concentration BTC, from a test performed in Malsta Brook, is presented in Figure 2. Detailed information about the tracer tests can be found in the appended Papers I and II.

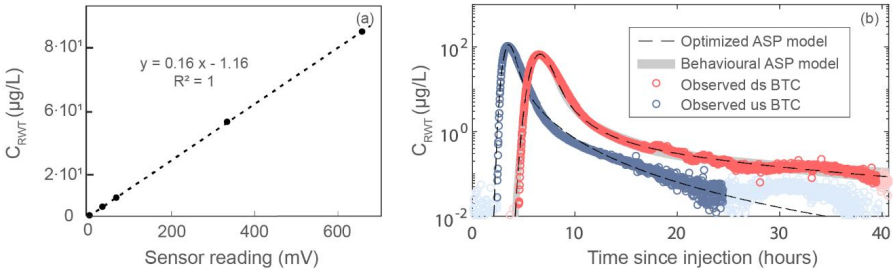

Figure 2. Example of tracer test data from Malsta Brook (reach R3 in Paper II), including a) a standard calibration curve linking the fluorimeter reading in mV to Rhodamine WT (RWT) concentration in µg/L; and b) the resulting upstream (us) and downstream (ds) observed break through curve (BTC) in µg/L, as well as the best (optimized) advective storage path (ASP) model of the us and ds BTC, and all the behavioral models of the ds BTC.

3.2.2 Hydraulic conductivity

The average hydraulic conductivity, K (m/s), was estimated in all investigated stream reaches through distributed in-situ falling head tests using a device referred to as a piezometer. The test was conducted by filling the piezometer with water and then allowing it to infiltrate into the streambed under constant hydraulic pressure while the pace at which the piezometer emptied was registered. The hydraulic conductivity was subsequently evaluated using the theory of Hvorslev (1951), which is described in more detail in Paper II. Hydraulic conductivity was measured with the piezometer at 3 and 7 cm depths, at 4 to 6 points in each cross-section, located approximately every 50-100 m along the reaches. In Paper I, the average hydraulic conductivity in all measuring points at each depth (3 and 7 cm) was used to parameterize a decay function for hydraulic conductivity, which is described in Section 3.4.3. In Paper II, isotropic hydraulic conductivity was assumed for the streambeds and the average of all hydraulic conductivity measurements was taken to parametrize the models used.

In the national investigation performed in Paper III, the hydraulic conductivity of the streambed was assumed to be 10^{-4} m/s everywhere. In Paper IV, where more detailed data were available, the geographically distributed hydraulic conductivity of the topsoils of the five catchments was estimated by correlating the Swedish soil map provided by ©Sveriges geologiska undersökning (SGU) to specific values of hydraulic conductivity taken from the literature. The hydraulic conductivity was then assumed to decay from 10^{-4} m/s at the streambed interface to the average hydraulic conductivity of the surrounding (underlying) soil. A hydraulic conductivity of 10^{-4} m/s was assumed based on the measurements of both this thesis (Table 1 and Table 2), and other studies (Riml et al., 2013, Stewardson et al., 2016, Ward et al., 2019).

3.2.3 Elevation surveying

Elevation surveys were performed in each of the investigated reaches to parameterize the developed mechanical model used to calculate the average exchange velocity across a multiscale streambed interface. All streambed elevation surveys were performed along the thalweg of the streams with a Leica Sprinter 50 automatic leveling instrument (Leica Geosystems AG, Switzerland), and a regular rod was used to measure the stream depth at the same point as the streambed elevation. The final elevation of the streambed had an instrumental accuracy of ± 2 mm, and the measurement of water surface elevations was estimated to have an accuracy of ± 7 mm, which was the sum of the instrumental accuracy and the ± 5 mm estimated uncertainty of the stream-depth measurements. In Paper I, the streambed elevation and stream depth were registered every 4-7 m. Since equal spacing was needed for the subsequent spectral analysis of the profiles, the profiles were interpolated to obtain an equal density of 2.45 m before analysis. In Paper II, measurements aimed for a distance between points of either 1 or 0.5 m. Since the

actual distances sometime differed from the predefined distances, those profiles were interpolated to a lag-distance between measured elevations between 0.23 m and 0.74 m, depending on the reach, before power spectral analysis was performed. The Leica Sprinter 50 automatic leveling instrument was also applied to measure the stream cross sections used as input in an HEC-RAS model that investigated the impact of stream restoration measures in Paper III (see Section 3.7.1)

3.2.4 Discharge and nitrogen load data

Information regarding the discharge for the entire stream network of Sweden was needed both to select relevant catchments within Paper III and IV, and to estimate the HEFs in the reaches within the selected catchments. Discharge in the outlet of all catchments of Sweden and the nitrogen load to each catchment was extracted from the Swedish Water Archive (SVAR). SVAR is an open-access database with information on Swedish hydrology, which divides the country into catchments and simulates runoff and nutrient transport in each catchment with the S-HYPE model (Lindström et al., 2010). The discharge out of each catchment and nitrogen load to each catchment were subsequently distributed per metre length of the stream network (Paper III) or for each pixel along the stream network (Paper IV). In Paper III, where network effects were accounted for, discharge and nitrogen load from upper catchments were added to the local discharge of each catchment.

3.2.5 Processing topography data

In Paper IV, no streambed or water surface elevation data were available, and a 2 m x 2 m digital elevation model (DEM) of the topography, provided by the Swedish mapping, cadastral and land registration authority (GSD-Elevation data, grid 2+, ©Lantmäteriet) was therefore processed to specify the longitudinal streambed elevation profiles for all of the investigated reaches. The DEM files were based on laser scanning of the topography surface, with >5 measuring points/m^2, which had horizontal and vertical accuracies of ±0.3 m and ±0.1 m, respectively. The geographical extension of the stream network within each of the five regional catchments was defined by calculating a flow accumulation raster from the DEM file and choosing a threshold accumulation area to only include streams with an annual mean low discharge of 0.5 L/s or more. After the stream network was defined, it was divided into stream reaches (sometimes referred to as segments), separated at the locations of stream junctions. However, only stream reaches with a length >50 m were included in the analysis. The longitudinal elevation was then extracted along all of the reaches.

The longitudinal elevation profiles were subsequently used both for parameterization of the HM model and for calculating a number of topographical indexes for each stream reach, later used in the regression analysis of Paper IV. Those indexes included the stream slope S (-) and the normalized standard deviation in stream slope σ_{z_b}/X (-), where X(m) is the length of the reach and σ_{z_b}

(m) is the standard deviation in streambed topography. Furthermore, these indexes included the median subcatchment area, MSC (m^2), which is the median of the local catchment area of each stream pixel upstream of the catchment or subcatchment outlet. In addition, the 2 m x 2 m DEM was also used to calculate a number of catchment average topographical indexes (see section 3.6). For each pixel of the DEM, the local catchment slope, S_{CM} (°), the gradient to stream GtS (-) and the elevation above stream EaS (m) were calculated. Subsequently, the average of S_{CM}, GtS, EaS and elevation, E (m), as well as the standard deviation in the elevation σ_{E} (m), were calculated for each catchment and subcatchments included in the study.

Elevation data provided by the Swedish mapping, cadastral and land registration authority were also used to calculate the average slope of each segment in the full stream network of Sweden (Paper III). However, a less dense DEM of 50 m x 50 m (GSD-Elevation data, grid 50+, ©Lantmäteriet) was used for this purpose.

3.3 The reactive advection storage path model

In this thesis, the ASP model (Wörman et al., 2002), was used to evaluate tracer tests and as a basis for deriving equations for nitrogen mass removal at the reach scale. The model was chosen because of how it couples the longitudinal solute transport in the stream with the advective transport of solutes along a continuous distribution of pathways within the HZ. Such a coupling was useful to investigate how changes in stream hydromorphology can affect the longitudinal transport of solutes in streams. The ASP-model, specified for nitrogen transport, is based on the general transport equation for solutes in streams, including a transversal flux across the streambed interface and first order mass removal in the main channel as well as the HZ (Equation 2.3 but with mass removal according to section 2.3). It reads:

$$\frac{dC}{dt} + \boldsymbol{u}\frac{dC}{dx} + D_L\frac{d^2C}{dx^2} = \frac{P}{A}J_{CS} - r_{MC}C \qquad (3.1)$$

where r_{MC} (1/s) is the mass removal rate in the main channel and C (kg/m^3) is the solute concentration in the stream water. In the ASP-model, the total transversal mass flux across the streambed interface, J_{CS}, is assumed to be due to advection only, thus excluding other processes such as turbulence or diffusion. It is parameterized by integrating the advective flux over a distribution of different pathways, defined as a continuous, flow-weighted residence time distribution, $f(T)$ where T (s) is the residence time along one streamline from entering to exiting the HZ. In Paper I, it was shown how the average could be calculated also by integration over the streambed length. The transformation between the spatial and time formulation was done by defining the flow-weighted residence time distribution as $f(T)dT = W(x)dx/(\langle W(x)\rangle X)$, where $W(x)$ (m/s) is the exchange velocity distributed spatially along the streambed, and X (m) is the length

of the full streambed. The squared brackets around $W(x)$ express the flow weighted average according to $\langle \dots \rangle = \int_0^\infty \dots f(T)dT$ and is a notation that will be used continuously throughout this thesis. This definition of $f(T)$ results in a hyporheic flux across the streambed interface according to:

$$J_{CS} = \frac{1}{2}\langle W(x)\rangle(-C(t) + \langle G(t,\tau)|_{\tau=T}\rangle) \quad (3.2)$$

where $G(t,\tau)|_{\tau=T}$ is the solute concentration when the pore water exits the HZ at residence time T. Furthermore, defining $f(T)$ as a function of the flow weighted average exchange velocity also leads to the expression:

$$\langle W(x)\rangle = \sqrt{\int_0^\infty \frac{W(x)^2}{X} dx} = \sigma_W \quad (3.3)$$

showing that the flow weighted average exchange velocity equals the standard deviation in the non-flow-weighted exchange velocity along the streambed, σ_W, (m/s). The derivations of Equations 3.2 and 3.3 are presented in detail in Paper I, and the equations constitute important stepping-stones for formally linking the longitudinal transport equations and the hydro mechanical model for the HEF that will be presented in Section 3.4. To specify the flow-weighted average of the solute concentration that exits the HZ at time t, i.e. $\langle G(t,\tau)|_{\tau=T}\rangle$, the flow along a single streamline in the HZ was defined in the ASP model as:

$$\frac{dG}{dt} + \frac{q_z}{\eta}\frac{dG}{dz} = -r_{HZ}G \quad (3.4)$$

where q_z is the Darcy velocity of a water parcel traveling within a stream tube with longitudinal coordinate z, η is the streambed porosity and r_{HZ} is the reaction rate along streamlines of the HZ (Wörman et al., 2002). Within this thesis, to account specifically for denitrification, two travel time ranges were specified along the hyporheic stream tubes, separated by the oxygen consumption time τ_{oxy} (s) (see section 2.3). For the travel time range $0 < \tau < \tau_{oxy}$, the reaction rate was set to zero, reflecting the oxygenated conditions that most likely occurs initially after the stream water has entered the HZ. As the water travels longer time within the HZ, one can assume that oxygen is consumed, leading to an oxygen depleted zone for travel times in the range $\tau_{oxy} < \tau < T$, where $r_{hz} \neq 0$. When evaluating RWT tracer tests (Paper I and II), both τ_{oxy} and r_{HZ} were set to zero, while when estimating the removal rate of nitrogen in the HZ (Papers I and III), r_{HZ} was specified to be denitrification only ($r_{HZ} = r_{den}$), and values of τ_{oxy} and r_{den} were estimated from the literature.

3.3.1 Solutions to the transport equation using the Laplace method

Several ways exist to solve the transport equation for solutes in streams, and in this thesis, exact solutions to Equations 3.1, 3.2 and 3.4 were either derived in the Laplace domain and then inversed numerically or solved analytically in the form of temporal moments. The governing equations for solute transport varied slightly between the three papers (I, II and III), but the final solutions are based on the same boundary and initial conditions. First, it was assumed that the solute entered the stream as an instantaneous mass pulse at time $t = 0$, defined by a Dirac delta pulse, $C(x = 0, t) = \frac{M_{inj}}{Q_0}\delta(t)$, where M_{inj} is the injected mass. Second, it was assumed that no solutes existed in the stream before that, i.e. $G(\tau, t = 0) = C(x, t = 0) = 0$ or at an infinite distance from the injection place, i.e. $C(x = \infty, t) = 0$. Finally, a boundary condition for the mass flux through the HZ was defined as: $G(\tau = 0, t) = C(x, t)$. In Papers I and III, the residence time distribution in the HZ was assumed exponential, since a one variable distribution was needed to find a closed form solution to the solute response. However, other types of residence time distributions have been shown to better represent the flow through the HZ. Therefore, in Paper II, I utilized the general solution presented by Wörman et al. (2002), which was derived for a conservative solute (i.e. $r_{MC} = r_{HZ} = \tau_{min} = K_{MC} = K_{HZ} = 0$), an arbitrary residence time distribution, dispersive flow in the main channel, and the same boundary conditions as in Paper I. The concentration in the stream was then calculated numerically, by assuming a log-normal residence time distribution.

3.3.2 Estimating the mass removal in stream reaches and networks

To quantify the effect of the transport of a solute through the HZ on the mass removal and retention at the reach scale, the zeroth temporal moments of the solute response were calculated, which is a common statistical measure used to characterize longitudinal solute transport (Gupta and Cvetkovic, 2000, Riml and Wörman, 2011, Schmid, 2003, Wörman et al., 2002). The temporal moment can be calculated directly from the Laplace transformed solutions of the solute transport equation, according to:

$$n_j = (-1)^j \frac{\partial^j \bar{f}(x,p)}{\partial p^j}\Big|_{p=0} \tag{3.5}$$

where $\bar{f}$ is the laplace transformed solution, p is the laplace variable and j is the order of the temporal moment. The zeroth temporal moment was used to derive the relative mass conservation along a stream reach according to $B = \frac{n_0}{M/Q}$, so that the mass removal along a stream reach, D (-), is:

$$D = 1 - \frac{n_0}{M/Q} \tag{3.6}$$

The derivation of the zeroth and first temporal moment of the solute concentration in the main channel (i.e. $\bar{f}(x,p) = \bar{C}(x,p)$) is found in the appended Paper I and in Morén et al., 2018. Furthermore, the final expressions for D (specified for nitrogen), with dispersion in the main channel (Paper I) and without dispersion (Paper III), are presented in the results section.

In addition to the relative mass removal, the absolute mass removal was estimated for all stream reaches in Sweden with a nitrogen load from agricultural sources and a discharge smaller than 1 m^3/s (Paper III). The absolute nitrogen mass removal within one of the reaches depends, apart from the relative mass removal (Equation 3.6), on the spatial distribution of the nitrogen load along the stream network (Riml and Wörman, 2011). The diffuse input of agricultural nitrogen to each reach was represented here by uniformly distributing the load to each regional catchment along the stream network of the catchment (see section 3.2.4). The path of downstream segments that water and mass followed to reach the final recipient was identified for each of the segments. The relative mass removal (of the mass loaded to segment i) along the full transport pathway from reach i to the recipient was subsequently denoted D^i and calculated according to:

$$D^i = \left(1 - B^i\right) = 1 - B_i \prod_{j=1}^{n} B_j \qquad (3.7)$$

where j is the number of reaches between reach i and the recipient, and B^i is the relative mass recovery along the full transport pathway from reach i to the recipient. Thus, the subscription index indicates the local mass removal and recovery of reach i, and the superscription index indicates the mass removal and recovery of the full transport pathway from reach i to the recipient. The absolute mass removal of the mass loaded to segment i, M_{in}^i (kg), was then calculated as $MR^i = M_{in}^i D^i = M_{in}^i\left(1 - B^i\right)$ (kg). Segments that represented lakes were excluded from the analysis by assuming a value of $B = 1$. The total agricultural N mass removal in small streams could then be calculated as the sum of mass removed in each of the separate segments.

3.3.3 Calibrating the advective storage path model

To quantify the variables of the ASP-model, it was calibrated to agree with the observed tracer breakthrough curves (Papers I and II). A formal parameter optimization was performed by minimizing the error between the observed tracer breakthrough curve and the numerical Laplace inversion of the calculated breakthrough. It was important that the minimized error emphasized the peak of the breakthrough as well as the tail, since the shape of the tail provides information regarding tracer flow through slow moving zones such as the HZ (e.g., Haggerty et al., 2002, Wörman and Wachniew, 2007). Therefore, before the error was calculated, the breakthrough curve concentration points were divided into two groups, where concentrations higher than 20% of the peak value were considered

the peak (group A) and concentrations lower than 20% of the peak were considered the tail (group B). To equally weight the contribution of the two parts of the dataset for the final error, the logarithmic form of the data in group B was used when the mean squared error was calculated according to:

$$e = min_e \left[\sqrt{\frac{1}{M_A+M_B}\left(\frac{\sum_{i=1}^{M_A}\left(C_{sim,A,i}-C_{obs,A,i}\right)^2}{\left(\max(C_{obs,A,i})-\min(C_{obs,A,i})\right)^2} + \frac{\sum_{i=1}^{M_A}\left(\log(C_{sim,B,i})-\log(C_{obs,B,i})\right)^2}{\left(\max(C_{obs,B,i})-\min(C_{obs,B,i})\right)^2} \right)} \right] \quad (3.8)$$

where M_A and M_B are the total number of observations in Groups A and B, respectively; C_{sim} is the simulated concentration (Laplace solution transformed back to the real domain); and C_{obs} is the observed concentration of each group (Bottacin-Busolin et al., 2011).

3.3.4 Sensitivity analysis

Even though it is satisfactory to arrive at a single set of variables describing the transport observed with a tracer test, it is also essential to report the uncertainties related to the estimated variables. In this thesis, the sensitivity of the model output to changes in the model parameters was investigated through a Monte-Carlo-based analysis of the parameter space (Papers I and II), in the line of several previous studies (Beven, 2006, Riml et al., 2013, Ward et al., 2017). The analysis was performed by modelling the BTC with a set of variables randomly sampled from predefined distributions and then comparing the simulated BTC with the observed BTC using equation 3.8. This was done more than 10000 times for each reach and tracer test. In Paper I, the uncertainty of all hydraulic variables U, D_L, $\langle W \rangle$ and $\langle T \rangle$ was investigated, while in Paper II, the velocity, U, was removed from the analysis because it was considered relatively certain. The uncertainty of the variables included in the Monte Carlo analysis was illustrated through so-called "dotty plots" (Figure 3), which is a projection of the multidimensional error with regard to one variable at the time. A dotty plot that forms a peaky minimum, indicates that the value provided by the formal optimization (if located at the minimum) is relatively certain since the error is sensitive to small changes in the value of this variable. In contrast, if the lowest values of the dotty plot are very wide, than the error is insensitive to changes in that variable, and the single value provided by the formal optimization is considered uncertain. To quantify the uncertainty illustrated through the dotty plots, an error limit, below which the relative parameter set was considered "behavioural", was stated. Behavioral variable sets were said to result in equally accurate simulations of the breakthrough curve. The range of each variable resulting in errors below the error limit was also reported as a substitute for a confidence interval, where a larger range was said to represent a more uncertain parameterization than a narrower range. The error limit was set to 50% of the lowest error in Paper I and 15% of the lowest error in Paper II (red markers in Figure 3). It should be noted that the choice of those limits was arbitrary, and

that the measure only allows for comparison between the reaches and variables estimated in this specific study.

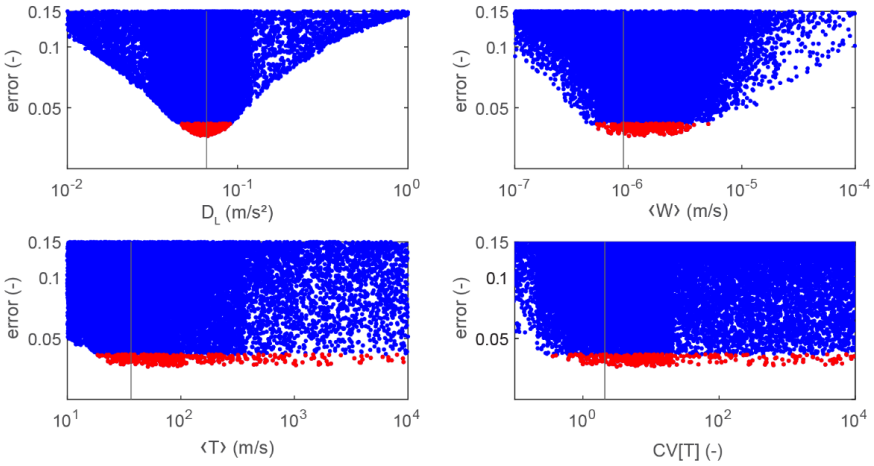

Figure 3. Dotty plots from Monte Carlo sensitivity analysis of the advective storage path (ASP) model calibrated using tracer test data from Malsta Brook (reach R3 of Paper II). Each dot represents a model run with randomly selected variables and the red dots represents behavioural models, with an error smaller than 15% of the minimal error. The vertical black line illustrates the parameter value from the formal optimization.

3.4 A hydromechanical model for hyporheic exchange flow

Streambed geomorphology has a documented major control on flow through the HZ and consequently on longitudinal solute transport in streams, and it is uniquely interesting from a stream restoration point of view since it can be engineered (see introduction section). A multiscale hydromechanical (HM) model was developed in this study to investigate how the streambed topography and changes in this topography influence the flow through the HZ. The model accounts for both static and dynamic head at the stream bottom and provides ways to decompose the flow along a reach for the two different drivers as well as for different spatial scales (wavelength). Scale decomposition was done by treating the upper hydraulic head boundary condition and the HEF across the streambed interface as spatial signals and analysing those signals using power spectral theory.

3.4.1 The flow-weighted average exchange velocity

The multiscale hydromechanical model was derived by acknowledging that the variance of any signal equals the integrated power spectral density (PSD) of the same signal according to:

$$\sigma_{f(x)}{}^2 = \int_{\lambda_{min}}^{\lambda_{max}} \frac{S_f(\lambda)}{\lambda^2} d\lambda \quad (3.9)$$

where $\sigma_{f(x)}{}^2$ is the variance of an arbitrary signal f and $S_f(\lambda)$ is the power spectral density (PSD) of that signal, which is a function of the wavelength λ (m), ranging between a minimum of λ_{min} (m) and a maximum of λ_{max} (m). Furthermore, in Paper I, it was shown that the flow weighted average exchange velocity across the streambed interface of a reach equals the standard deviation in the exchange velocity along the reach (Equation 3.3) according to:

$$\langle W(x) \rangle = \sqrt{\int_{\lambda_{min}}^{\lambda_{max}} \frac{S_W(\lambda)}{\lambda^2} d\lambda} \quad (3.10)$$

where $S_W(\lambda)$ (m3/s2) is the power spectral density of the exchange velocity longitudinal variations along the reach. To parameterize Equation 3.10, $S_W(\lambda)$ was estimated from the PSD of the hydraulic head at the streambed interface, $S_h(\lambda)$ (m3), which in turn was estimated from streambed geomorphology and hydraulics. The linkages between $S_W(\lambda)$, $S_h(\lambda)$ and the stream characteristics were specified by introducing a discrete form of the PSDs, for which the variance can be written as $\sigma_{f(x)}{}^2 = \sum_{i=1}^{N} \Delta S_f(\lambda_i) \lambda_i{}^{-2} \Delta\lambda_i$. As shown in the theory section, previous research has suggested that the multiscale hydraulic head variation along a stream bottom and the resulting HEF can be modelled as a Fourier series (Equations 2.10 and 2.11). With this in mind, it was recognized that the total variance of a real Fourier series (representing the signal f) is equal to the sum of squared amplitudes divided by two according to $\sigma_{f(x)}{}^2 = \sum_{i=1}^{N} A_{f,i}{}^2 /2$, where $A_{f,i}$ is the amplitude of harmonic i in the series $\sum_{i=1}^{N} A_{f,i} \sin\left(\frac{2\pi}{\lambda_i} x\right)$. These two ways of writing the variance of the signal f provide a formal link between the real Fourier sum and the PSD of the signal according to:

$$\sum_{i=1}^{N} \frac{A_f{}^2}{2} = \sum_{i=1}^{N} \Delta S_f(\lambda_i) \lambda_i{}^{-2} \Delta\lambda_i \quad (3.11)$$

Since the variance of a sum equals the sum of a variance, it was assumed that the link provided by Equation 3.11 also is valid for a single harmonic function according to $\frac{A_f(\lambda_i)^2}{2} = \Delta\lambda_i \frac{S_f(\lambda_i)}{\lambda_i{}^2}$. Substituting the arbitrary signal f for the hydraulic head and exchange velocity along a reach the linkages becomes:

$$\frac{A_h(\lambda_i)^2}{2} = \Delta\lambda_i \frac{S_h(\lambda_i)}{\lambda_i^2} \quad (3.12)$$

$$\frac{A_W(\lambda_i)^2}{2} = \Delta\lambda_i \frac{S_W(\lambda_i)}{\lambda_i^2} \quad (3.13)$$

where $A_W(\lambda_i) = 2\pi K \frac{A_h(\lambda_i)}{\lambda_i}\alpha(\lambda_i)$ is the amplitude of the velocity spectrum (see Equation 2.11). Equations 3.12 and 3.13 can then be combined to define the PSD of the HEF velocity along the reach according to:

$$S_W(\lambda) = (2\pi K)^2\alpha(\lambda)^2 \frac{S_h(\lambda)}{\lambda^2} \quad (3.14)$$

The hydraulic head spectrum was subsequently decomposed into its static and dynamic contribution according to:

$$S_h(\lambda) = S_{h_s} + S_{h_d}(\lambda) \quad (3.15)$$

where $S_{y_b}(\lambda)$ is the streambed topography PSD and $S_{h_d}(\lambda)$ is the dynamic head PSD.

3.4.2 Estimating hydraulic head power spectral densities

A central part of the HM model developed and used in this thesis involves the estimation of the hydraulic head PSD, which in this work was done by first estimating the hydraulic head variations in real space and, in a second step, calculating the PSD. The longitudinal variations in the water surface profile were used directly as the static part of the real hydraulic head in the cases where they were measured (Papers I and II) or modelled (Paper III). However, in Paper IV, the only available data were those extracted from the DEM (3.2.5). A comparison with measured streambed topographies and WSPs showed that the DEM seemed to reflect the WSP, rather than the streambed topography. Therefore, the topography extracted from the DEM was used as the static head distribution in real space at the stream bottoms of the five catchments in Paper IV, and a constant scaling factor was derived from field data to estimate the streambed topography elevation. The dynamic part of the hydraulic head distributions was calculated as a simple damped version of the multiscale streambed topography utilizing Equation 2.9, and estimating the bedform height as $H = 2\sqrt{2}\sigma_{y_b}$ in Paper I and $H = 2\sqrt{2}\sigma_{y_b}$ in Paper IV. In Paper II and the local modelling in Paper III, longitudinal variations in the stream hydraulics within the separate reaches were accounted for when calculating Fehlmans constant. It should be noted again that in the HM model, the streambed topography is assumed flat, and the estimated hydraulic head variations are assumed to act upon this flat bed.

After the streambed topographies and hydraulic head distributions were measured or calculated in real space, their PSDs were estimated using Welsh's method and the MATLAB function *pwelch*. This common approach results in a spectrum with less noise than the simpler standard periodogram estimation method. Welsh's method includes decomposition of the data series into overlapping, windowed segments followed by calculations of a periodogram for each segment using the discrete Fourier transform (Welch, 1967). The different periodograms are subsequently averaged to get the final spectrum.

Figure 4 shows an example of the derived power spectral densities for the streambed topography, water surface profile and dynamic hydraulic head estimated from a) measurements in reach R6a (Paper II) and b) data extracted from the DEM at the same position as reach R6a (Paper IV). Both methods result in streambed topography spectra that have higher magnitudes than the water surface profile and much higher magnitudes than the dynamic head spectra. However, when accounting for longitudinal variations in the hydraulic variables (in Paper II and III) the dynamic head PSDs have a different shape compared to the streambed PSD. Moreover, the static head PSD, resulting from the measured water surface profiles (Papers I, II and III) has a different shape than the streambed topography PSD. In contrast, in the method used in Paper IV, all three spectra have the same shape and only the spectral level differs between them.

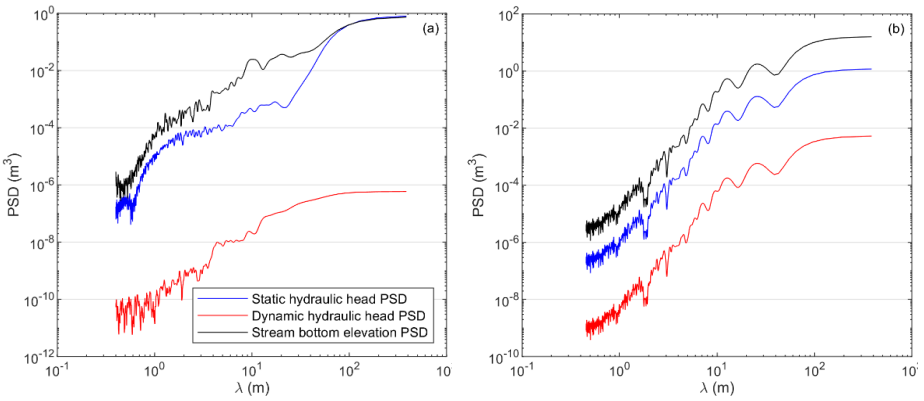

Figure 4. Power spectral density (PSD) of static and dynamic hydraulic head fluctuations as well as stream bottom elevation fluctuations along the thalweg of the stream based on a) elevation measurements along reach R6a of Paper II and b) data extracted from the DEM at the same position as reach R6a.

3.4.3 The geological damping factor

The geological damping factor, $\alpha(\lambda)$, controls the decay in the HEF velocity with streambed depth due to geological constraints and is part of Equations 2.11 and

3.14 in different forms. The factor results from the derivation of the exchange velocity field in the real domain, and it was defined differently in the four papers included in the thesis. In Papers II and III, homogenous hydraulic conductivity was assumed down to an impermeable layer at depth ε (m), which is similar to the solution by Wörman et al. (2006), but here derived in 2D and resulting in a geological damping factor according to:

$$\alpha(\lambda) = \frac{1-\exp(-4\pi\varepsilon/\lambda)}{1+\exp(-4\pi\varepsilon/\lambda)} \tag{3.16}$$

This factor quickly approaches 1 when ε exceeds $\lambda/3$. The impermeable layer does allow for an exact solution of the average exchange velocity since no streamlines reach a depth of infinity. However, the saturated hydraulic conductivity of streambeds and deeper geological layers is rarely homogenous and has been shown to decrease with depth. A relatively common way to account for this decay, which was also done in Paper IV, is to use an exponential decay function according to $K = K_0 \exp[-c_K y]$, where y is the depth into the streambed and c_K (1/m) is a constant (Marklund et al., 2008, Ameli et al., 2016). Including the decay in hydraulic conductivity when deriving the hyporheic flow field leads to a geological damping factor according to:

$$\alpha(\lambda) = \exp\left(\left(-\frac{c_K\lambda}{4\pi} + \sqrt{\left(\frac{c_K\lambda}{4\pi}\right)^2 + 1}\right)\frac{2\pi y}{\lambda}\right) \tag{3.17}$$

Equation 3.17 will approach unity if c_K is very small and approach zero if c_K is very large. The average hydraulic conductivity will thus decrease with increasing c_K. In Paper I, a combination of the two assumptions was used: an impermeable layer was assumed above which the hydraulic conductivity was assumed to decay exponentially. With these assumptions, the geological damping factor becomes:

$$\alpha(\lambda) = \left(-\frac{c_K\lambda}{4\pi} + \sqrt{\left(\frac{c_K\lambda}{4\pi}\right)^2 + 1}\right)\frac{1+exp\left(-\left(-\frac{c_K\lambda}{4\pi}+\sqrt{\left(\frac{c_K\lambda}{4\pi}\right)^2+1}\right)\frac{4\pi}{\lambda}\varepsilon\right)}{1-exp\left(-\left(-\frac{c_K\lambda}{4\pi}+\sqrt{\left(\frac{c_K\lambda}{4\pi}\right)^2+1}\right)\frac{4\pi}{\lambda}\varepsilon\right)} \tag{3.18}$$

All three geological damping factors imply that the exchange velocity induced by hydraulic head gradients across longer wavelengths dampens and that the contribution of large-scale topographical features to the average HEF generally becomes less important than that of small-scale features.

3.4.4 The hyporheic residence time

In addition to the flow-weighted average exchange velocity derived in section 3.4.1, the hyporheic residence time distribution provides an important control for the

transport of both inert and reactive solutes in streams. It was estimated in three different ways in this thesis. In Paper I, it was shown that if the areas of upwelling and downwelling hyporheic flow are the same, the average depth of the HZ can be derived according to:

$$\varepsilon = \frac{\langle W \rangle \langle T \rangle}{2} \tag{3.19}$$

Equation 3.19 was used in Paper I and the local investigation of Paper III to estimate ε. Furthermore, in the local investigation of Paper III, ε was assumed not to be impacted by the stream restoration, equation 3.10 was used to calculate $\langle W \rangle$ after implementation of weirs or alteration of the hydraulic conductivity, and the residence time was then calculated as $\langle T \rangle = \frac{2\varepsilon}{\langle W \rangle}$.

In Paper II, the log-normal residence time distribution associated with the hydro-mechanical mode was derived numerically through a particle tracing routine. The hyporheic velocity field was calculated using the multivariate groundwater equations 2.11a and 2.11b, in combination with the calculated hydraulic head PSDs and the formal link between Fourier amplitudes and the PSD (equation 3.11). Different values of streambed porosity and depth were assumed, resulting in a number of different flow fields. Subsequently, particles were released at recharge (inflow) locations along the streambed interface and traced within each of the flow fields until they reached the interface again. For the travel of each particle, in each flow field, the residence time was logged. A histogram of particle residence times was created and flow weighted, and a continuous log-normal function was fitted to the discrete distribution. The fitting provided values of the mean and standard deviation of the distribution, and subsequently those were used to calculate the flow weighted average residence time, $\langle T \rangle$ (s) and the coefficient of vatiaiton, $CV[T]$ (-). Thus, the particle tracing methodology, which is described in more detail in Paper II, resulted in one residence time distribution for each assumption of streambed porosity and HZ depth.

In the national investigation of Paper III a scaling law introduced by Wörman et al. (2002) was utilized to calculate the average residence time of all reaches according to:

$$\frac{\langle T \rangle K}{d} = 0.013 \frac{1}{Fr^2}, \tag{3.20}$$

where $Fr = \frac{U}{\sqrt{gd}}$ is the Froude number (-) and the constant 0.013 was estimated by fitting the equation to data from a set of field investigations in agricultural reaches of Sweden (including some of the sites in Paper II).

3.5 Estimating hydraulic variables in nongauged streams

The derived models, presented in section 3.3 and 3.4, needed to be parameterized with relevant hydraulic variables to evaluate the effect of HEF on longitudinal transport in and on upwelling groundwater. In Papers III and IV, in which the HEF and nitrogen mass removal were estimated for a large number of stream reaches where no field experiments were performed, the hydraulic conditions were also estimated using different models. This was done according to the following procedure. First, the discharge at all catchment outlets (extracted from the SVAR database), was distributed over the stream network as described in section 3.2.4. Second, the discharge was averaged over short distances, resulting in the local mean annual discharge Q (m3/s), specified for each stream reach or segment. Third, the local mean annual discharge was used to estimate the stream velocity and stream depth in each of the reaches; this was done differently in Papers III and IV.

In Paper III, simplified routing was performed at the national scale using a corrected form of Manning's equation according to:

$$\frac{Q}{A} = \frac{1}{n_c} S^{1/2} R_h^{2/3} \tag{3.21}$$

where, R_h (m) is the hydraulic radius and $n_c = \zeta_n \cdot n$ (s/m$^{1/3}$) is the corrected Manning coefficient. n (s/m$^{1/3}$) is the Manning coefficient, which was set as a constant, and ζ_n (-), a correction factor, which was introduced to account for the nonuniform flow conditions that can be expected in the investigated agricultural reaches. The correction factor was determined by comparing the flow velocity derived from a set of tracer experiments in agricultural streams (including some of tracer tests in Papers I and II) with the equivalent variables estimated from the uncorrected Manning equation. The stream slope was derived from the stream network map and the 50 m x 50 m elevation DEM, and the hydraulic radius and depth were calculated based on the assumption that all reaches had a stream bottom width of 1.5 m and a trapezoidal cross-section with a side slope of 1:3.

In Paper IV, a regression model was used to represent the average stream velocity U and average stream width w in all reaches according to the two equations below:

$$U = 10^{X_U} \cdot Q^{Y_U} \cdot \left(\frac{Q}{\mathrm{MQ}}\right)^{Z_U} \tag{3.22}$$

$$w = 10^{A_w} \left(\frac{Q}{\mathrm{U}}\right)^{B_w + C_w {}^{10}\log\left(\frac{Q}{\mathrm{U}}\right)} \tag{3.23}$$

where A_w, B_w and C_w and X_U, Y_U, and Z_U are regression constants. This work was conducted for assumed annual mean discharge conditions and thus $Q = Q_M$. Those regression constants were previously quantified for 11 geographical regions

in Sweden using an extensive dataset (Rosberg, 2003) and this quantification was used in Paper IV. Subsequently, a rectangular channel geometry was assumed to calculate the average stream depth for all reaches according to $d = \frac{Q}{Uw}$. It should be mentioned that Equations 3.22 and 3.23 were used in several established models for water resource assessments in Sweden, i.e. the HBV-model (Pers, 2007) and HYPE (Lindström et al., 2010).

3.6 Generalization of the average hyporheic exchange velocity

The methodologies to quantify HEF that were mentioned above (assessment of stream tracer tests and the multiscale hydro mechanical model) are simplified in many ways compared to 3D hydromechanical and numerical models or distributed in-stream measurements of HEF. Nevertheless, the methods rely on relatively complicated and extensive data processing and field measurements that are commonly not available for managers or researchers at larger scales. Therefore, this thesis also explored general linkages between the HEF velocity and other independently measurable properties, such as stream and catchment geographical and hydromorphological characteristics. These linkages were tested statistically in Paper IV using principal component and regression analyses and generalized the understanding that could be gained from the cross-validation between the two approaches for quantifying HEF, performed in Paper II. Furthermore, regression analysis was also performed in Paper IV to investigate in which geographical and hydromorphological condition HEF is expected to have an impact on deep upwelling groundwater.

3.6.1 Tested dependent and independent variables

Before performing the regression analysis in Paper IV, dependent and independent variables were calculated for all subcatchments (related to specific stream segments and with an area of between 0.0051 km^2 and 7.714 km^2), intermediate subcatchments (areas of 6.68 km^2 and 37.75 km^2) and the five full regional catchments. Both the modelled flow weighted average HEF velocity, and the ratio between the average deep groundwater discharge velocity and the average HEF velocity, $\delta_W = \frac{\overline{W_{dGWF}}}{\langle W \rangle}$, were used as dependent variables. The HEF velocity was calculated using the HM model parametrized according to section 3.2.5. To specify the average deep groundwater discharge velocity, $\overline{W_{dGWF}}$, the topographically controlled groundwater flow fields in the five regional catchments were first modelled using a steady state numerical model described in the appended Paper IV. Particles were then released at a depth of 500 m and traced to the surface. Finally, the velocity of all particles discharging within the sub-catchment or full catchment of interest was averaged.

To explain the variability in the dependent variables, a large number of independent variables were derived, representing catchment topography characteristics,

catchment geology characteristics and stream reach characteristics (both hydraulic and topographical indexes). As described in section 3.2.5, topographical indexes were derived from the DEM file. In addition, the average hydraulic conductivity of the topsoil in each sub-catchment, K, was estimated from hydraulic conductivity related to specific soil types, and the average soil depth (quaternary deposits), D_{QD}, was calculated from the soil depth model provided by the Geological survey of Sweden (© SGU). Furthermore, fractal properties of the WSP (i.e. PSD magnitude and slope), were included in the regression analysis and noted a_{WSP} and b_{WSP}. Finally, stream hydraulic characterizing variables, i.e. the Reynolds number $Re = \frac{Ud}{\nu}$, the Frouds number $Fr = \frac{U}{\sqrt{gd}}$, the stream power per unit channel length, $\Omega = \rho g S Q$ (kg m/s^2) and the Darcy-Weibash friction factor $f = \frac{8gdS}{U^2}$, were calculated using values of discharge, velocity, and depth, estimated according to section 3.5 and stream slope, S, according to section 3.2.5.

To avoid multicollinearity in the multivariate regression analysis, reduce the degrees of freedom and select the most relevant dependent variables, a PCA was performed and the variance of inflation factor was calculated for the dependent parameter set. Both these statistical analyses are described in more detail in the appended Paper IV. The analysis lead to that ten independent variables (A_{CM}, S_{CM}, GtS, MSC, K_{CM}, D_{QD}, U, Fr, Re, Ω, f, a_{WSP}, and b_{WSP}) were selected to be included in the regression analysis.

3.6.2 Regression analysis

Regression analysis is a statistical method that estimates the relationship between one or several dependent variables and one or several independent variables. Since the dependent variables in Paper IV were shown to follow a log-normal distribution, a power law equation was used in the regression analysis. Both single and multivariate regression analyses were performed, where the latter was done both in ae stepwise matter, and with two independent variables at the time. To evaluate the significance of the included independent variables in the regression models, statistical t-tests were performed and a significant model was defined as having a p-value < 0.05. Furthermore, to estimate the explanatory power of the model, three different coefficients of determination were calculated (Montgomery et al., 2012). First, the ordinary coefficient of determination was calculated as:

$$R^2 = 1 - \frac{\sum_{i=1}^{n}(Y_i - \hat{Y}_i)^2}{\sum_{i=1}^{n}(Y_i - \bar{Y})^2} \quad (3.24)$$

where Y_i is the true dependent variable, $\hat{Y}_i$ is the predicted dependent variable and $\bar{Y}$ is the mean of the true values. Second, to compensate for the number of included independent variables that naturally increase the explanatory power of a model, the adjusted coefficient of determination was calculated as:

$$R^2_{Adj} = 1 - \frac{(1-R^2)(i-1)}{i-k-1} \quad (3.25)$$

where k is the number of independent variables, and i is the number of datapoints in the regression plot. Finally, the predictive coefficient of determination was calculated by first performing a 3-fold cross validation of the regression model and repeating this 10 times. The R^2 value was then calculated for each of the 30 tests and finally averaged to obtain the predictive coefficient of variation, R^2_{Pred}.

3.7 Testing the potential of stream restoration

A number of simple remediation strategies were tested as part of this thesis to examine the practical possibility of increasing the nitrogen mass removal along a specific reach (Papers I and III). The impact of specific designs was assessed in two local stream reaches, and the theoretical potential was assessed at the national scale.

3.7.1 The local effects of specific stream restoration designs

The HM model (section 3.4) was parameterized with estimates of the upper hydraulic head PSD and the in-stream hydraulics to approximate the impact of stream restoration in two short stream reaches.

In Paper I, the measured hydraulic head PSD (in Reach 3) was compared with a theoretical PSD intended to represent a remediation measure resulting in a step shaped WSP. The hydraulic conditions of the stream, including the advective travel time and the stream depth, were assumed not to be impacted by the implementation of this generic step.

In Paper III, HEC-RAS (USACE, USA), was used to model the impact of a number of restoration designs on both the water surface profile and in-stream velocity and depth. HEC-RAS solved the 1D energy equation using the standard step method and calculated the distributed variation in discharge, exchange velocity and stream depth. The model was calibrated for the base-case conditions (i.e. the current geomorphologic conditions, without restoration measures), towards stream depth and velocities assessed from the tracer test measurements performed in the reach. The tested designs, presented in Table 3, included alterations of hydraulic conductivity as well as the implementation of weirs of different heights H (m) and in-between distances, L (m), designed to represent in-stream structures such as cross-vanes or boulder clusters. The different designs were then analyzed during three discharge conditions: low discharge LMQ = 0.01 m3/s, mean discharge MQ = 0.12 m3/s, and high discharge HMQ = 0.41 m3/s.

Table 3. The base case condition and restoration designs tested in Malsta Brook (Paper III), including in-stream structures in the form of weirs of varying height (H) and in-between distance (L) and modification of the average hydraulic conductivity (K) of the streambed. (From Paper III)

	Design notation	Design details	
Base-case	**BC**	Observed topography	K = $1 \cdot 10^{-3}$ m/s
Installing in-stream structures	**S1**	H =0.2 m, L=57 m, H/L = 0.004	K = $1 \cdot 10^{-3}$ m/s
	S2	H= 0.4 m, L =57 m, H/L= 0.007	K = $1 \cdot 10^{-3}$ m/s
	S3	H = 0.2 m, L=114 m, H/L= 0.002	K = $1 \cdot 10^{-3}$ m/s
	S4	H = 0.4 m, L =114 m, H/L= 0.004	K = $1 \cdot 10^{-3}$ m/s
Modifying streambed material	**K1**	Observed topography	K = $1 \cdot 10^{-2}$ m/s
	K2	Observed topography	K = $1 \cdot 10^{-4}$ m/s
	K3	Observed topography	K = $1 \cdot 10^{-5}$ m/s

3.7.2 The theoretical potential of stream restoration at the national scale

In addition to the reach scale stream restoration scenario analysis described in section 3.7.1, Paper III included an estimation of the potential for stream restoration in all small agricultural streams in Sweden. It was done by calculating the current as well as maximal nitrogen removal rate and relative mass removal and comparing these; thus the national scale analysis did not consider specific stream restoration designs. The equations used for this national analysis are presented as results in Section 4.2.1 (Equations 4.3 and 4.6). To estimate the current mass removal, Equation 4.3 was parameterized with the HEF parameters $\langle T \rangle$ and $\langle W \rangle$, which were calculated using Equation 3.19 and Equation 3.20 and assuming ε= 0.1 m in all stream segments. Furthermore, it was assumed that r_{den}= 0.1 h^{-1} and τ_{oxy}= 1 h^{-1} in all stream segments, and the denitrification in the main channel, R_{MC}, was assumed to be zero and thus $R_{sys} = R_{HZ}$. Subsequently, the maximal nitrogen removal rate and relative mass removal in the HZ were derived in the same way but assuming $\langle T \rangle = \langle T \rangle_{opt}$, where $\langle T \rangle_{opt}$ is the optimal hyporheic residence time, estimated for each reach using Equation 4.6.

The network effect was accounted for by aggregating the relative and absolute mass removal in all small agricultural stream reaches in Sweden, according to Equation 3.7, for both current and optimal conditions. The potential was then stated as the difference between current and optimal conditions. Temporal variation in the removal rate was not analyzed explicitly but instead assessed by performing a sensitivity analysis including three static discharge scenarios, that is: mean discharge (MQ), low mean discharge (LMQ) and high mean discharge (HMQ), estimated as the yearly averages of modeled discharge provided by SMHI (SMHI, 2021).

4 RESULTS AND DISCUSSION

The general aim of this thesis was to better understand the physical controls for HEF and how HEF influences solute transport in stream reaches and networks. Specifically, a modelling framework was established that provides a physically based way to parameterize HEF variables in transport models and assess the mass removal at the stream reach, and network, scale. The modelling framework is in itself an important result of this thesis and is presented in Figure 5. The big white arrows in Figure 5 indicates the models and methodologies that were linked together and the blue markers how models were used in different papers. First, the multiscale hydro mechanical (HM) model was developed (section 3.4) and utilized to quantify the 2D subsurface flow; and the transport model (ASP model) was used simultaneously to quantify the in stream solute transport, including HEF. The temporal moments of the solute transport were then derived to estimate the reach scale mass removal (Equation 3.6); and the reach scale response was aggregated to estimate the network scale mass removal (Equation 3.7).

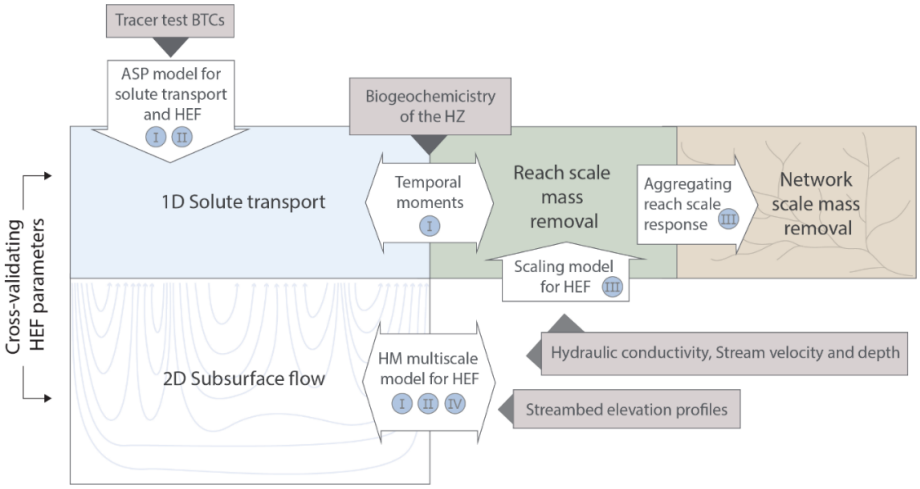

Figure 5. The interlinkages between different models and papers in this thesis, indicating both subsurface and surface water modelling (lower and upper boxes) and modelling at different spatial scales (increasing scale towards the right in the figure). The big white arrows illustrates the models that are part of the framework including the multiscale, hydro mechanical (HM) model used for 2D subsurface flow modeling; the advective storage path (ASP) model used to quantify the 1D solute transport with surface water; temporal moment derivation to estimate the reach scale mass removal; and aggregation of the reach scale response to estimate the network scale mass removal. The cross-validation between the surface and subsurface models is also shown to the left. The brown fields and small arrows denotes the data needed to limit the models, and the blue markers illustrates which models that were part of which papers.

Figure 5 also illustrates that in Paper III, a scaling model (Equation 3.20) was used to estimate the hyporheic residence times, due to lack of streambed elevation profiles from all agricultural streams of Sweden. Field observations and extraction of data from maps and literature reviews were used to limit the model results and these are shown in the brown fields in Figure 5. Furthermore, the cross-validation between HEF variables derived with the transport model and the HM model is shown in Figure 5 since it motivates to use the HM model to parameterize ASP model. In this thesis, the model framework in Figure 5 was specifically used in the clockwise direction to estimate the mass removal from specific hydromorphological characteristics. However, the bidirectional arrows are representing the ambition to in the future follow the modelling framework in the opposite direction, i.e., to estimate the hydromorphology needed to reach a specific reach or network scale mass removal.

4.1 Physical controls on hyporheic exchange flow

One of the main objectives of this thesis was to advance the physical understanding of how HEF is controlled at different spatial scales. Therefore, linkages between the multiscale stream hydromorphologic characteristics and HEF quantifying parameters were thoroughly investigated. The results from these investigations are presented in this section and includes: 1) the cross-validation of two different approaches for HEF quantification; 2) the advanced understanding of key spatial scales and drivers for measuring and modelling HEF; and 3) assessed statistical correlations between the average exchange velocity and geographic and hydromorphological stream and catchment characteristics.

4.1.1 Cross-validating two approaches for estimating hyporheic exchange

The cross validation performed in Paper II show that the results from HM modelling and tracer test assessments of HEF generally agreed in terms of the flow-weighted average exchange velocity, $\langle W \rangle$ (Figure 6a). However, the results also show that the residence time distributions (quantified in terms of the average residence time $\langle T \rangle$, and coefficient of variation $CV[T]$) agreed to a lesser extent (Figure 6b and 6c). The horizontal uncertainty bars in Figure 6 are related to the MC analysis, performed to investigate parameter sensitivities in the ASP model, and show that the observed tracer breakthrough curves are accurately described by a large range of HEF parameters. The vertical uncertainty bars show the range of values resulting from the HM model when assuming a range of reasonable HZ depths (0-1 m) and streambed porosities (0.2-0.5). If both error bars crossed the 1:1 line, it was considered an acceptable cross-validation between the two approaches. Thus, the results show that $\langle W \rangle$ assessed using the two methods agreed in the seven reaches with the smallest discharge, shallowest depth and lowest Reynolds number. In contrast, in the three largest reaches, $\langle W \rangle$ was lower when induced from the tracer test than when derived with the HM model, even when the model uncertainty was accounted for.

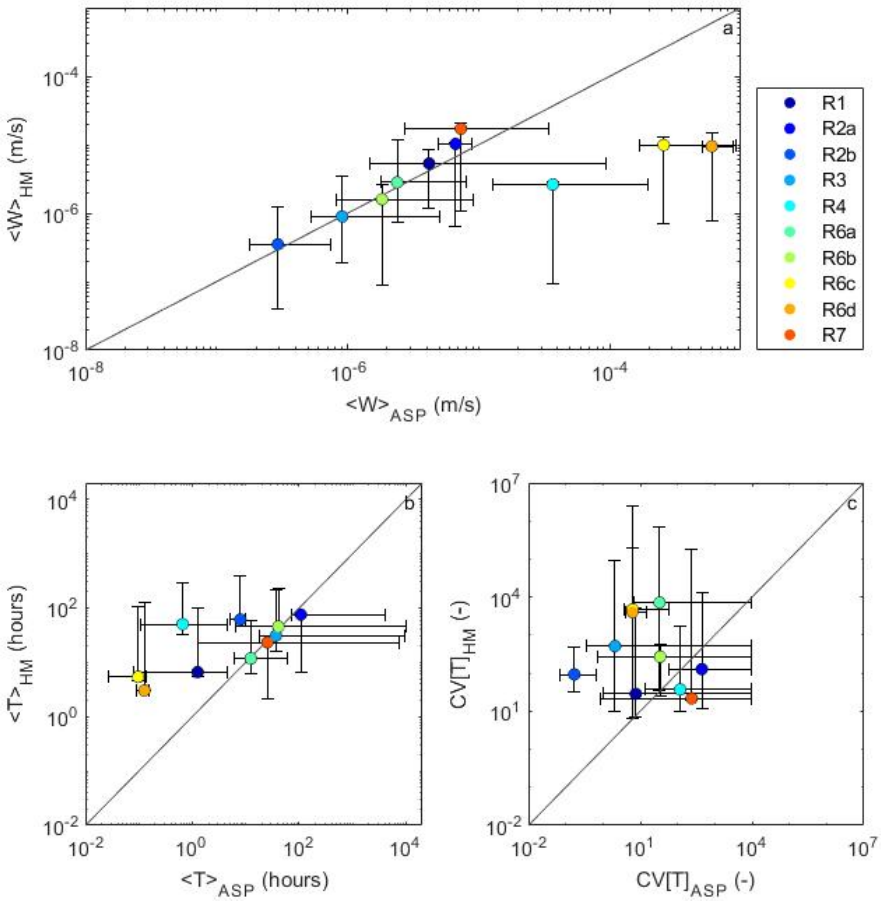

Figure 6. Cross-validation of inductive assessments of tracer tests using the advective storage path (ASP) model and deductive modelling using the mulstiscale hydro mechanical (HM) model, in terms of: a) the average exchange velocity, $\langle W \rangle$; b) the average of the hyporheic residence time, $\langle T \rangle$; and c) the coefficient of variation of the residence time distribution, $CV[T]$. Horizontal error bars represents the variable range leading to behavioral models, while the vertical error bars represents the sensitivity in the variables due to different assumptions of the hyporheic zone depth, ε, and streambed porosity, η. (From Paper II)

In terms of $\langle T \rangle$, comparable results were reached with the two models in only five out of ten reaches (Figure 6b), and an even lower agreement was found in terms of $CV[T]$ (Figure 6c). Note that only three of the reaches were cross-validated in terms of both $\langle T \rangle$ and $CV[T]$. More emphasis was placed on the longer residence times when applying the HM model than when tracer tests were evaluated, and generally, the HM model resulted in wider RTDs compared to the optimized tracer test. The largest difference in $\langle T \rangle$ was found in the same three reaches where $\langle W \rangle$

was not cross-validated and those were the three largest, and deepest, reaches. The divergence between models could be attributed to model technical differences between the approaches, which generally emphasize different parts of the residence time distributions (Stonedahl et al., 2012). A tracer test detect only the transport of the injected tracer that reaches the downstream measuring point within the length and time scale of the tracer test (i.e. within the so-called window of detection) (Harvey and Wagner, 2000, Schmadel et al., 2016). Thus, the longest streamlines and residence times will be missed if part of the tracer bypasses the measuring point and recharges into the main channel further downstream; if part of the tracer reaches the measuring point after measurements are ended; or if the concentration is below the detection limit of the measuring device (Bencala et al., 2011, Drummond et al., 2012). In contrast, HM models are restricted by their resolution. A too small resolution of input data, in this case the longitudinal distance between elevation measurements, or uncertainty in high density data, might result in uncertain estimates of the shortest residence times of the RTD.

Another reason for deviation between the HEF variables estimated with the two approaches is that while the HM only accounts for so-called pumping, occurring vertically and longitudinally along the stream thalweg, the ASP model induces all of the transported tracer within the reach. Exchange with stagnant surface water and lateral exchange with the riparian zone (Briggs et al., 2009, Johnson et al., 2014) could, for example, be expected in the three reaches with the largest deviation between the two approaches since these three reaches were the largest in terms of both depth and width. The same reaches also had the highest Reynolds numbers, and therefore, turbulence could have been an important exchange mechanism there (Packman et al., 2004, Grant et al., 2018).

Finally, deviation between the two approaches in terms of $\langle T \rangle$ and $CV[T]$ could be attributed to uncertainties in the model parameterization and input data. Equifinality in the parameterization of the ASP model is indicated by the MC analysis. Specifically, there exists a statistical relationship between the mean and the variance of a log-normal distribution, whereby if $\langle T \rangle$ is uncertain, so is $CV[T]$ (Wörman and Wachniew, 2007). Parameter uncertainty exist also in the HM model and is mainly related to how the streambed hydraulic conductivity, permeability and depth are estimated and conceptually described. When modelling HEF in the Paper II using the HM model, the average hydraulic conductivity was estimated from point measurements in the field, and the depth and permeability was parameterized by minimizing a specific error between the HM model results and the tracer test assessment. In reality however, heterogeneities often exists in streambed material and hydraulic conductivity, and it is difficult to specify the maximum depth below which there is no hyporheic flow. Heterogeneities in streambed sediments can cause both increases and decreases in HEF parameters (Cardenas and Wilson, 2004). One way of easily accounting for heterogeneity in the model defined here, is to assume a decay in hydraulic conductivity with depth,

as was done in Papers I and IV. However, variation in both hydraulic conductivity and HZ depth over relatively short distances, due to heterogeneities such as clay lenses or rocks, can also be expected in some streams and can impact the hyporheic flow field (Earon et al., 2020, Gomez-Velez et al., 2014). Such heterogeneity was not accounted for in the modelling performed in this thesis.

In summary, although uncertainty existed, the general result of Paper II was that the tracer test assessments and HM model could be cross-validated relatively well in terms of $\langle W \rangle$ in small alluvial streams, with shallow depth, small width and moderate slope. This indicates that the HEF is largely controlled by longitudinal gradients in the water surface elevation profile or stream bottom elevation profile. Furthermore, these results provide a physical explanation for the parameters of the ASP model, which can also easily be transformed into variables of other transport models.

4.1.2 Static and dynamic hyporheic exchange at different spatial scales

The multiscale HM model, developed as part of this thesis, can be used to study the physical basis of HEF in detail and when distributed over a range of spatial scales. The contribution of different spatial scales and different drivers to the total HEF is relevant for a phenomenological understanding of the processes and benefits management when planning stream restorations or monitoring stream hydromorphology and water quality.

The HEF velocity PSDs from reach R3 are plotted in Figure 7, and the PSDs from the rest of the reaches are found in the appended Paper II. The peaks around wavelengths of approximately 1-2 m shows that the HEF was mainly generated by hydraulic head gradients over features with this length. Furthermore, Figure 7 shows that the static head driven HEF velocity was considerably larger than the dynamic head-driven HEF velocity over all observed wavelengths and this was the case in all stream reaches. The domination of relatively small-scale features over larger features in all investigated reaches was also observed for the average HEF velocity $\langle W \rangle$, which was conceded by integrating over the PSDs. Increasing the upper cutoff wavelength used in the integration, λ_{max}, showed that more than 90% of the average exchange velocity was driven by features with wavelengths smaller than 5 m and that it was the case in all reaches (Figure 8). Thus, the results indicates that spatial scales smaller than 5 meters are crucial to consider to satisfactory quantify HEF in small alluvial streams, both in measurements and models, whereas larger scales might be acceptable to neglect. Several previous studies that have modelled HEF over a range of spatial scales, also concluded that small-scale features contribute to a large part of the total hyporheic flux (Wörman et al., 2006, Stonedahl et al., 2012, Stonedahl et al., 2013, Gomez-Velez and Harvey, 2014).

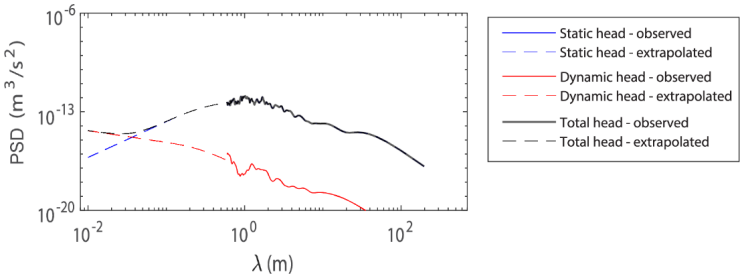

Figure 7. The power spectral densities (PSDs) of the static, dynamic and total head driven hyporheic exchange flow (HEF) velocity distributed over observed and extrapolated wavelength. Note that the blue lines (solid and dashed) are disappearing behind the black line for larger wavelength, since the dynamic head is too small to influence the total HEF velocity at these scales. This is an example from Malsta Brook (Reach R3), while results from the rest of the reaches are found in Paper II.

Previous studies that have separated between the HEF driven by static and dynamic head gradients have disagreed on which of the two that drives the main part of the exchange. It is generally thought that HEF in high-order reaches, which are normally steep with low discharge and low relative submergence of bedforms, is mainly driven by static head gradients. Subsequently, when moving toward lower stream order reaches with lower slopes and higher discharges, dynamic head gradients becomes increasingly important (Wondzell et al., 2019). This theory could explain why static head domination that was found in two mountainous catchments (Marzadri et al., 2014, Mojarrad et al., 2019), while dynamic head domination was observed in less steep reaches and catchments (Stonedahl et al., 2013, Gomez-Velez and Harvey, 2014). However, the reason for the domination of dynamic head exchange according to some models could also possibly be related to the presumption that no static head gradients exist below a certain wavelength, as in Stonedahl et al. (2013).

To test whether the resolution in the input data and the resulting PSD minimum wavelength control the relative importance of the static and dynamic heads according to the HM model, the hydraulic head spectrum was extrapolated to wavelengths smaller than what was observed. This extrapolation was also performed to investigate whether the agreement between the HM model and the tracer test assessment (Section 4.1.1) was dependent on the resolution of the PSDs. When extrapolated, the static and dynamic head spectra intersected in some of the reaches at wavelengths between 0.01 and 1 m (see example in Figure 7, dashed lines). The intersection indicates that at the smallest scales, hydraulic head variations exist in the stream bottom profile that are not evident in the overlying water surface. Nevertheless, this intersection did not affect the relative importance of the static and dynamic heads for the average HEF velocity, and the static head driven HEF was still dominant in most reaches.

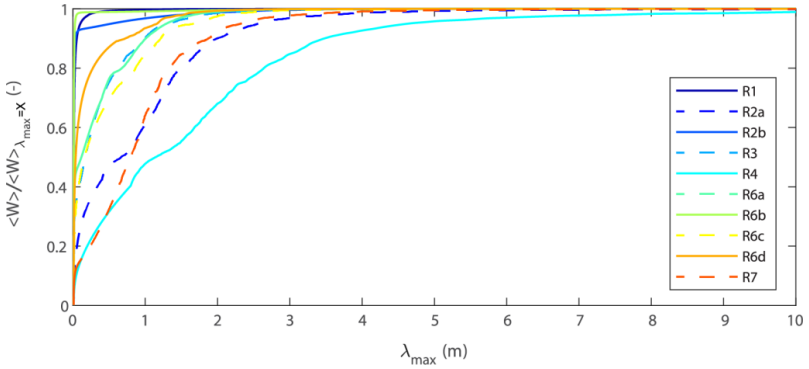

Figure 8. The average hyporheic exchange flow (HEF) velocity calculated with increasingly high cutoff wavelength (λ_{max}) and normalized with the HEF velocity calculated with the maximal upper wavelength equal to the stream reach length (X), for the ten different study reaches of Paper II. (Modified from Paper II)

However, in two of the reaches, R2b and R6b, the dynamic average HEF velocity became larger than the static when all scales were included. This finding is probably attributed to the relatively low slopes of reaches R6b and R2b, which does exert a limitation for the longitudinal static head gradients, as discussed thoroughly in Paper I. Thus, this thesis indicates that the importance of dynamic head gradients for the average HEF velocity might be missed if an excessively low longitudinal resolution of the streambed topography or hydraulic head at the surface water interface is used in hydromechanical models estimating HEF. However, the thesis also shows that static head gradients might be important at scales less than a meter and should therefore not be dismissed beforehand.

It is also possible that the inclusion of small spatial scales influences the cross-validation of the HM model and the tracer test assessment described in Section 4.1.1. This prospect was investigated in Papers I and II by integrating over the exchange velocity PSDs with an increasingly large value of the minimum wavelength, λ_{min}. In Paper I, the estimated stream topography PSD had an original minimum wavelength of approximately 5 m; when the PSD was extrapolated down to wavelengths of 1 mm, the HEF velocity increased substantially, and a better agreement with the tracer test results was reached. In Paper II, the minimal observed wavelength ranged between 0.2 m and 1.4 m, depending on the reach, leading to relatively good agreement between the two approaches in most reaches, as shown in Figure 6. When extrapolating the hydraulic head PSDs towards nonobserved wavelengths, it only had a minor impact on $\langle W \rangle$, not large enough to considerably affect the agreement with the tracer test assessment in any of the ten reaches.

4.1.3 Reach and catchment characteristics controlling hyporheic exchange

The agreement found between the HM model and tracer test assessments in terms of $\langle W \rangle$ provides a physical explanation for the HEF parameters of the ASP model and other similar solute transport models, in certain types of streams. However, the usefulness of the HM model and other similar models are limited by their complexity and the need for high density input data. Extrapolation of the hydraulic head spectrum towards nonobserved wavelengths could partly resolve this problem. However, the method of extrapolation does incorporate uncertainties and assumes that the topographical power spectrum slope is strictly fractal over the shortest wavelength, which might not always be the case. Therefore, it might be valuable to investigate new methods for the collection of high-resolution topography data (Passalacqua et al., 2015, Woodget et al., 2017) or other methods for parameterization of the HEF. In Papers I and Paper II, simple relationships between the $\langle W \rangle$ and certain hydromophological independent variables were derived and discussed. In Paper IV, a multivariate regression analysis was performed to find more advanced, and statistically significant, relationships between the $\langle W \rangle$ derived with the HM model and a large number of independent reach and catchment characteristics. The most relevant relationships is presented and discussed in this section.

From groundwater flow theory, $\langle W \rangle$ is linearly related to the pressure gradient and the hydraulic conductivity of the streambed. In Paper I, an analytical solution was derived, showing that $\langle W \rangle$ was also linearly related to the standard deviation in hydraulic head along the streambed interface, normalized with the maximum wavelength of the hydraulic head PSD, $\frac{\sigma_h}{\lambda_{max}}$. In addition, the exchange velocity was shown to depend on the distribution of the hydraulic head gradients along the streambed, quantified by the slope of the hydraulic head PSD, b_h, where $\langle W \rangle$ increased with decreasing b_h. Finally, the smallest included wavelength $\lambda_{\min} = \frac{\lambda_{max}}{N}$ in the hydraulic head spectra, and the geological damping factor α_i (Equation 3.18), also impacted the exchange velocity according to:

$$\langle W \rangle = K\pi \frac{\sigma_h}{\lambda_{max}} \sqrt{\sum_{i=1}^{N} \frac{2(b_h-1)}{(i^2+1)(i^{b_h-4})} {\alpha_i}^2} \quad (4.1)$$

Equation 4.1 is a simpler version of the general form of the HM model (Equation 3.10), where the hydraulic head spectrum is not divided into static and dynamic parts, and is assumed to be fractal over the whole range of wavelengths.

In Paper II, the Buckingham pi-theorem was used to generalize the more complex form of the HM model by relating the dimensionless exchange velocity $\langle W \rangle / K$ to seven independent dimensionless parameter groups. Four of the tested relationships are presented in Figure 9, and the rest can be found in the appended

Paper II. The investigation indeed showed that $\langle W \rangle / K$ increased with the standard deviation in both static and dynamic hydraulic heads, but uncertainties existed, mainly related to the reaches where the HM model did not agree with the tracer test assessments (Figure 9a). It is also relevant to note that the reaches where the two approaches did not agree, had relatively high submergence of streambed features (d/σ_{y_b}) (Figure 9b). Thus, dynamic hydraulic head is theoretically an important driver of HEF in these reaches and possibly underestimated in the HM model because of the difficulty in measuring the small-scale features and conceptual model uncertainties related to the use of the Fehlmans formula. Furthermore, both the squared Froude number, Fr^2, and Reynold's number, Re (based on stream depth), were positively related to $\langle W \rangle / K$ (Figure 9c and 9d). Note that the worst agreement between the two approaches was found in the reaches with the highest Re (Figure 9c), indicating that turbulence, which was not accounted for by the HM model, could be an important HEF driving mechanism in those reaches. The relationship between HEF and Fr^2 (Figure 9d) has been shown previously in e.g., Wörman et al. (2002) where it was explained by the linear relationship between the HEF velocity and dynamic head fluctuations at the streambed (accounted for here using Equations 2.8 and 2.9). In Paper II, it was found that static hydraulic head-driven hyporheic exchange dominated dynamic hydraulic head-driven HEF in most reaches. Thus, the relationship is most likely mainly due to the existing relationship between gradients in the WSP over a short distance and Fr, which is known from basic hydraulic theory and is discussed in, e.g., Sawyer et al. (2011) and Mojarrad et al. (2019).

In the statistical investigation of Paper IV, several significant multivariate regression models successfully linked $\langle W \rangle$ to different reach and catchment hydromorphologic and geographic independent variables (Paper IV). The best regression model was selected as the one in which the explorative and predictive R^2 value did not decrease by more than 2% if one of the included variables were removed. For variables averaged at the reach scales (average reach length of 1230 m), the best regression model is plotted in Figure 10a and is stated as follows:

$$\langle W \rangle = 1.17 \cdot 10^{-2}\, {a_{WSP}}^{0.31} {b_{WSP}}^{-2.06} {K_{CM}}^{0.17} \qquad (4.2)$$

where a_{WSP} and b_{WSP} are the magnitude and slope of the water surface profile PSD, respectively, and K_{CM} (m/s) is the average hydraulic conductivity of the stream reach subcatchment topsoil. These three variables together explained 72% of the observed variance in $\langle W \rangle$ between reaches.

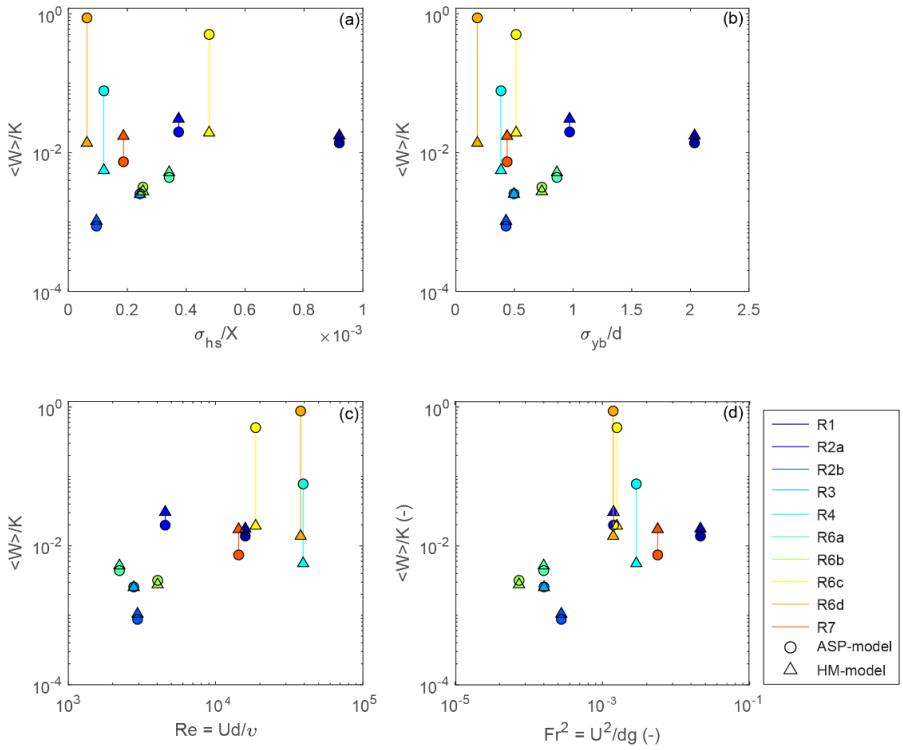

Figure 9. The hyporheic exchange flow velocity, $\langle W \rangle$, normalized with the hydraulic conductivity, K, as a function of; a) the standard deviation in the water surface profile along the reach normalized with the stream reach length σ_{hs}/X; b) the standard deviation in streambed topography normalized with stream depth, σ_{yb}/d; c) the Reynold number calculated from streamdepth, $Re = Ud/\nu$; and d) the squared Froude number $Fr^2 = U^2/dg$. Triangles and circles represents values estimated with the multiscale hydromechanical (HM) model and the advective storage path (ASP) model, respectively. Colors refer to the reaches investigated in Paper II, according to the legend. Lines between markers indicate that the data is coming from the same reach; thus longer lines indicates a higher disagreement between the models. (Modified from Paper II)

In Paper IV, the power law with variables a_{WSP} and b_{WSP} was only fitted to the lower range of the WSP PSD with wavelengths < 20 m. Variables that represented the hydraulic head variations at larger scales, such as the overall standard deviation in hydraulic head, were thus not as important as the fractal properties of the lower range of the hydraulic head spectrum. This indicated that the small scales are essential to include when calculating the HEF at the reach scale. Note also that none of Reynold's number, Froude's number, or Darcy Weisbach friction factor increased the explanatory power considerably when included in the analysis. These dimensionless numbers are closely related to the dynamic head variation along the streambed but not necessarily to the static hydraulic head variation. The fact that

they were not included in the best regression models might be due to the simple way in which the stream velocity and depth were estimated in Paper IV, which resulted in relatively small variations in these parameters within the catchments. However, the exclusion of these variables could also be because the static head gradients were more important than the dynamic as drivers of HEF, which was already indicated in Paper II. Previous studies have also shown that the fractal properties of the streambed topography (or the water surface profile) provide important controls for the HEF (Marzadri et al. 2014, Lee et al. 2020). In more general terms, it means that $\langle W \rangle$ usually is larger in reaches with large variation in the streambed or WSP across small scales (high a_{WSP} in this study). Furthermore, the largest $\langle W \rangle$ are found in reaches where the variability is distributed equally over all spatial scales and the streambed topography or WSP is rough also over the shorter scales (low positive b_{WSP} in this study). In Paper IV, b_{WSP} ranged between approximately 1 and 6, with most values between 2.5 and 4 and a_{WSP} ranged between 10^{-8} and 10^{-3}. If the fractal variables were excluded from the regression analysis, then the Darcy Weisbach friction factor controlled a large part of the exchange velocity, agreeing with previous research (e.g., Harvey et al. 2003, Zarnetske et al. 2007).

This thesis also investigated how regression models for the average exchange velocity changed when the averaging area increased, and that the changes were in terms of both the included independent variables and the explanatory power. The results showed that at the intermediate catchment scale (catchment area between 6.7 km2 and 37.8 km2), the best regression model included the independent variable a_{WSP} and the Darcy-Weisbach friction factor, f_{IC}, which explained 90% of the observed variability between catchments (Figure 10b). At the regional catchment scale, only single regression models were tested, and surprisingly, the Darcy-Weisbash friction factor, f_{RC}, alone explained 96% of the variability in the exchange velocity between the five regional catchments (Figure 10c). However, due to the very small dataset (5 catchments), the results should be interpreted with caution, and larger datasets are needed to confirm this relation. The general change in regression models and their explanatory power, when set up for different scales, is, however, interesting. This indicates the complexity of using average variables when assessing the transport of solutes with groundwater and HEF.

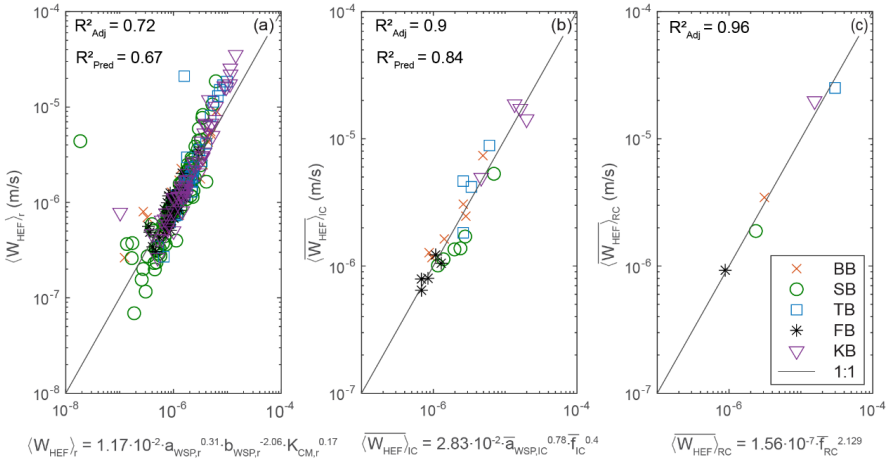

Figure 10. The best performing regression models, estimating the average hyporheic exchange flow (HEF) velocity at a) the reach scale (r), b) the intermediate catchment (IC) scale and, c) the regional catchment (RC) scale. Adjusted R^2 and predictive R^2 are shown in each graph. The different markers indicates that data are derived from the different regional catchments Bodals Brook (BB), Säva Brook (SB), Tullstorps Brook (TB), Forsmark Brook (FB) and Krycklan Catchment (KC) and the grey line represents the I:I reference. (From Paper IV).

4.2 Impact of hyporheic exchange on stream nitrogen removal

After investigating methods to parameterize the reach average HEF velocity, this thesis sought to improve the understanding of how the local HEF can impact solute transport at the reach and catchment scales. In this section, analytical solutions for the reach scale nitrogen removal is presented and discussed, subsequently followed by results from using these solutions to evaluate the impact of HEF on stream water quality before and after stream restoration, at the reach scale as well as at the network scale.

4.2.1 Analytical solutions for nitrogen removal at the reach scale

A key result of this thesis is the analytical expression for the reach scale mass removal, which was derived from the zeroth temporal moment of the in-stream solute transport according to section 3.3.2. In Paper III, the longitudinal dispersion of the initial transport equation (Equation 3.1) was neglected before the temporal moment was derived, and it resulted in an expression of the relative nitrogen mass removal, D (-) according to:

$$D = 1 - \exp\left(-\frac{X}{U}(R_{MC} + R_{HZ})\right) \quad 4.3$$

Equation 4.3 shows that mass removal within a reach is controlled by the product between the in-stream residence time, defined as X/U, and the sum of the mass

removal rate in the main channel (R_{MC}) and in the HZ (R_{HZ}). This agrees with a previous solution presented by Runkel (2007), which was based on the transient storage model. When dispersion is included in the initial transport equation (Paper I), the relative mass removal instead becomes:

$$D = 1 - \exp\left[\left(\frac{U}{2D_L} - \sqrt{\left(\frac{U}{2D_L}\right)^2 + \frac{R_{MC}+R_{HZ}}{D_L}}\right)X\right] \quad 4.4$$

Thus, increased dispersion will lead to decreased mass removal. This is explained by Runkel (2007) to be due to a faster downstream transport with dispersion compared to conditions without dispersion, which results in shorter residence times and thus lower D. However, the impact of dispersion is minor when the velocity is low, and Equation 4.4 was assumed appropriate to estimate the mass removal in all agricultural reaches of Sweden in Paper III. Furthermore, the derivation of the zeroth temporal moment resulted in an expression for the effective mass removal rate in the HZ, R_{HZ}, and its dependency on the HEF and biogeochemical variables according to:

$$R_{HZ} = -\frac{P}{A}\frac{\langle W\rangle\langle T\rangle}{2}\frac{r_{den}\exp[-\tau_{oxy}/\langle T\rangle]}{(1+r_{den}\langle T\rangle)}. \quad 4.5$$

Equation 4.5 shows that in addition to being linearly related to the hyporheic denitrification rate, r_{den}, R_{HZ} is controlled by three dimensionless parameter groups. The magnitude of R_{HZ} is linearly correlated to the size of the HZ relative to the stream depth, $\frac{P}{A}\frac{\langle W\rangle\langle T\rangle}{2} = \frac{\varepsilon}{d}$, Thus increasing stream depth will decrease the removal rate, while a larger HZ depth allows more water to be transported into the HZ and leads to a higher R_{HZ}. Furthermore, R_{HZ} is dependent on two Damkhöler numbers, which are known to be useful measures of the relative importance of reaction and transport processes (e.g., Ocampo et al., 2006, Pinay et al., 2015). First, R_{HZ} is negatively correlated to the hyporheic denitrification Damkhöler number defined as $Da_{den} = r_{den}\langle T\rangle$. If denitrification starts immediately after stream water enters the HZ, that is $\tau_{oxy} = 0$, R_{HZ} is limited only by how much nitrogen that is transported to the HZ and is highest when $\langle T\rangle$ and Da_{den} is low. Moreover, R_{HZ} is exponentially related to the oxygen Damkhöler number, defined according to $Da_{oxy} = \langle T\rangle/\tau_{oxy}$. Increasing Da_{oxy} increase R_{HZ}, since it leads to longer time for the nitrogen within anoxic conditions. The diversified impact that the two Damkhöler numbers have on R_{HZ} means there exists an optimal residence time in the HZ, $\langle T\rangle_{opt}$, which leads to a maximal R_{HZ}, given that the biogeochemical conditions of the stream are constant. The optimal residence time is a function of both characteristic timescales $1/r_{den}$ and τ_{oxy} according to:

$$\langle T\rangle_{opt} = \left(\frac{\tau_{oxy}}{2} + \sqrt{\left(\frac{\tau_{oxy}}{2}\right)^2 + \frac{\tau_{oxy}}{r_{den}}}\right) \quad (4.6)$$

Subsequently there also exist an optimal Damkhöler number defined according to $Da_{den,opt} = \langle T \rangle_{opt} r_{den}$. Comparing the current Da_{den} in a specific reach with $Da_{den,opt}$, provides valuable guidance when designing stream restorations. If $Da_{den} < Da_{den,opt}$, R_{HZ} is reaction controlled and increases with increasing $\langle T \rangle$. Contradictory, if $Da_{den} > Da_{den,opt}$, R_{HZ} is transport controlled and decreases with increasing $\langle T \rangle$, since the inverse relationship between $\langle T \rangle$ and $\langle W \rangle$ leads to that less nitrogen is transported into the HZ and subjected to denitrification. In reality, hyporheic denitrification is a much more complex process than what equation 4.3 and 4.5 indicates and it varies e.g. with concentrations of nitrate and labile dissolved organic carbon; microbial abundance; and temperature. Nevertheless, previous works have indicated that HEF velocities and residence times control the variability of R_{HZ} to a large extent (Zarnetske et al. 2011; Harvey et al. 2013), which makes the equations derived here important tools when evaluating the reach-scale mass removal.

4.2.2 Current hyporheic nitrogen removal at the national scale

In Paper III, the current hyporheic nitrogen removal rate, R_{HZ}, and subsequently the relative nitrogen mass removal, D, was estimated in all stream segments in Sweden in agricultural areas with nitrogen leakage and with an annual mean discharge smaller than 1 m^3/s. These stream segments together represented 33.5% of the full stream network in Sweden and equations 4.3 and 4.5 were parameterized for all stream segments according to section 3.7.2.

The resulting wide pdfs of the hyporheic nitrogen removal rate, R_{HZ}, (Figure 11) reflect the impact of the spatial variability in stream hydraulics between stream segments. At mean discharge conditions (MQ), 75% of the segments had R_{HZ} between 0.053 and 0.551 day^{-1}, and the median R_{HZ} over all segments was 0.2562 $days^{-1}$. A literature review, performed as part of Paper III, showed that stream system denitrification rates, R_{sys}, estimated from tracer tests in snowy and warm-temperate climates, vary between approximately 0.05 and 0.52 day^{-1}, with an interquartile range between 0.03 and 0.36 day^{-1}. Thus, the results in Paper III are in well agreement with existing estimations in previous studies, given that the main channel nitrogen removal rate R_{MC} is small enough to be neglected.

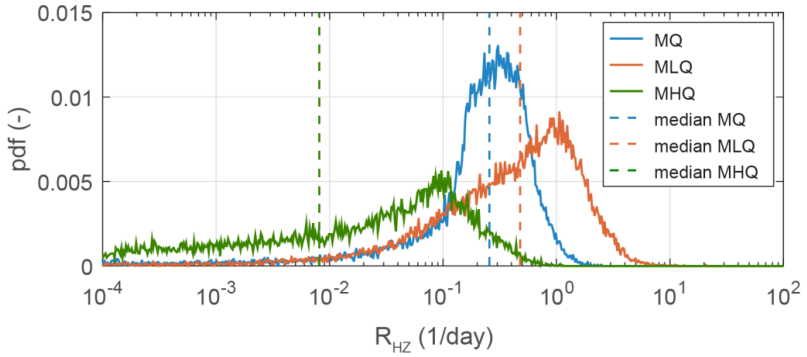

Figure 11. Probability density functions of the system reaction rate, R_{HZ}, in all small local agricultural stream reaches in Sweden at yearly mean discharge (MQ), yearly mean low discharge (MLQ) and yearly mean high discharge (MHQ) conditions. (Modified from Paper III)

Furthermore, the estimated current R_{HZ} was largely dependent on the discharge conditions (Figure 11). An increase in discharge in all reaches from MQ to high mean discharge (HMQ) resulted in a decrease in the current R_{HZ} to a median of 0.008 (0.000-0.13) days^{-1} (values in parentheses represent the inner quartile). In contrast, a decrease in discharge from MQ to low mean discharge (LMQ) leads to an increase in the current R_{HZ} to a median of 0.479 (0.053-1.575) days^{-1}. This large variability with discharge is due to the relationship between stream hydraulics and HEF, and the fact that $\langle T \rangle$ was estimated for all reaches utilizing Equation 3.20. High discharges generally lead to large Froude numbers and consequently high $\langle W \rangle$ and low $\langle T \rangle$. It should be noted here that the relationship between in-stream discharge and hyporheic flow is complex and widely discussed, since discharge varies with both time and space (Ward et al., 2019) and impacts different types of HEF drivers differently (Wondzell et al., 2019). Nevertheless, this study showed that under MLQ conditions approximately 85% of all stream segments had a current R_{HZ} that was transport controlled, i.e., $Da_{den} > Da_{den,opt}$. However, under higher discharge conditions, the situation was shifted, with 28% and 9% of transport controlled reaches in MQ and MHQ conditions respectively. This shift is essential to account for in designing stream restoration measures, which will be discussed later in this Section as well as in Section 4.2.3.

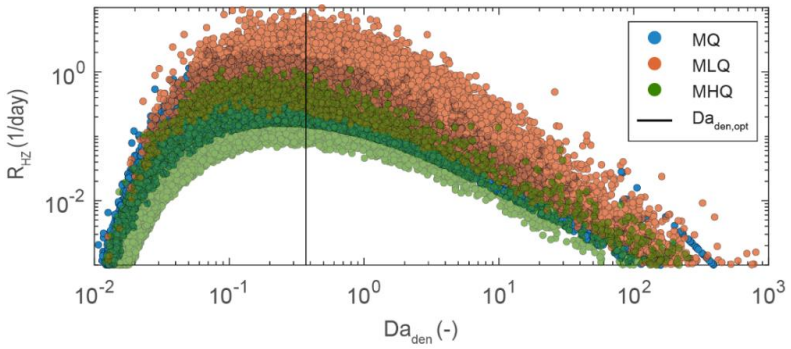

Figure 12. The hyporheic removal rate, R_{HZ}, as a function of the Damkhöler number Da at conditions of yearly mean discharge (MQ), yearly mean low discharge (MLQ) and yearly mean high discharge (MHQ). The black vertical line denotes the optimal Damkhöler number $Da_{den,opt}$. Presented results are based on the assumption that ε=0.1, r_{HZ}=0.1 h^{-1} and τ_{oxy}=1 h while stream hydraulics varies between stream reaches (Modified from Paper III).

The calculated R_{HZ} values were subsequently used to estimate the relative mass removal (D) for all small agricultural stream segments in Sweden, assuming a main channel nitrogen removal rate $R_{MC} = 0$. It resulted in a median D of 4.9 % (0.5-14.1 %), 0.1 % (0.0-1.0 %), and 30.2 % (3.3-63.7 %), for MQ, MHQ and MLQ, respectively. Subsequently, the network effect on the mass removal was assessed by aggregating D of all segments from the source of the nitrogen load to the recipient, utilizing Equation 3.7, and multiplied by the yearly nitrogen load to each reach segment. This aggregation resulted in a total absolute mass removal in agricultural reaches, MR_{tot}, of 4060.5, 11628 and 289 tons per year, in MQ, MLQ and MHQ conditions respectively. Comparing these numbers with the total load of nitrogen to all small agricultural reaches in Sweden resulted in an estimated total HZ relative mass removal, D_{tot}, of 13%, 38% and 0.1% in MQ, MLQ and MHQ discharge conditions respectively.

4.2.3 Potential hyporheic nitrogen removal at the national scale

The theoretical potential for nitrogen removal in the HZ through restoration measures in local agricultural stream segments was also estimated in Paper III by comparing the current R_{HZ} distribution (the variation between segments) with the distribution of potential R_{HZ}, i.e. R_{HZ} under optimal hyporheic conditions, when $\langle T \rangle = \langle T \rangle_{opt}$. Modelling results show that in MQ conditions, the pdf of the potential R_{HZ} in all stream segments had a median of 0.518 days^{-1}, with 75% of the reaches between 0.184 days^{-1} and 1.215 days^{-1}, which is a small increase compared to the estimated current removal rates (Figure 13a). Similar patterns were found when estimating the potential D, which during MQ conditions had a median value of 9.4%, compared to the estimated current median value of 4.9% (Figure 13b).

Aggregating this result over the full network resulted in a relative mass removal, D_{tot}, which was 15, 2 and 62%, in MQ, MHQ and MLQ respectively, which is an increase in mass removal with 2, 1 and 24 percentage points. This large spatiotemporal variability in the mass removal enhancement potential indicates that stream restorations could be a useful strategy, but only if implemented in the right streams and designed for the right discharge conditions. It is also possible that the potential is slightly underestimated, since it relies on the assumption that restoration measures only impact the residence time in the HZ and not the in-stream residence time, which constitutes a major control for mass removal according to equation 4.3. In reality many stream restoration designs, such as embankments that cause steps in the WSP, likely increase both X/U and R_{HZ}.

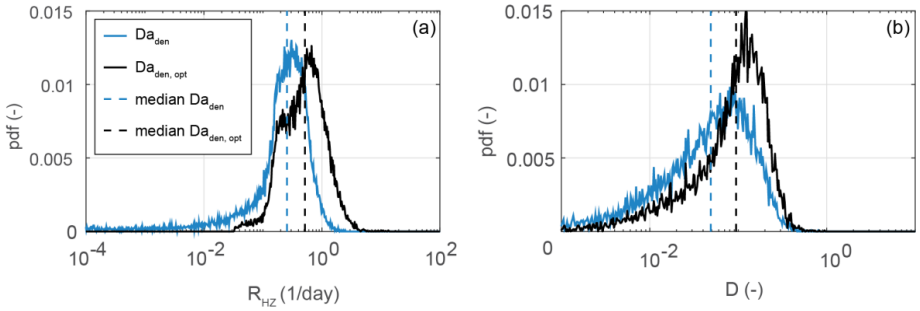

Figure 13. Variability in a) the current and potential hyporheic removal rate, R_{HZ} and b) the current and potential relative mass removal, D, in all local agricultural stream reaches during mean flow conditions (MQ). Presented results are based on the assumption that ε=0.1, r_{den}=0.1 h^{-1} and τ_{oxy}=1 h in all reaches, while stream hydraulics varies between stream reaches.(Modified from Paper III)

Finally, it should be noted that this investigation does not provide any information regarding which type of stream restoration measures can achieve the optimal hyporheic conditions. However, it was recognized that to alter mass removal in transport controlled reaches, the average hyporheic residence time should be increased, while in reaction controlled reaches, residence times needs to be lower is thus desired to increase mass removal in these reaches. The task of designing remediation actions is further complicated since transition between transport- and reaction-controlled conditions with time can be expected in some streams.

4.2.4 Impacts of stream restoration design on nitrogen mass removal

The estimated potential for enhancing nitrogen mass removal in the HZ through stream restoration presented in Section 4.2.2 is merely theoretical. However, the possibility of reaching the identified potential for nitrogen mass removal through a few simple restoration measures was examined in Papers I and III by comparing mass removal in current geomorphological conditions in Tullstorps Brook and Malsta Brook, respectively, with a set of modelled restoration scenarios presented

in Section 3.7.1. The current geomorphological conditions are from here on referred to as the base-case conditions.

In general, the results from the scenario analysis show that it is possible to increase the nitrogen mass removal at the reach scale through changes in the stream hydromorphology. However, the results also show that designing the stream restoration measures is delicate and that there is a risk that a certain design has no impact or even lowers the nitrogen mass removal compared to the current hydromorphologic conditions. Furthermore, the effect of some designs may depend on the discharge conditions, and thus may vary in time. To determine the optimal stream restoration design for improved water quality, first, the local stream must be assessed for its nitrogen removal status, and then the restoration design must be chosen to optimize mass removal over time. Below, details from the scenario analysis are presented and discussed, pointing out the different aspects that are important to consider, including if the depth of the HZ is constrained by the geology and if the system reaction rate is transport or reaction controlled at different discharges.

In Paper I, mass removal was calculated from the observed hydraulic head fluctuations along a specific stream reach in Tullstorps Brook (base-case conditions) and compared with mass removal in a theoretical reach of the same length and slope but with a step-shaped WSP (section 3.7.1). The steps were shown to increase the HEF velocity, $\langle W \rangle$, and decrease the average residence time, $\langle T \rangle$, but the impact on the hyporheic nitrogen removal rate was largely dependent on the assumed HZ depth and the length of the steps (Figure 14). If the HZ was constrained to 1.9 cm, which was indicated by the tracer test, the natural streambed resulted in the highest mass removal. This is because that depth, in combination with the assumption of $r_{den} = 0.1$ h^{-1} and $\tau_{oxy} = 1$ h, indicated the nitrogen removal in the HZ was reaction limited ($Da_{den} < Da_{den,opt}$) and that $\langle T \rangle$ and Da_{den} needed to be altered in order for the mass removal to increase. Steps were shown to increase $\langle W \rangle$ and decrease $\langle T \rangle$, thus having an unwanted impact on mass removal. However, when assuming a larger HZ depth, the increase in $\langle W \rangle$ caused only a minor decrease in $\langle T \rangle$ (since $\langle T \rangle = 2\varepsilon/\langle W \rangle$) and the step-shaped WSP led to substantially larger mass removal than the more natural hydraulic head fluctuations. Consequently, larger steps (longer and higher) needed a deeper HZ to be effective, compared to shorter steps. When the HZ was assumed to be infinitely deep, the size of the step did have no impact on the HEF variables, and the stream slope alone controlled the HEF. Note that the dynamic head at the streambed-water interface was assumed not to change as a result of stream restoration. In reality, the dynamic hydraulic head gradients might change but will likely not impact the results considerably since the static head gradients dominated as drivers of HEF in the streams investigated in this thesis.

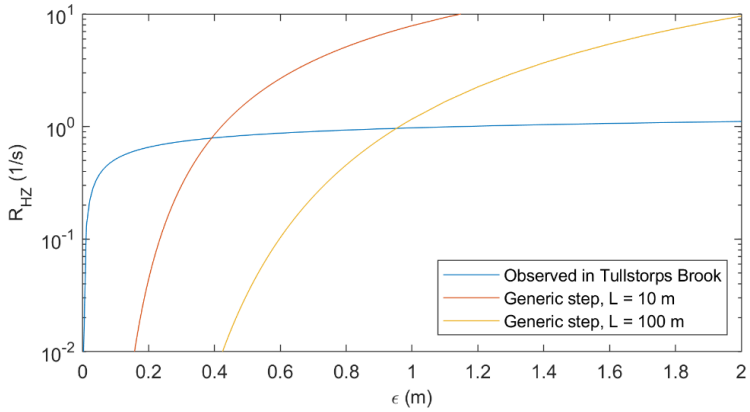

Figure 14. The nitrogen removal rate, R_{HZ}, as a function of hyporheic zone depth, ε, derived assuming hydraulic head variations along the streambed estimated from measurements in the Tullstorps Brook, and hydraulic head distributions shaped as a generic horizontal step. Two different step sizes were tested, which differed in length (L) and height (H), but had the same ratio height/length equal to the stream slope. (Modified from Paper I).

In Paper III, restoration designs, including embankments (steps) and changes of streambed hydraulic conductivity, were tested in Malsta Brook by combining hydraulic modelling in HEC-RAS and the HM model (section 3.7.1). Furthermore, three different in-stream discharge rates were tested in HEC-RAS to account for the impact of discharge on the removal. As in the national scale investigation (section 4.2.2) $\langle T \rangle$ and Da_{den} was largely dependent on discharge. At the base-case condition, the lowest discharge resulted in $Da_{den} > Da_{den,opt}$, and the mean and high discharge led to $Da_{den} < Da_{den,opt}$. Thus, for stream restoration measures to be effective under a variety of conditions, they need to have a bidirectional impact on $\langle T \rangle$, i.e., restoration measures should increase the residence time under high discharge conditions and decrease the hyporheic residence time under low discharge conditions.

In fact, the scenario analysis in Malsta Brook showed that the implemented embankments impacted $\langle T \rangle$ differently depending on discharge. At low flow conditions, all designs increased $\langle W \rangle$ due to altered hydraulic head gradients at the stream bottom across the weirs. The increase in $\langle W \rangle$ resulted in lower $\langle T \rangle$ and Da_{den}, than under the base-case condition (Figure 15a, blue circles). The weir height controlled the magnitude of the change in Da_{den}, and the lower weirs heights of 0.2 m lead to a hyporheic nitrogen removal rate closer to the optimum compared to the base-case.

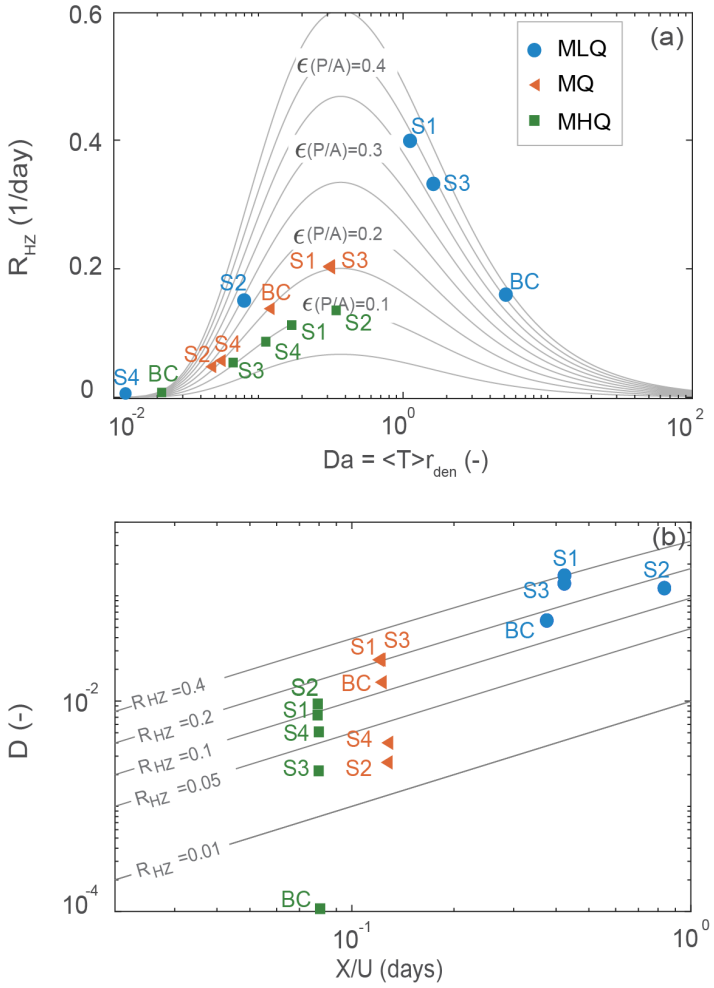

Figure 15. Effect of stream different stream restoration design scenarios (S1-S4) in Malsta Brook compared to base-case (BC) conditions on a) the denitrification Damkhöler number and its impact on the nitrogen removal rate of the hyporheic zone, R_{HZ}, and b) the in stream residence time, and its impact on the relative mass removal, D. The scenarios were tested in mean low discharge conditions (MLQ), mean discharge conditions (MQ) and mean high discharge conditions (MHQ). The grey lines in the upper panel represents different values of the ratio $\frac{P}{A}\frac{\langle W\rangle\langle T\rangle}{2} = \varepsilon\frac{P}{A}$, and the gray lines in the lower panel represents different values of R_{HZ} in 1/day. In both the base-case conditions and the different scenarios the hyporheic zone depth was assumed to be ε=0.05, and the denitrification rate r_{den} = 0.1 h^{-1} and the oxygen consumption time τ_{oxy}= 1 h. (Modified from Paper III)

In contrast, weir heights of 0.4 m transformed the system from being transport limited to reaction limited and had a negative impact on the hyporheic nitrogen removal rate compared to the base-case (Figure 15a, markers S2 and S4). In addition to the decrease in $\langle T \rangle$, the weirs resulted in higher stream depth (A/P), which exaggerated the negative impact on R_{HZ}. During high flow conditions, the implementation of weirs had a smoothening effect on the WSP across the smaller scales, more than it increased the total variance of the WSP. The smoothening of the WSP increased the slope of the WSP power spectrum, without increasing its overall magnitude, which in turn led to a decrease in $\langle W \rangle$ and the wanted altering of $\langle T \rangle$ and Da_{den}. This smoothening effect was shown to increase with weir height and decrease with distance between weirs.

Finally, at the MQ condition, large weir heights (designs S2 and S4) resulted in an increase in Da_{den}, thus reflecting the impacts found in low flow conditions, while low weir heights (designs S1 and S3) decreased Da_{den}, and thus had the same effects as all structures under the high flow conditions. Since R_{HZ} was reaction controlled at mean flow conditions, designs S1 and S3 were effective for increasing mass removal.

Increasing hydraulic conductivity effectively modified the average hyporheic residence time, and the impact was relatively simple to predict since K is inversely proportional to $\langle T \rangle$. An increase in K will increase the system denitrification rate of mass removal if the HZ system is transport-limited and have the opposite effect if the hyporheic system is reaction-limited. The challenge of this design lies instead in finding K that optimize the hyporheic nitrogen removal rate over the full range of discharges in a reach. Furthermore, it might be complicated to change the streambed substrate without negative impacts on the established streambed ecology. Because of these challenges, local actions at targeted places, such as the in-stream structures tested here, might be a preferred restoration design

Although this thesis mainly focused on the nitrogen removal rate in the HZ, it was noticed that in cases with low X/U, a change in R_{HZ} within the potential range will have limited impact on D. In such cases, increases in the in-stream residence time X/U by, for example, changing the course of the stream or installing flood-zones alongside the stream will not only be more simple to design but possibly more effective than using measures aiming to alter HEF. It should also be noticed that the measures creating steps in the water surface profile probably often lowers the in stream velocity and thus increases the in-stream residence time, although this was not the case in most of the design scenarios tested in Malsta Brook (Figure 15b). There, the mass removal was controlled by the increased in-stream residence time rather than the slight decrease in R_{HZ} only in one case, and that was the design with the highest ratio H/L, tested under low flow conditions (Figure 15b, blue markers).

4.3 Surface water and deep groundwater interactions

The fate and transport of solutes that discharge into streams with groundwater can be influenced by the HEF at the surface water interface. To investigate in which geographic and hydromorphologic conditions this influence is most prevalent, the spatial variability in the ratio between the deep ground water flow (dGWF) velocity and the HEF velocity, noted δ_W was investigated in Paper IV. The results show that both dGWF and HEF velocities generally varied largely between the different stream segments but that the HEF velocities generally were larger than the dGWF velocities and thus, that the ratio was much smaller than one in most reaches (Figure 17). In reaches where the ratio is much smaller than 1, one can expect the groundwater to discharge into small pinholes, with a relatively high velocity compared to that estimated by the groundwater model alone (Mojarrad et al., 2022). In reaches where the velocity ratio is larger than one, the impact of the HEF on the dGWF discharge pattern is most likely minor or nonexisting. However, it should be noted that the dGWF discharge velocities presented in Paper IV result from particles released at a 500 m depth. Higher discharge velocities, which are less impacted by the HEF, are expected for shallower groundwater discharge. Contaminants that discharges into the stream with deep and old groundwater, and for which this analysis is relevant, are e.g., radioactive compounds leaching from high level radioactive waste depositories (Alexander et al. 2003, Kautsky et al. 2013), or legacy nitrogen (Tesoriero et al., 2013, Van Meter et al., 2016).

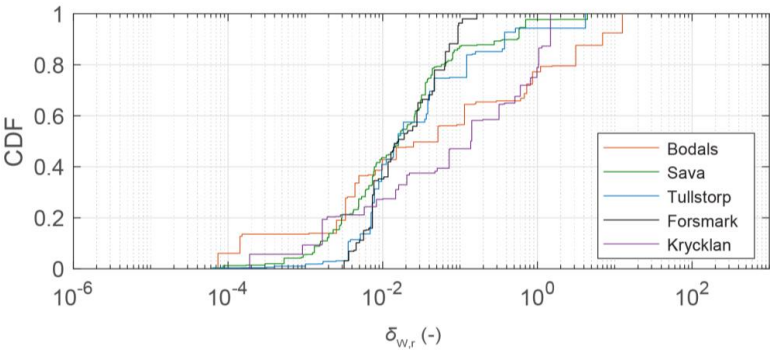

Figure 16. The empirical cumulative distribution function of the ratio between the average deep GWF discharge velocity and the average flow weighted HEF velocity at the streambed-water interface, $\delta_{W,r}$, in all stream segments in the five catchments modelled in Paper IV. (From Paper IV)

Subsequently, a multivariate regression analysis was performed to explain the observed variability of Figure 16. One significant model (p-value <0.05) was found at the reach scale, which explained approximately 50% of the observed variability between the stream segments. The model showed that the velocity ratio decreased with the magnitude of the WSP PSD, $a_{WSP,r}$ and increased with the slope of the

WSP PSD, $b_{WSP,r}$, the catchment average hydraulic conductivity, K_r, and the catchment average slope, S_r, according to:

$$\delta_{W,r} = 4.65 \cdot 10^{-3}\, a_{WSP,r}^{-0.52}\, b_{WSP,r}^{1.92}\, K_r^{0.74}\, S_r^{1.30} \quad (4.7)$$

where the index r indicates that the variables were averaged at the reach scale. Equation 4.7 shows that the impact of the HEF on the dGWF is most prevalent in stream reaches with high variability in the WSP, where the variability mainly occurs over relatively short spatial scales, which are not correlated with the surrounding landscape topographic variations. This type of variability is likely highest in the low slope sub-catchment (low S_r) with low hydraulic conductivity (low K_r), thus in the most downstream parts of the regional catchments, where the discharging dGWF velocity is low. When the same analysis was performed with dependent and independent variables averaged at the intermediate catchment scale, the variability in $\delta_{W,IC}$ between catchments was relatively small and no significant models were found at the 95% confidence level.

5 FUTURE PROSPECTS

Although the modelling framework presented here is based on current state-of-the-art methods and theories, there are several sources of uncertainty, which could be reduced or better understood by validation of parts of the model against observations, more thorough sensitivity analysis or development of the conceptual and mathematical model. In this section, I present a few ideas for improvement of the specific methodology used in this thesis, as well as more general thoughts on the future prospects of HEF research in relation to stream restoration.

A large part of the structural errors and parameter uncertainties of the HM model are related to the assessment of the hydraulic head fluctuations at the streambed-water interface. Although equation 2.9 has been used to estimate the multiscale dynamic hydraulic head in several previous studies (Wörman et al., 2006, Stonedahl et al., 2010, Mojarrad et al., 2019), it has not been validated against distributed hydraulic head measurements along a streambed outside the lab. In future studies a thorough validation of the generality of the equation and its empirical coefficients would be valuable. It would also be interesting to assess how uncertainty in the small scale hydraulic head data is reflected in the extrapolation of the PSDs, and in the resulting HEF velocities. Furthermore, the parameter uncertainties could be limited in future studies by utilizing evolving measurement techniques for the assessment of both stream bottom variation and WSPs (Passalacqua et al., 2015, Woodget et al., 2017).

There are also several uncertainties related to the biochemical part of the model framework. Studies have e.g. shown that the biological activity needed for denitrification is mostly abundant in the few top centimeters of the streambed

sediments (Berner, 1980; Inwood et al., 2007) and, furthermore, in hot spots along the streambed (Briggs et al., 2015). Also temporal variation in the reaction rate probably exists due to temporal variation in controlling parameters such as temperature, discharger or nutrient concentration. Thus, the model, which now has biogeochemical coefficients that are constant in time as well as space, could be improved by accounting for these controls on the biocemical variables or simply by considering an arbitrary distribution of coefficients. Furthermore, more realistic nitrogen transformation within the HZ can possibly be represented in the model by using for example Mondo kinetics. However, more complex models would require thorough calibration and validation against not only conservative tracer tests as in this study but also against reactive tracer tests (Haggerty et al., 2009, Mulholland et al., 2009, Riml et al., 2016) or direct observations of the biogeochemistry of the streambed (Zarnetske et al., 2011, Schaper et al., 2018). Non-conservative tracer tests would also be useful to parameterize or validate the relatively simple model framework developed in this study.

This thesis provides equations for the integrated mass removal in stream reaches, and shows that it depends on both the in-stream residence time and the system mass removal rate. However, the focus when assessing the nationwide stream restoration efficiency was mainly on the removal rate within the HZ. To be more practically useful, future studies should assess the impact of stream restoration on both the removal rate and the in-stream residence time. Other limitations for stream restoration designs, such as risk for flooding due to the implementation of steps, should also be accounted for. Furthermore, the dynamic aspects of HEF and nitrogen removal is not accounted for in this study other than through a simple test of three different discharges in Paper III, which shows that the mass removal in streams probably is highly variable over time. To optimize restoration practices over time an improved representation of the temporal variations in both stream hydraulics, HEF, groundwater discharge and biogeochemical reactions is needed. Furthermore, the largest impact on mass removal should be correlated with the highest nitrogen load to the stream, and it is still debated how this load varies with time as well as space (Minaudo et al., 2019; Liu et al, 2020; Royer et al., 2006).

The modelling framework developed here, as well as the large body of other models that have been developed during the last decades, have greatly improved our understanding of HEF and how it impacts solute transport. However, recent review studies ask for a higher degree of conceptual consensus between different approaches for studying HEF and points out that in order to be useful new models needs to clearly specify the limits and conditions for which they are valid (Knapp and Kelleher, 2020, Ward and Packman, 2019, Lewandowski et al., 2019). This thesis takes a step towards a larger consensus between different theories by cross-validating two common approaches for assessing vertical, pressure driven HEF in small alluvial streams. However, there are deviations from the cross-validation that are specifically evident in the three streams with high discharge, Froudes number,

Reynolds number and relative submergence of bedforms, which indicates model limitations that needs to be investigated further. Moreover, both approaches relies on mathematical modelling for quantification of HEF. To describe reality, direct measurements of the HEF is also needed and this thesis points out that observations preferably should be done at a wide range of spatial scales. Monitoring over long timescales are also essential in stream restoration projects to evaluate the efficiency of specific stream restoration designs.

6 CONCLUSIONS

This thesis highlights the importance of the hyporheic zone as a biochemical and mechanical filter for solutes transported through the stream network, which can largely influence the quality of both discharging groundwater and the surface water in local stream reaches and downstream recipients. By using mathematical modelling and field measurements this thesis explains the close correlation between streambed geomorphology and HEF, and shows that stream restoration measures can enhance the HEF and the nitrogen mass removal in the HZ. Through the cross-validation of HEF variables estimated with two different approaches, this thesis has contributed to an increased physical understanding of how HEF is driven in small alluvial streams with moderate slope, shallow depth and low discharge. Furthermore, the consensus between the models connects theories that previously were quite dis-joint and provides a physically based tool for parameterizing network scale solute transport models, including the upscaling of HEF from very small scales (<1m) to the scale of river-basin wide reaches. Predictive tools for upscaling are essential to estimate the impact of specific stream restoration measures on solute transport at the catchment scale, which is the scale at which water managers commonly works and monitoring most often is done.

More explicitly, this thesis assess the differences in magnitude between static and dynamic head driven HEF at different scales and hydraulic conditions, which is important to understand when designing stream-specific restoration measures. Section 5 discusses several ways that the established modelling framework and the input data, can be improved, which would increase the certainty of the results of this thesis. Nevertheless, based on the data collected in Paper II in mall alluvial streams with moderate slopes, low discharges and shallow stream depths, hydraulic head gradients across scales of approximately 10 centimeters to 5 meters constituted the main drivers of the hyporheic flux across the streambed. Furthermore, the static head fluctuations dominated over dynamic head fluctuations as the main driving mechanism of HEF, even when gradients were observed over scales less than a meter and in most cases when the HEF power spectrum were extrapolated down to the scale of one centimeter. The finding that static head gradients drives the dominating part of HEF makes DEMs developed from Lidar measurements, if reliable and with high resolution, potentially useful as input data in hydraulic models for estimating HEF in stream networks were

measurements are lacking. When the methodology was tested in Paper IV, it resulted in reach scale average HEF velocities of between approximately 10^{-7} m/s and 10^{-5} m/s, which varied both within and between five regional catchments of Sweden. This variation is consistent with general tracer test results and was statistically explained using regression analysis, which showed that the fractal properties of the longitudinal hydraulic head variations at the stream bottom provides an important control on the reach scale average HEF velocity. Increasing hydraulic head power specral density (PSD) magnitude results in a proportional increase in the hyporheic flux across the streambed, while increases in the hydraulic head PSD slope decreases the average exchange velocity. In general, a smoother water surface profile, often related to a highly submerged streambed topography, will result in a lower HEF velocity. The thesis also showed that there is a linear relationship between the reach average HEF velocity and the reach scale Froudes number, which is valid both if the static or dynamic head fluctuations is the main driving mechanism of HEF.

The second part of this thesis considers the derivation of analytical solutions to the solute transport equations with account taken to HEF and nitrogen mass removal in the hyporheic zone. The results shows that the HZ nitrogen removal rate is linearly related to the denitrification rate along streamlines but also is largely controlled by the characteristic flow of water through the HZ. Specifically, there exists an optimal hyporheic residence time, corresponding to a specific Damköhler number, that result in a maximum nitrogen removal rate within the hyporheic zone, given constant denitrification and oxygen consumption timescales. If the average residence time is lower than the optimal, mass removal in the hyporheic zone is transport controlled, while it is reaction controlled if the average residence time is higher than the optimal. By using the developed solutions to assess the reach-scale relative nitrogen removal together with a thorough assessment of stream hydraulics, the model estimated that during annual mean discharge conditions the current nitrogen removal within the hyporheic zone of all small agricultural streams in Sweden of approximately 13 % of the total nitrogen load to these streams. This assessment is unique since the modelling approach accounts both for the cumulative effects of HEF and mass removal in the dense network of small, low order streams, which has been simplified or neglected in most previous studies. Assuming optimal hyporheic conditions in all streams indicated a potential to enhance nitrogen removal with 2, 1 and 25 percentage points through stream restoration in mean, low and high discharge conditions respectively. Even though the potential was relatively low at the two higher discharges, the large spatiotemporal variation in the potential between reaches makes stream restoration a promising strategy at some sites, given the restorations are designed for the condition with highest enhancement potential.

A scenario analysis of stream restoration efforts in Malsta Brook, which modified the streambed hydraulic conductivity and created steps in the water surface profile, indicates that these measures in theory can reach the estimated optimal nitrogen removal at the stream reach scale. Interestingly, features that created steps in the water surface, of the right size and length, did have both positive and negative impact on the average exchange velocity through the hyporheic zone, depending on the assumed discharge conditions. Thereby the measures could be effective in both high and low flow conditions. However, this means there is also a risk that restoration actions decrease the nitrogen removal in some conditions. Thus, before stream restoration can be applied in a specific stream there is a need to thoroughly investigate the current site-specific biogeochemical as well as hydromorphological conditions. One important aspect is to determine from data if the mass removal within the hyporheic zone is transport or reaction controlled. Furthermore, it is relevant to have a site-specific understanding of which processes that are driving the current HEF, e.g., if the dynamic or static head is most important; or if there exists head gradients at a specific scale that drives HEF and therefore should be preserved. Thus, designing stream restoration for the removal of nitrogen in the hyporheic zone is a delicate matter but if carefully done, and if implemented over large areas, stream restorations could be useful for reducing the nitrogen load from Swedish agriculture to downstream watercourses and the Baltic sea.

References

Åkesson, A., Wörman, A., Riml, J., & Seibert, J. (2016). Change in streamflow response in unregulated catchments in Sweden over the last century, Water Resour. Res.,. 52(8), 5847-5867. https://agupubs.onlinelibrary.wiley.com/doi/abs/10.1002/2015WR018116

Alexander, R. B., Smith, R. A., & Schwarz, G. E. (2000). Effect of stream channel size on the delivery of nitrogen to the Gulf of Mexico. Nature, 403(6771), 758-761. https://doi.org/10.1038/35001562

Alexander, W.R., Smith, P.A., Mckinley, I.G. (2003) Chapter 5 Modelling radionuclide transport in the geological environment: a case study from the field of radioactive waste disposal. In: Scott, E.M., (Eds.) Radioactivity in the environment, (pp. 109-145), Elsevier,

Ameli, A. A., McDonnell, J. J., & Bishop, K. (2016). The exponential decline in saturated hydraulic conductivity with depth: a novel method for exploring its effect on water flow paths and transit time distribution. Hydrological Processes, 30(14), 2438-2450. https://onlinelibrary.wiley.com/doi/abs/10.1002/hyp.10777

Anderson, J. K., Wondzell, S. M., Gooseff, M. N., Haggerty, R. (2005) Patterns in stream longitudinal profiles and implications for hyporheic exchange flow at the H.J. Andrews Experimental Forest, Oregon, USA, Hydrological Processes, 19(50), 2931-2949.

Aubeneau, A. F., Martin, R. L., Bolster, D., Shumer, R., Jerolmack, D., & Packman, A. I. (2015). Fractal patterns in river bed morphology produce fractal scaling of water storage times. Geophysical Research Letters, 42, 5309–5315.

Azinheira, D. L., Scott, D. T., Hession, W., & Hester, E. T. (2014). Comparison of effects of inset floodplains and hyporheic exchange induced by in-stream structures on solute retention. Water Resources Research, 50(7), 6168-6190. http://dx.doi.org/10.1002/2013WR014400

Azizian, M., Grant, S. B., Kessler, A. J., Cook, P. L. M., Rippy, M. A., & Stewardson, M. J. (2015). Bedforms as Biocatalytic Filters: A Pumping and Streamline Segregation Model for Nitrate Removal in Permeable Sediments. Environmental Science & Technology, 49, 10993−11002

Bencala, K. E. (1993). A Perspective on Stream-Catchment Connections. Journal of the North American Benthological Society, 12(1), 44-47. http://www.jstor.org/stable/1467684

Bencala, K. E., Gooseff, M. N., & Kimball, B. A. (2011). Rethinking hyporheic flow and transient storage to advance understanding of stream-catchment connections. Water Resources Research, 47(3), http://dx.doi.org/10.1029/2010WR010066

Bencala, K. E., & Walters, R. A. (1983). Simulation of Solute Transport in a Mountain Pool-and-Riffle Stream: A Transient Storage Model. Water Resources Research, 19(3), 718-724.

Berg, J., Burch, J., Cappuccitti, D., Filoso, S., Fraley-McNeal, L., Goerman, D., et al. (2014). Recommendations of the Expert Panel to Define Removal Rates for Individual Stream Restoration Projects. In: Chesapeake Bay Program (2014) Ellicott City, MD.

Berner, R. A. (1980), Early Diagenesis: A Theoretical Approach. Princeton, New Jersey: Priceton University Press.

Bernhardt, E. S., Palmer, M. A., Allan, J. D., Alexander, G., Barnas, K., Brooks, S., Carr, J., Clayton, S., Dahm, C., Follstad-Shah, J., Galat, D., Gloss, S., Goodwind, P., Hart, D., Hassett, B., Jenkinson, R., Katz, S., Kondolf, G. M., Lake, P. S., Lave, R., Meyer, J. L., O'donnell, T. K., Pagano, L., Powell B. & Sudduth, E. (2005). Syntesizing U.S. River Restoration Efforts. Sience, 308(5722), 636-637.

Bernot, M. J., & Dodds, W. K. (2005). Nitrogen Retention, Removal, and Saturation in Lotic Ecosystems. Ecosystems, 8(4), 442-453. https://doi.org/10.1007/s10021-003-0143-y

Betterle, A., Jaeger, A., Posselt, M., Coll, C., Benskin, J. P., & Schirmer, M. (2021). Hyporheic exchange in recirculating flumes under heterogeneous bacterial and morphological conditions. Environmental Earth Sciences, 80(6), 234. https://doi.org/10.1007/s12665-021-09472-2

Beven, K. (2006). A manifesto for the equifinality thesis. Journal of Hydrology, 320(1–2), 18-36. http://www.sciencedirect.com/science/article/pii/S002216940500332X

Birgand, F., Skaggs, R. W., Chescheir, G. M., & Gilliam, J. W. (2007). Nitrogen Removal in Streams of Agricultural Catchments—A Literature Review. Critical Reviews in Environmental Science and Technology, 37(5), 381-487.

Boano, F., Camporeale, C., Revelli, R., & Ridolfi, L. (2006). Sinuosity-driven hyporheic exchange in meandering rivers. Geophysical Research Letters, 33(18).

Boano, F., Demaria, A., Revelli, R., & Ridolfi, L. (2010). Biogeochemical zonation due to intrameander hyporheic flow. Water Resources Research, 46(2), http://dx.doi.org/10.1029/2008WR007583

Boano, F., Harvey, J. W., Marion, A., Packman, A. I., Revelli, R., Ridolfi, L., & Wörman, A. (2014). Hyporheic flow and transport processes: Mechanisms, models, and biogeochemical implications.Reviews of Geophysics 52(4), 603-679. https://agupubs.onlinelibrary.wiley.com/doi/abs/10.1002/2012RG000417

Boano, F., Revelli, R., & Ridolfi, L. (2009). Quantifying the impact of groundwater discharge on the surface–subsurface exchange. Hydrological Processes, 23(15), 2108-2116. http://dx.doi.org/10.1002/hyp.7278

Boano, F., Revelli, R., & Ridolfi, L. (2011). Water and solute exchange through flat streambeds induced by large turbulent eddies. Journal of Hydrology, 402(3), 290-296. http://www.sciencedirect.com/science/article/pii/S0022169411002034

Bottacin-Busolin, A., & Marion, A. (2010). Combined role of advective pumping and mechanical dispersion on time scales of bed form-induced hyporheic exchange. Water Resources Research, 46(8), W08518.

Bottacin-Busolin, A., Marion, A., Musner, T., Tregnaghi, M., & Zaramella, M. (2011). Evidence of distinct contaminant transport patterns in rivers using tracer tests and a multiple domain retention model. Advances in Water Resources, 34(6), 737-746.

Boudreau, B. P. (2000). The mathematics of early diagenesis: from worms to waves. Reviews of Geophysics, 38(3), 389-416.

Boyer, E. W., Alexander, R. B., Parton, W. J., Li, C., Butterbach-Bahl, K., Donner, S. D., et al. (2006). Modeling denitrification in terrestrial and aquatic ecosystems at regional scales. Ecological Applications, 16(6), 2123-2142. https://esajournals.onlinelibrary.wiley.com/doi/abs/10.1890/1051-0761%282006%29016%5B2123%3AMDITAA%5D2.0.CO%3B2

Briggs, M. A., Day-Lewis, F. D., Zarnetske, J. P., & Harvey, J. W. (2015). A physical explanation for the development of redox microzones in hyporheic flow.

Geophysical Research Letters, 42(11), 4402-4410. http://dx.doi.org/10.1002/2015GL064200

Briggs, M. A., Gooseff, M. N., Arp, C. D., & Baker, M. A. (2009). A method for estimating surface transient storage parameters for streams with concurrent hyporheic storage. Water Resources Research, 45(4), W00D27.

Brunke, M., & Gonser, T. (1997). The ecological significance of exchange processes between rivers and groundwater. Freshwater Biology 37(1), 1-33. https://onlinelibrary.wiley.com/doi/abs/10.1046/j.1365-2427.1997.00143.x

Böhlke, J. K., Antweiler, R. C., Harvey, J. W., Laursen, A. E., Smith, L. K., Smith, R. L., & Voytek, M. A. (2009). Multi-scale measurements and modeling of denitrification in streams with varying flow and nitrate concentration in the upper Mississippi River basin, USA. Biogeochemistry, 93(1), 117-141. http://pubs.er.usgs.gov/publication/70042388

Böhlke, J. K., Harvey, J. W., & Voytek, M. A. (2004). Reach-scale isotope tracer experiment to quantify denitrification and related processes in a nitrate-rich stream, midcontinent United States. Limnology and Oceanography, 49(3), 821-838. http://dx.doi.org/10.4319/lo.2004.49.3.0821

Cardenas, M. B. (2009). A model for lateral hyporheic flow based on valley slope and channel sinuosity. Water Resources Research, 45, W01501.

Cardenas, M. B. (2015). Hyporheic zone hydrologic science: A historical account of its emergence and a prospectus. Water Resources Research, 51(5), 3601-3616. https://agupubs.onlinelibrary.wiley.com/doi/abs/10.1002/2015WR017028

Cardenas, M. B., & Wilson, J. L. (2004). Impact of heterogeneity, bed forms, and stream curvatureon subchannel hyporheic exchange. Water Resources Research, 40(8), W08307.

Cardenas, M. B., & Wilson, J. L. (2007). Hydrodynamics of coupled flow above and below a sediment–water interface with triangular bedforms. Advances in Water Resources, 30(3), 301-313.

Carrera, J., Sánchez-Vila, X., Benet, I., Medina, A., Galarza, G., & Guimerà, J. (1998). On matrix diffusion: formulations, solution methods and qualitative effects. Hydrogeology Journal, 6(1), 178-190. https://doi.org/10.1007/s100400050143

Caruso, A., Ridolfi, L., & Boano, F. (2016). Impact of watershed topography on hyporheic exchange. Advances in Water Resources, 94, 400-411. https://www.sciencedirect.com/science/article/pii/S0309170816301671

Chen, Y., Wang, Y., Chia, B., & Wang, D. (2021). Upstream-downstream water quality comparisons of restored channelized streams. Ecological Engineering, 170, 106367. https://www.sciencedirect.com/science/article/pii/S0925857421002226

Choi, J., Harvey, J. W., & Conklin, M. H. (2000). Characterizing multiple timescales of stream and storage zone interaction that affect solute fate and transport in streams. Water Resour. Res., 36, 1511.

Chow, V. T. (1959). Open-channel hydraulics. New York: McGraw-Hill.

Chow, V. T., Maidment, D. R., & Mays, L. W. (1988). Applied hydrology. New York: McGraw-Hill

Conant, B., Cherry, J. A., & Gillham, R. W. (2004). A PCE groundwater plume discharging to a river: influence of the streambed and near-river zone on contaminant distributions. Journal of Contaminant Hydrology, 73(1), 249-279. https://www.sciencedirect.com/science/article/pii/S0169772204000555

Drummond, J. D., Covino, T. P., Aubeneau, A. F., Leong, D., S., P., Shumer, R., & Packman, A. I. (2012). Effects of solute breakthrough curve tail truncation on residence time estimates: A synthesis of solute tracer injection studies. Journal of Geophysical Research, 117, G00N08.

Duff, J. H., & Triska, F. J. (2000). 8 - Nitrogen Biogeochemistry and Surface–Subsurface Exchange in Streams A2 - Jones, Jeremy B. In: P. J., Mulholland, (Eds.), Streams and Ground Waters, (pp 197-220), San Diego: Academic Press.

Dufour, S., & Piégay, H. (2009). From the myth of a lost paradise to targeted river restoration: forget natural references and focus on human benefits. River Research and Applications, 25(5), 568-581. http://dx.doi.org/10.1002/rra.1239

Earon, R., Riml, J., Wu, L., & Olofsson, B. (2020). Insight into the influence of local streambed heterogeneity on hyporheic-zone flow characteristics. Hydrogeology Journal, 28(8), 2697-2712. https://doi.org/10.1007/s10040-020-02244-5

EEA. (2018). European watersAssessment of status and pressures 2018. EEA Report 7/2018. Luxembourg: Publications Office of the European Union. doi:10.2800/303664.

EEA. (2019). Nutrient enrichment and eutrophication in Europe's seas - Moving towards a healthy marine environment. EEA Report 14/2019, .Luxembourg: Publications Office of the European Union. doi:10.2800/092643.

EEA. (2022). Nutrient trends in European Water Bodies. Available online: https://www.eea.europa.eu/data-and-maps/daviz/rivers-nutrient-trend-4/#tab-dashboard-01 (accessed on 12 April 2022)

Elliott, H. A. (1990). Transfer of solutes into and out of streambeds. (PhD). California Institution of Technology, Passadena, California.

Elliott, H. A., & Brooks, H. N. (1997a). Transfer of non sorbing solutes to a streambed with bed forms: Theory. Water Resources Research, 33(1), 123-136.

Elliott, H. A., & Brooks, H. N. (1997b). Transfer of nonsorbing solutes to a streambed with bed forms: Laboratory experiments. Water Resources Research, 33(1), 137-151.

Ensign, S. H., & Doyle, M. W. J. J. o. G. R. B. (2006). Nutrient spiraling in streams and river networks. J. Geophys. Res., 111, G04009, doi:10.1029/2005JG000114.

Fehér, J., Gáspár, J., Szurdiné-Veres, K., Kiss, A., Kristensen, P., Peterlin, M., et al. (2012). Hydromorphological alterations and pressures in European rivers, lakes, transitional and coastal waters. Thematic assessment for EEA Water 2012. Euoropean Topic Center/Inland, costal, marine waters Technical Report 2/2012. Prague. ETC.

Fehlman, H. M. (1985). Resistance components and velocity distributions of open channel flows over bedforms. (MSc). Colorado State University, Fort Collins, Colorado.

Findlay, S., & Sobczak, W. V. (2000). 12 - Microbial Communities in Hyporheic Sediments. In J. B. Jones & P. J. Mulholland (Eds.), Streams and Ground Waters (pp. 287-306). San Diego: Academic Press.

Fischer, H. B., List, J. E., Koh, C. R., Imberger, J., & Brooks, N. H. (1979). Mixing in Inland and Coastal Waters. San Diego: Accademic Press.

Fisher, T. R., Fox, R. J., Gustafson, A. B., Koontz, E., Lepori-Bui, M., & Lewis, J. (2021). Localized Water Quality Improvement in the Choptank Estuary, a Tributary of Chesapeake Bay. Estuaries and Coasts, 44(5), 1274-1293. https://doi.org/10.1007/s12237-020-00872-4

Galloway, J. N., Aber, J. D., Erisman, J. W., Seitzinger, S. P., Howarth, R. W., Cowling, E. B., & Cosby, B. J. (2003). The Nitrogen Cascade. BioScience, 53(4), 341-356. https://doi.org/10.1641/0006-3568(2003)053[0341:TNC]2.0.CO;2

Galloway, J. N., Dentener, F. J., Capone, D. G., Boyer, E. W., Howarth, R. W., Seitzinger, S. P., et al. (2004). Nitrogen Cycles: Past, Present, and Future. Biogeochemistry, 70(2), 153-226. https://doi.org/10.1007/s10533-004-0370-0

Gomez-Velez, J. D., & Harvey, J. W. (2014). A hydrogeomorphic river network model predicts where and why hyporheic exchange is important in large basins. Geophysical Research Letters, 41(18), 6403-6412. http://dx.doi.org/10.1002/2014GL061099

Gomez-Velez, J. D., Harvey, J. W., Cardenas, B. M., & Kiel, B. A. (2015). Denitrification in the Mississippi River network controlled by flow through river bedforms. Nature Geoscience.

Gomez-Velez, J. D., Krause, S., & Wilson, J. L. (2014). Effect of low-permeability layers on spatial patterns of hyporheic exchange and groundwater upwelling. Water Resour. Res. 50, 5196–5215. https://agupubs.onlinelibrary.wiley.com/doi/abs/10.1002/2013WR015054

Gooseff, M. N., Hall, J. R. O., & Tank, L. J. (2007). Relating transient storage to channel complexity in streams of varying land use in Jackson Hole, Wyoming. Water Resources Research, 43. W01417, doi:10.1029/2005WR004626.

Gooseff, M. N., Wondzell, S. M., Haggerty, R., & Anderson, J. (2003). Comparing transient storage modeling and residence time distribution (RTD) analysis in geomorphically varied reaches in the Lookout Creek basin, Oregon, USA. Advances in Water Resources, 26(9), 925-937.

Gordon, R. P., Lautz, L. K., & Daniluk, T. L. (2013). Spatial patterns of hyporheic exchange and biogeochemical cycling around cross-vane restoration structures: Implications for stream restoration design. Water Resources Research, 49(4), 2040-2055. http://dx.doi.org/10.1002/wrcr.20185

Grant, S. B., Gomez-Velez, J. D., & Ghisalberti, M. (2018). Modeling the Effects of Turbulence on Hyporheic Exchange and Local-to-Global Nutrient Processing in Streams. 54(9), 5883-5889. https://agupubs.onlinelibrary.wiley.com/doi/abs/10.1029/2018WR023078

Grant, S. B., Stolzenbach, K., Azizian, M., Stewardson, M. J., Boano, F., & Bardini, L. (2014). First-Order Contaminant Removal in the Hyporheic Zone of Streams: Physical Insights from a Simple Analytical Model. Environmental Science & Technology, 48(19), 11369-11378. http://dx.doi.org/10.1021/es501694k

Gupta, A., & Cvetkovic, V. (2000). Temporal moment analysis of tracer discharge in streams: Combined effect of physicochemical mass transfer and morphology. Water Resources Research, 36(10), 2985-2997.

Haggerty, R., Martí, E., Argerich, A., von Schiller, D., & Grimm, N. B. (2009). Resazurin as a "smart" tracer for quantifying metabolically active transient storage in stream ecosystems. J. Geophys. Res., 114, G03014. https://agupubs.onlinelibrary.wiley.com/doi/abs/10.1029/2008JG000942

Haggerty, R., McKenna, S. A., & Meigs, L. C. (2000). On the late-time behavior of tracer test breakthrough curves. 36(12), 3467-3479. https://agupubs.onlinelibrary.wiley.com/doi/abs/10.1029/2000WR900214

Haggerty, R., Wondzell, S. M., & Johnson, M. A. (2002). Power-law residence time distribution in the hyporheic zone of a 2nd-order mountain stream. Geophysical Research Letters, 29(13), 18-11-18-14. http://dx.doi.org/10.1029/2002GL014743

Hancock, P. J. (2002). Human impacts on the stream-groundwater exchange zone. Environ Manage, 29(6), 763-781.

Harvey, J. W., & Bencala, K. E. (1993). The Effect of streambed topography on surface-subsurface water exchange in mountain catchments. Water Resources Research, 29(1), 89-98. https://agupubs.onlinelibrary.wiley.com/doi/abs/10.1029/92WR01960

Harvey, J. W., Böhlke, J. K., Voytek, M. A., Scott, D., & Tobias, C. R. (2013). Hyporheic zone denitrification: Controls on effective reaction depth and contribution to whole-stream mass balance. Water Resources Research, 49(10), 6298-6316. http://dx.doi.org/10.1002/wrcr.20492

Harvey, J. W., & Wagner, B. J. (2000). 1 - Quantifying Hydrologic Interactions between Streams and Their Subsurface Hyporheic Zones. In J. B., Jones & P. J., Mulholland (Eds.), Streams and Ground Waters (pp. 3-44). San Diego: Academic Press.

Hassan, M. A., Tonina, D., Beckie, R. D., & Kinnear, M. (2015). The effects of discharge and slope on hyporheic flow in step-pool morphologies. Hydrological Processes, 29(3), 419-433. http://dx.doi.org/10.1002/hyp.10155

Hays, J. R. (1966). Mass transport mechanisms in open channel flow: 138. Nashville, Tennessee: Vanderbilt University.

Hedin, L. O., von Fischer, J. C., Ostrom, N. E., Kennedy, B. P., Brown, M. G., & Robertson, G. P. (1998). Thermodynamic Constraints on Nitrogen Transformations and Other Biogeochemical Processes at Soil-Stream Interfaces. Ecology, 79(2), 684-703. http://www.jstor.org/stable/176963

HELCOM. (2021). HELCOM Baltic Sea Action Plan – 2021 update. 31. Helsinki, Finland: Baltic Marine Environment Protection Commission – Helsinki Comission.

HELCOM. (2018). Sources and pathways of nutrients to the Baltic Sea. Baltic Sea Environment Proceedings No. 153. Helsinki, Finland: Baltic Marine Environment Protection Commission – Helsinki Comission.

Hester, E. T., & Doyle, M. W. (2008). In stream geomorphic structures as drivers for hyporheic exchange. Water Resources Research, 44.

Hester, E. T., & Gooseff, M. N. (2010). Moving Beyond the Banks: Hyporheic Restoration Is Fundamental to Restoring Ecological Services and Functions of Streams. Environmental Science & Technology, 44(5), 1521-1525.

Hester, E. T., & Gooseff, M. N. (2011). Hyporheic Restoration in Streams and Rivers. In Simon, A., Bennett, S. J., Castro, J. M., (Ed) Stream Restoration in Dynamic Fluvial Systems (pp. 167-187). Washington DC: American Geophysical Union.

Hester, E. T., Hammond, B., & Scott, D. T. (2016). Effects of inset floodplains and hyporheic exchange induced by in-stream structures on nitrate removal in a headwater stream. Ecological Engineering, 97, 452-464. http://www.sciencedirect.com/science/article/pii/S092585741630564X

Hino, M. (1968). Equilibrium-range spectra of sand waves formed by flowing water. Journal of Fluid Mechanics, 34(3), 565-573. https://www.cambridge.org/core/article/equilibrium-range-spectra-of-sand-waves-formed-by-flowing-water/4A58FF4D8D92A64D0C70067DE04D0067

Holmes, R. M., Jones, J. B., Fisher, S. G., & Grimm, N. B. (1996). Denitrification in a nitrogen-limited stream ecosystem. Biogeochemistry, 33(2), 125-146. https://doi.org/10.1007/BF02181035

Howarth, R. (2014). Nitrogen in Freshwater Systems and Estuaries Nitrogen☆. In Reference Module in Earth Systems and Environmental Sciences: Elsevier.

Hvorslev, M. J. (1951). Time lag and soil permeability in ground-water observations. Vicksburg, Miss.: Waterways Experiment Station, Corps of Engineers, U.S. Army.

Inwood, S.E., Tank, J.L. & Bernot, M.J. (2007). Factors Controlling Sediment Denitrification in Midwestern Streams of Varying Land Use. Microb Ecol 53, 247–258. https://doi.org/10.1007/s00248-006-9104-2

Janssen, F., Cardenas, M. B., Sawyer, A. H., Dammrich, T., Krietsch, J., & de Beer, D. (2012). A comparative experimental and multiphysics computational fluid dynamics study of coupled surface–subsurface flow in bed forms. Water Resources Research 48(8), W08514. https://agupubs.onlinelibrary.wiley.com/doi/abs/10.1029/2012WR011982

Jones, J. B., Fisher, S. G., & Grimm, N. B. (1995). Nitrification in the Hyporheic Zone of a Desert Stream Ecosystem. Journal of the North American Benthological Society 14(2), 249-258. https://www.journals.uchicago.edu/doi/abs/10.2307/1467777

Jones, J. B., & Holmes, R. M. (1996). Surface-subsurface interactions in stream ecosystems. Trends in Ecology and Evolution, 11(6).

Kasahara, T., & Hill, A. R. (2006). Hyporheic exchange flows induced by constructed riffles and steps in lowland streams in southern Ontario, Canada. Hydrological Processes, 20, 4287–4305.

Kilpatrick, F. A., & Wilson, J. F. (1989). Measurement of time of travel in streams by dye tracing. U.S. Geological Survey, Techniques of Water-Resources Investigations 3-A9. USGS. http://pubs.er.usgs.gov/publication/twri03A9

Knapp, J. L. A., & Kelleher, C. (2020). A Perspective on the Future of Transient Storage Modeling: Let's Stop Chasing Our Tails. Water Resources Research, 56, e2019WR026257. https://agupubs.onlinelibrary.wiley.com/doi/abs/10.1029/2019WR026257

Krause, S., Hannah, D. M., Fleckenstein, J. H., Heppell, C. M., Kaeser, D., Pickup, R., et al. (2011). Inter-disciplinary perspectives on processes in the hyporheic zone. Ecohydrology, 4(4), 481-499. https://onlinelibrary.wiley.com/doi/abs/10.1002/eco.176

Krause, S., Tecklenburg, C., Munz, M., & Naden, E. (2013). Streambed nitrogen cycling beyond the hyporheic zone: Flow controls on horizontal patterns and depth distribution of nitrate and dissolved oxygen in the upwelling groundwater of a lowland river. J. Geophys. Res. Biogeosci., 118(1), 54-67. https://agupubs.onlinelibrary.wiley.com/doi/abs/10.1029/2012JG002122

Krug, A. (1993). Drainage history and land use pattern of a Swedish river system — their importance for understanding nitrogen and phosphorus load. Hydrobiologia, 251(1), 285-296. https://doi.org/10.1007/BF00007188

Lammers, R. W., & Bledsoe, B. P. (2017). What role does stream restoration play in nutrient management? Critical Reviews in Environmental Science and Technology, 47(6), 335-371. https://doi.org/10.1080/10643389.2017.1318618

Laudon, H., Taberman, I., Ågren, A., Futter, M., Ottosson-Löfvenius, M., & Bishop, K. (2013). The Krycklan Catchment Study—A flagship infrastructure for hydrology, biogeochemistry, and climate research in the boreal landscape. Water Resources Research, 49(10), 7154-7158. https://agupubs.onlinelibrary.wiley.com/doi/abs/10.1002/wrcr.20520

Lautz, L. K., & Fanelli, R. M. (2008). Seasonal biogeochemical hotspots in the streambed around restoration structures. Biogeochemistry, 91(1), 85-104. journal article. http://dx.doi.org/10.1007/s10533-008-9235-2

Lautz, L. K., Siegel, D. I., & Bauer, R. L. J. H. P. A. I. J. (2006). Impact of debris dams on hyporheic interaction along a semi-arid stream. Hydrological Processes, 20(1), 183-196.

Lee, A., Aubeneau, A. F., & Cardenas, M. B. (2020). The Sensitivity of Hyporheic Exchange to Fractal Properties of Riverbeds. Water Resources Research 56(5), e2019WR026560. https://agupubs.onlinelibrary.wiley.com/doi/abs/10.1029/2019WR026560

Lewandowski, J., Arnon, S., Banks, E., Batelaan, O., Betterle, A., Broecker, T., et al. (2019). Is the Hyporheic Zone Relevant beyond the Scientific Community?, Water, 11(11), 2230. https://www.mdpi.com/2073-4441/11/11/2230

Lindström, G., Pers, C., Rosberg, J., Strömqvist, J., & Arheimer, B. (2010). Development and testing of the HYPE (Hydrological Predictions for the Environment) water quality model for different spatial scales. Hydrology Research, 41(3-4), 295-319. https://doi.org/10.2166/nh.2010.007

Lowe, W. H., & Likens, G. E. (2005). Moving Headwater Streams to the Head of the Class. BioScience, 55(3), 196-197. https://doi.org/10.1641/0006-3568(2005)055[0196:MHSTTH]2.0.CO;2

Magliozzi, C., Coro, G., Grabowski, R. C., Packman, A. I., & Krause, S. (2019). A multiscale statistical method to identify potential areas of hyporheic exchange for river restoration planning. Environmental Modelling & Software, 111, 311-323. https://www.sciencedirect.com/science/article/pii/S1364815218301476

Mallard, J., McGlynn, B., & Covino, T. (2014). Lateral inflows, stream-groundwater exchange, and network geometry influence stream water composition. Water Resources Research 50(6), 4603-4623. https://agupubs.onlinelibrary.wiley.com/doi/abs/10.1002/2013WR014944

Marklund, L., Wörman, A., Geier, J., Simic, E., & Dverstorp, B. (2008). Impact of Landscape Topography and Quaternary Overburden on the Performance of a Geological Repository of Nuclear Waste. Nuclear Technology, 163(1), 165-179. https://doi.org/10.13182/NT08-A3979

Marzadri, A., Tonina, D., & Bellin, A. (2011). A semianalytical three-dimensional process-based model for hyporheic nitrogen dynamics in gravel bed rivers. Water Resources Research 47(11). W11518. https://agupubs.onlinelibrary.wiley.com/doi/abs/10.1029/2011WR010583

Marzadri, A., Tonina, D., McKean, J. A., Tiedemann, M. G., & Benjankar, R. M. (2014). Multi-scale streambed topographic and discharge effects on hyporheic exchange at the stream network scale in confined streams. Journal of Hydrology, 519, 1997-2011. http://www.sciencedirect.com/science/article/pii/S0022169414007689

Mason, S. J. K., McGlynn, B. L., & Poole, G. C. (2012). Hydrologic response to channel reconfiguration on Silver Bow Creek, Montana. Journal of Hydrology, 438–439, 125-136. http://www.sciencedirect.com/science/article/pii/S0022169412002077

McClain, M. E., Boyer, E. W., Dent, C. L., Gergel, S. E., Grimm, N. B., Groffman, P. M., Hart, S. C., Harvey, J. W., Johnston, C. A., Mayorga, E., McDowell, W. H., & Pinay, G. (2003). Biogeochemical Hot Spots and Hot Moments at the Interface of Terrestrial and Aquatic Ecosystems. Ecosystems, 6(4), 301-312. http://www.jstor.org/stable/3659030

McDonnell, J.J., McGuire, K., Aggarwal, P., Beven, K.J., Biondi, D., Destouni, G., Dunn, S., James, A., Kirchner, J., Kraft, P., Lyon, S., Maloszewski, P., Newman, B., Pfister, L., Rinaldo, A., Rodhe, A., Sayama, T., Seibert, J., Solomon, K., Soulsby, C., Stewart, M., Tetzlaff, D., Tobin, C., Troch, P., Weiler, M., Western, A., Wörman, A. & Wrede, S. How old is streamwater? Open questions in catchment transit time conceptualization, modelling and analysis. Hydrological Processes, 24(12), 1745-1754.

Melland, A. R., Fenton, O., & Jordan, P. (2018). Effects of agricultural land management changes on surface water quality: A review of meso-scale catchment research. Environmental Science & Policy, 84, 19-25. https://www.sciencedirect.com/science/article/pii/S1462901117309784

Minaudo, C., Dupas, R., Gascuel-Odoux, C., Roubeix, V., Danis, P.-A., & Moatar, F. (2019). Seasonal and event-based concentration-discharge relationships to identify catchment controls on nutrient export regimes. Advances in Water Resources, 131, 103379. https://www.sciencedirect.com/science/article/pii/S030917081830616X

Mojarrad BB (2021). Multi-Scale Surface Water-Groundwater Interaction: Implications for Groundwater Discharge Patterns (PhD), KTH Royal Institute of Technology, Stockholm, Sweden.

Mojarrad, B. B., Riml, J., Wörman, A., & Laudon, H. (2019). Fragmentation of the Hyporheic Zone Due to Regional Groundwater Circulation. Water Resources Research, 55(2), 1242-1262. https://doi.org/10.1029/2018WR024609

Morén, I., Riml, J. and Wörman, A. (2018) In-stream water management strategies for reducing nutrient loads to the Baltic Sea. BONUS Soils2Sea Deliverable 4.4. Stockholm , Sweden: Royal Institute of Technology (KTH). http://soils2sea.eu/xpdf/d4_4-bonus-soils2sea-in-stream-water-management-strategies.pdf

Montgomery, D. C., Peck, E. A., & Vining, G. G. (2012). Introduction to linear regression analysis (5th ed.). 821 p. Hoboken: Wiley.

Mulholland, P. J., Hall, R. O., Sobota, D. J., Dodds, W. K., Findlay, S. E. G., Grimm, N. B., et al. (2009). Nitrate removal in stream ecosystems measured by 15N addition experiments: Denitrification. Limnology and Oceanography, 54(3), 666-680. http://dx.doi.org/10.4319/lo.2009.54.3.0666

Mulholland, P. J., Helton, A. M., Poole, G. C., Hall, R. O., Hamilton, S. K., Peterson, B. J., et al. (2008). Stream denitrification across biomes and its response to anthropogenic nitrate loading. Nature, 452(7184), 202-205. http://dx.doi.org/10.1038/nature06686

Nagaoka, H., & Ohgaki, S. J. W. R. (1990). Mass transfer mechanism in a porous riverbed. Water Research, 24(4), 417-425.

Nagorski, S. A., & Moore, J. N. (1999). Arsenic mobilization in the hyporheic zone of a contaminated stream. Water Resources Research 35(11), 3441-3450. https://agupubs.onlinelibrary.wiley.com/doi/abs/10.1029/1999WR900204

Neilson, B. T., Chapra, S. C., Stevens, D. K., & Bandaragoda, C. (2010). Two-zone transient storage modeling using temperature and solute data with multiobjective calibration: 1. Temperature. Water Resour. Res., 46(12). https://agupubs.onlinelibrary.wiley.com/doi/abs/10.1029/2009WR008756

Neilson, B. T., S. C. Chapra, D. K. Stevens, and C. Bandaragoda (2010), Two-zone transient storage modeling using temperature and solute data with multiobjective

calibration: 2. Temperature and solute, Water Resour. Res., 46, W12521, https://doi.org/10.1029/2009WR008759

Newcomer Johnson, T., Kaushal, S., Mayer, P., Smith, R., & Sivirichi, G. (2016). Nutrient Retention in Restored Streams and Rivers: A Global Review and Synthesis. Water, 8(4), 116. http://www.mdpi.com/2073-4441/8/4/116

Nikora, V., I., Sukhodolov, A. N., & Rowiński, P. M. (1997). Statistical sand wave dynamics in one-directional water flows. Journal of Fluid Mechanics, 351.

O'Connor, L. B., Hondzo, M., & Harvey, J. W. (2010). Predictive Modeling of Transient Storage and Nutrient Uptake: Implications for Stream Restoration. Journal of Hydraulic Engineering, 136(Special Issue on River Flow Hydrodynamics: Physical and Ecological Aspects), 1018-1032.

Ocampo, C. J., Oldham, C. E., & Sivapalan, M. (2006). Nitrate attenuation in agricultural catchments: Shifting balances between transport and reaction. Water Resources Research 42(1), W01408. https://agupubs.onlinelibrary.wiley.com/doi/abs/10.1029/2004WR003773

Opdyke, M. R., David, M. B., & Rhoads, B. L. (2006). Influence of Geomorphological Variability in Channel Characteristics on Sediment Denitrification in Agricultural Streams. Journal of Environmental Quality 35(6), 2103-2112. https://acsess.onlinelibrary.wiley.com/doi/abs/10.2134/jeq2006.0072

Orghidan, T. J. A. H. (2010). A new habitat of subsurface waters: the hyporheic biotope. Fundam. Appl. Limnol., 176(4), 291–302

Packman, A. I., & Bencala, K. E. (2000). 2 - Modeling Surface–Subsurface Hydrological Interactions. In J. B. Jones & P. J. Mulholland (Eds.), Streams and Ground Waters (pp. 45-80). San Diego: Academic Press.

Packman, A. I., Brooks, N. H., & Morgan, J. J. (2000). A physicochemical model for colloid exchange between a stream and a sand streambed with bed forms. Water Resources Research, 36(8), 2351-2361. http://dx.doi.org/10.1029/2000WR900059

Packman, A. I., Salehin, M., & Zaramella, M. (2004). Hyporheic Exchange with Gravel Beds: Basic Hydrodynamic Interactions and Bedform-Induced Advective Flows. Journal of hydraulic engineering, 130(7), 647-656.

Passalacqua, P., Belmont, P., Staley, D. M., Simley, J. D., Arrowsmith, J. R., Bode, C. A., et al. (2015). Analyzing high resolution topography for advancing the understanding of mass and energy transfer through landscapes: A review. Earth-Science Reviews, 148, 174-193. http://www.sciencedirect.com/science/article/pii/S0012825215300015

Pell, M., & Wörman, A. (2008). Biological Wastewater Treatment Systems. In Jørgensen, S. E., (Eds.) Ecosystem Ecology. (pp. 166-180) Amsterdam, The Netherlands: Elsevier

Pers, C. (2007). HBV-NP Model Manual, Hydrology nr 103. (80 p.) Norrköping, Sweden: SMHI

Petersen, R., Gíslason, G., & Vought, L. (1995). Rivers of the Nordic Countries. Ecosystems of the World, 22, 295-341.

Peterson, B. J., Wollheim, W. M., Mulholland, P. J., Webster, J. R., Meyer, J. L., Tank, J. L., et al. (2001). Control of Nitrogen Export from Watersheds by Headwater Streams. Science, 292(5514), 86-90.

Pinay, G., Peiffer, S., De Dreuzy, J.-R., Krause, S., Hannah, D. M., Fleckenstein, J. H., et al. (2015). Upscaling Nitrogen Removal Capacity from Local Hotspots to Low

Stream Orders' Drainage Basins. Ecosystems, 18(6), 1101-1120. https://doi.org/10.1007/s10021-015-9878-5

Pinder, G. F., & Sauer, S. P. (1971). Numerical Simulation of Flood Wave Modification Due to Bank Storage Effects. Water Resources Research 7(1), 63-70. https://agupubs.onlinelibrary.wiley.com/doi/abs/10.1029/WR007i001p00063

Rana, S. M. M., Scott, D. T., & Hester, E. T. (2017). Effects of in-stream structures and channel flow rate variation on transient storage. Journal of Hydrology, 548, 157-169. http://www.sciencedirect.com/science/article/pii/S0022169417301294

Refsgaard, J. C., Hansen, A. L., Højberg, A. L., Olesen, J. E., Hashemi, F., Wachniew, P., et al. (2019). Spatially differentiated regulation: Can it save the Baltic Sea from excessive N-loads? Ambio, 48(11), 1278-1289. https://www.ncbi.nlm.nih.gov/pmc/articles/PMC6814693/

Ren, J., Zhang, W., Yang, J., & Zhou, Y. (2019). Using water temperature series and hydraulic heads to quantify hyporheic exchange in the riparian zone. Hydrogeology Journal, 27(4), 1419-1437. https://doi.org/10.1007/s10040-019-01934-z

Riml, J., Morén, I., Wörman, A., Zieba, D., & Wachniew, P. (2016). Tracer Tests and the effect of solute retention and attenuation on the stream reach scale. BONUS Soils2Sea Deliverable 4.2. Stockholm, Sweden: Royal Institute of Technology (KTH). http://soils2sea.eu/xpdf/soils2sea_d4-2_10dec2016.pdf

Riml, J., & Wörman, A. (2011). Response functions for in-stream solute transport in river networks. Water Resources Research, 47(6), W06502, doi:10.1029/2010WR009412.

Riml, J., Wörman, A., Kunkel, U., & Radke, M. (2013). Evaluating the fate of six common pharmaceuticals using a reactive transport model: Insights from a stream tracer test. Sience of the Total Environment, 458-460, 344-354.

Rodhe, A., Nyberg, L., & Bishop, K. (1996). Transit Times for Water in a Small Till Catchment from a Step Shift in the Oxygen 18 Content of the Water Input. Water Resources Research 32(12), 3497-3511. https://agupubs.onlinelibrary.wiley.com/doi/abs/10.1029/95WR01806

Rodríguez-Iturbe, I., Rinaldo, A., Rigon, R., Bras, R. L., Marani, A., & Ijjász-Vásquez, E. (1992). Energy dissipation, runoff production, and the three-dimensional structure of river basins. Water Resources Research 28(4), 1095-1103. https://agupubs.onlinelibrary.wiley.com/doi/abs/10.1029/91WR03034

Rosberg, J. (2003). Modeling phosphorus transport and retention in river networks. (MSc), Uppsala University, Uppsala.

Royer, T. V., David, M. B., & Gentry, L. E. (2006). Timing of Riverine Export of Nitrate and Phosphorus from Agricultural Watersheds in Illinois: Implications for Reducing Nutrient Loading to the Mississippi River. Environmental Science & Technology, 40(13), 4126-4131. https://doi.org/10.1021/es052573n

Runkel, R. L. (2007). Toward a transport-based analysis of nutrient spiraling and uptake in streams. Limnol. Oceanogr. Methods, 5(1), 50-62. https://doi.org/10.4319/lom.2007.5.50

Rutherford, J. C., Chiu, T. W., Hatherell, T. V. J., Elliott, H. A., & Boyle, J. D. (1995). Modeling Benthic Oxygen Uptake by Pumping. Journal of Environmental Engineering, 121(1).

Saenger, N., Kitanidis, P. K., & Street, R. L. (2005). A numerical study of surface-subsurface exchange processes at a riffle-pool pair in the Lahn River, Germany. Water

Resources Research, 41(12), W12424. https://agupubs.onlinelibrary.wiley.com/doi/abs/10.1029/2004WR003875

Savant, S. A., Raible, D. D., & Thibodeaux, L. J. (1987). Convective Transport Within Stable River Sediments. Water Resources Research, 23(9).

Sawyer, A. H., Bayani Cardenas, M., & Buttles, J. (2011). Hyporheic exchange due to channel-spanning logs. Water Resources Research, 47(8), W08502. https://agupubs.onlinelibrary.wiley.com/doi/abs/10.1029/2011WR010484

Sawyer, A. H., Bayani Cardenas, M., & Buttles, J. J. W. R. R. (2012). Hyporheic temperature dynamics and heat exchange near channel-spanning logs, Water Resources Research, 48(1), W01529. https://doi.org/10.1029/2011WR011200

Sawyer, A. H., & Cardenas, M. B. (2012). Effect of experimental wood addition on hyporheic exchange and thermal dynamics in a losing meadow stream. Water Resources Research, 48(10), W10537. http://dx.doi.org/10.1029/2011WR011776

Schaper, J. L., Posselt, M., McCallum, J. L., Banks, E. W., Hoehne, A., Meinikmann, K., Shanafield, M. A., Batelaan, O. & Lewandowski, J. (2018). Hyporheic Exchange Controls Fate of Trace Organic Compounds in an Urban Stream. Environmental Science & Technology, 52(21), 12285-12294. https://doi.org/10.1021/acs.est.8b03117

Schindler, D. W. (1974). Eutrophication and recovery in experimental lakes: implications for lake management. Science, 184(4139), 897-899.

Schmadel, N. M., Ward, A. S., Kurz, M. J., Fleckenstein, J. H., Zarnetske, J. P., Hannah, D. M., et al. (2016). Stream solute tracer timescales changing with discharge and reach length confound process interpretation. Water Resources Research, 52(4), 3227-3245. https://agupubs.onlinelibrary.wiley.com/doi/abs/10.1002/2015WR018062

Schmid, B. H. (2003). Temporal moments routing in streams and rivers with transient storage Advances in Water Resources, 26(9), 1021-1027.

Shrivastava, S., Stewardson, M. J., & Arora, M. (2021). Influence of Bioturbation on Hyporheic Exchange in Streams: Conceptual Model and Insights From Laboratory Experiments. Water Resources Research, 57(2), e2020WR028468. https://agupubs.onlinelibrary.wiley.com/doi/abs/10.1029/2020WR028468

Singh, T., Wu, L., Gomez-Velez, J. D., Lewandowski, J., Hannah, D. M., & Krause, S. (2019). Dynamic Hyporheic Zones: Exploring the Role of Peak Flow Events on Bedform-Induced Hyporheic Exchange. Water Resources Research, 55(1), 218-235. https://agupubs.onlinelibrary.wiley.com/doi/abs/10.1029/2018WR022993

SMHI, 2021, Modelldata hela Sverige, Available online: https://vattenwebb.smhi.se/modelregion/ (accessed August 2022)

Song, J., Chen, X., Cheng, C. J. F. o. E. S., & China, E. i. (2010). Observation of bioturbation and hyporheic flux in streambeds. Frontiers of Environmental Science & Engineering in China, 4(3), 340-348.

Stewardson, M. J., Datry, T., Lamouroux, N., Pella, H., Thommeret, N., Valette, L., & Grant, S. B. (2016). Variation in reach-scale hydraulic conductivity of streambeds. Geomorphology, 259, 70-80. http://www.sciencedirect.com/science/article/pii/S0169555X16300216

Stonedahl, S. H., Harvey, J. W., Detty, J., Aubeneau, A., & Packman, A. I. (2012). Physical controls and predictability of stream hyporheic flow evaluated with a multiscale model. Water Resources Research, 48(10), W10513.

Stonedahl, S. H., Harvey, J. W., & Packman, A. I. (2013). Interactions between hyporheic flow produced by stream meanders, bars, and dunes. Water Resources Research, 49(9), 5450– 5461.

Stonedahl, S. H., Harvey, J. W., Wörman, A., Salehin, M., & Packman, A. I. (2010). A multiscale model for integrating hyporheic exchange from ripples to meanders. Water Resources Research, 46(12), W12539.

Storey, R. G., Williams, D. D., & Fulthorpe, R. R. (2004). Nitrogen processing in the hyporheic zone of a pastoral stream. Biogeochemistry, 69(3), 285-313. https://doi.org/10.1023/B:BIOG.0000031049.95805.ec

Stream Solute Workshop (1990). Concepts and Methods for Assessing Solute Dynamics in Stream Ecosystems. Journal of the North American Benthological Society, 9(2), 95-119 https://www.journals.uchicago.edu/doi/abs/10.2307/1467445

Tesoriero, A. J., Duff, J. H., Saad, D. A., Spahr, N. E., & Wolock, D. M. (2013). Vulnerability of Streams to Legacy Nitrate Sources. Environmental Science & Technology, 47(8), 3623-3629. https://doi.org/10.1021/es305026x

Teutschbein, C., Grabs, T., Laudon, H., Karlsen, R. H., Bishop, K., Simulating streamflow in ungauged basins under a changing climate: The importance of landscape characteristics. Journal of Hydrology, 561, 160-178. https://doi.org/10.1016/j.jhydrol.2018.03.060

Thackston, E. L., & Schnelle, K. B. (1970). Predicting Effects of Dead Zones on Stream Mixing. Journal of the Sanitary Engineering Division, 96(2), 319-331. https://ascelibrary.org/doi/abs/10.1061/JSEDAI.0001078

Thibodeaux, L. J., & Boyle, J. D. (1987). Bedform-generated convective transport in bottom sediment. Nature, 325(6102), 341-343. 10.1038/325341a0. http://dx.doi.org/10.1038/325341a0

Thompson, J., Pelc, C. E., Brogan, W. R., & Jordan, T. E. (2018). The multiscale effects of stream restoration on water quality. Ecological Engineering, 124, 7-18. https://www.sciencedirect.com/science/article/pii/S0925857418303537

Tonina, D., & Buffington, J. M. (2007). Hyporheic exchange in gravel bed rivers with pool-riffle morphology: Laboratory experiments and three-dimensional modeling. Water Resources Research, 43(1), W01421. http://dx.doi.org/10.1029/2005WR004328

Tonina, D., & Buffington, J. M. (2009). Hyporheic Exchange in Mountain Rivers I: Mechanics and Environmental Effects. Geography Compass, 3(3), 1063-1086. http:https://dx.doi.org/10.1111/j.1749-8198.2009.00226.x

Tonina, D., & Buffington, J. M. (2011). Effects of stream discharge, alluvial depth and bar amplitude on hyporheic flow in pool-riffle channels. Water Resources Research, 47(8), W08508. https://agupubs.onlinelibrary.wiley.com/doi/abs/10.1029/2010WR009140

Tóth, J. (1963). A theoretical analysis of groundwater flow in small drainage basins. Journal of Geophysical Research 68(16), 4795-4812. https://agupubs.onlinelibrary.wiley.com/doi/abs/10.1029/JZ068i016p04795

Triska, F. J., Duff, J. H., & Avanzino, R. J. (1993). The role of water exchange between a stream channel and its hyporheic zone in nitrogen cycling at the terrestrial-aquatic interface. Hydrobiologia, 251(1), 167-184. https://doi.org/10.1007/BF00007177

Tullstorpsån Ekonomisk Förening (2022). Tullstorpsåprojektet – Från källa till mynning. Available online: https://www.tullstorpsan.se/. (Accessed April 2022).

Turcotte, D. L. (1992). Fractals and chaos in geology and geophysics. Great Britain: Cambridge University Press

Van Meter, K. J., Basu, N. B., Veenstra, J. J., & Burras, C. L. (2016). The nitrogen legacy: emerging evidence of nitrogen accumulation in anthropogenic landscapes. Environmental Research Letters, 11(3), 035014. http://dx.doi.org/10.1088/1748-9326/11/3/035014

Vaux, W. G. (1962). Interchange of stream and intragravel water in a salmon spawning riffle. United States Fish and Widelife Service Special Scientific Report No. 405. Washington DC: University of Washington http://hdl.handle.net/2027/mdp.39015086538777

Vaux, W. G. (1968). Intragravel flow and interchange of water in a streambed. Fishery Bulletin, 66(3), 479-489.

Voermans, J. J., Ghisalberti, M., & Ivey, G. N. (2017). The variation of flow and turbulence across the sediment–water interface. Journal of Fluid Mechanics, 824, 413-437. https://www.cambridge.org/core/article/variation-of-flow-and-turbulence-across-the-sedimentwater-interface/E4ADF6CD754ADDF9482C8EDF611B91C7

Voermans, J. J., Ghisalberti, M., & Ivey, G. N. (2018). A Model for Mass Transport Across the Sediment-Water Interface. Water Resources Research, 54(4), 2799-2812. https://agupubs.onlinelibrary.wiley.com/doi/abs/10.1002/2017WR022418

Vought, L. B.-M., & Lacoursière, J. O. (2010). Restoration of Streams in the Agricultural Landscape. In: Eiseltová, M., (Eds.), Restoration of Lakes, Streams, Floodplains, and Bogs in Europe: Principles and Case Studies (pp. 225-242). Dordrecht: Springer Netherlands.

Ward, A. S., Kelleher, C. A., Mason, S. J. K., Wagener, T., McIntyre, N., McGlynn, B., Runkel, R. L. & Payn, R. A. (2017). A software tool to assess uncertainty in transient-storage model parameters using Monte Carlo simulations. Freshwater Science, 36(1), 195-217. https://www.journals.uchicago.edu/doi/abs/10.1086/690444

Ward, A. S., & Packman, A. I. (2019). Advancing our predictive understanding of river corridor exchange. Water, 6(1), e1327. https://onlinelibrary.wiley.com/doi/abs/10.1002/wat2.1327

Ward, A. S., Wondzell, S. M., Schmadel, N. M., Herzog, S., Zarnetske, J. P., Baranov, V., Blaen, P. J., Brekenfeld, N., Chu, R., Derelle, R., Drummond, J., Fleckenstein, J. H., Garayburu-Caruso, V., Graham, E., Hannah, D., Harman, C. J., Hixson, J., Knapp, J. L. A., Krause, S., Kurz, M. J., Lewandowski, J., Li, A., Martí, E., Miller, M., Milner, A. M., Neil, K., Orsini, L., Packman, A. I., Plont, S., Renteria, L., Roche, K., Royer, T., Segura, C., Stegen, J., Toyoda, J., Wells, J., & Wisnoski, N. I. (2019). Spatial and temporal variation in river corridor exchange across a 5th-order mountain stream network. Hydrol. Earth Syst. Sci., 23(12), 5199-5225. https://hess.copernicus.org/articles/23/5199/2019/

Ward, J. V., Tockner, K., Uehlinger, U., & Malard, F. (2001). Understanding natural patterns and processes in river corridors as the basis for effective river restoration. Regulated Rivers: Research & Management, 17(4-5), 311-323. http://dx.doi.org/10.1002/rrr.646

Welch, P. (1967). The use of fast Fourier transform for the estimation of power spectra: A method based on time averaging over short, modified periodograms. IEEE Transactions on Audio and Electroacoustics, 15(2), 70-73.

Winter, T. C., Harvey, J. W., Franke, O. L., & Alley, W. M. (1998). Ground water and surface water: A single resource. U.S. Geological Survey Circular 1139. Denver, Colorado: USGS http://pubs.er.usgs.gov/publication/cir1139

Woessner, W. W. (2000). Stream and Fluvial Plain Ground Water Interactions: Rescaling Hydrogeologic Thought. Groundwater 38(3), 423-429. https://ngwa.onlinelibrary.wiley.com/doi/abs/10.1111/j.1745-6584.2000.tb00228.x

Wohl, E., Lane, S. N., & Wilcox, A. C. (2015). The science and practice of river restoration. Water Resources Research, 51(8), 5974-5997. http://dx.doi.org/10.1002/2014WR016874

Wollheim, W. M., Vörösmarty, C. J., Peterson, B. J., Seitzinger, S. P., & Hopkinson, C. S. (2006). Relationship between river size and nutrient removal. Geophysical Research Letters, 33(6), L06410. https://agupubs.onlinelibrary.wiley.com/doi/abs/10.1029/2006GL025845

Wondzell, S. M. (2011). The role of the hyporheic zone across stream networks. Hydrological Processes 25(22), 3525-3532. https://onlinelibrary.wiley.com/doi/abs/10.1002/hyp.8119

Wondzell, S. M., Herzog, S. P., Gooseff, M. N., Ward, A. S., & Schmadel, N. M. (2019). Geomorphic Controls on Hyporheic Exchange Across Scales—Watersheds to Particles☆. In Reference Module in Earth Systems and Environmental Sciences: Elsevier.

Woodget, A. S., Austrums, R., Maddock, I. P., & Habit, E. (2017). Drones and digital photogrammetry: from classifications to continuums for monitoring river habitat and hydromorphology. WIREs Water, 4(4), e1222. https://onlinelibrary.wiley.com/doi/abs/10.1002/wat2.1222

Wroblicky, G. J., Campana, M. E., Valett, H. M., & Dahm, C. N. (1998). Seasonal variation in surface-subsurface water exchange and lateral hyporheic area of two stream-aquifer systems. Water Resources Research, 34(3), 317-328. https://agupubs.onlinelibrary.wiley.com/doi/abs/10.1029/97WR03285

Wu, L., Singh, T., Gomez-Velez, J., Nützmann, G., Wörman, A., Krause, S., & Lewandowski, J. (2018). Impact of Dynamically Changing Discharge on Hyporheic Exchange Processes Under Gaining and Losing Groundwater Conditions. Water Resources Research, 54(12), 10,076-10,093. https://agupubs.onlinelibrary.wiley.com/doi/abs/10.1029/2018WR023185

Wörman, A., Packman, A. I., Johansson, H., & Jonsson, K. (2002). Effect of flow-induced exchange in hyporheic zones on longitudinal transport of solutes in streams and rivers. Water Resources Research, 38(6), doi:0043-1397/02/2001WR00769.

Wörman, A., Packman, A. I., Marklund, L., Harvey, J. W., & Stone, S. (2007). Fractal topography and subsurface water flows form from fluvial bedforms to the continential sheild. Geophysical Research Letters, 34, L07402.

Wörman, A., Packman, A. I., Marklund, L., Harvey, J. W., & Stonedahl, S. H. (2006). Exact three-dimensional spectral solution to surface-groundwater interactions with arbitrary surface topography. Geophysical Research Letters, 33(7), L07402.

Wörman, A., & Wachniew, P. (2007). Reach scale and evaluation methods as limitations for transient storage properties in streams and rivers. Water Resources Research, 43(10), W10405.

Zarnetske, J. P., Gooseff, M. N., Brosten, T. R., Bradford, J. H., McNamara, J. P., & Bowden, W. B. (2007), Transient storage as a function of geomorphology, discharge, and

permafrost active layer conditions in Arctic tundra streams, Water Resour. Res., 43(7), W07410, doi:10.1029/2005WR004816.

Zarnetske, J. P., Haggerty, R., Wondzell, S. M., & Baker, M. A. (2011). Dynamics of nitrate production and removal as a function of residence time in the hyporheic zone. Journal of Geophysical Research, 116(G1), G01025, doi:10.1029/2010JG001356.

Zarnetske, J. P., Haggerty, R., Wondzell, S. M., Bokil, V., A., & Gonzalez-Pinzon, R. (2012). Coupled transport and reaction kinetics control the nitrate source-zink function of hyporheic zones. Water Resources Research, 48(11), W11508, doi:10.1029/2012WR011894.

Zhao, S., Zhang, B., Sun, X., & Yang, L. (2021). Hot spots and hot moments of nitrogen removal from hyporheic and riparian zones: A review. Science of The Total Environment, 762, 144168. https://www.sciencedirect.com/science/article/pii/S0048969720376993

.